2IPRiy

Engineering Experiment Station

NEW MEXICO STATE UNIVERSITY

ADVANCED STUDY OF VIDEO SIGNAL PROCESSING IN LOW SIGNAL TO NOISE ENVIRONMENTS

By

Frank Carden
Robert Henry

A Final Report

Submitted to

NATIONAL AERONAUTICAL SPACE ADMINISTRATION
WASHINGTON, D. C.

NASA RESEARCH GRANT NGR-32-003-037

Electrical Engineering Department
Communication Research Group

June 1972 - August 1973

(NASA-CR-136897) ADVANCED STUDY OF VIDEO SIGNAL PROCESSING IN LOW SIGNAL TO NOISE ENVIRONMENTS Final Report, Jun. 1972 - Aug. 1973 (New Mexico State Univ.) ~~101~~ 100 p HC $8.25 CSCL 12A

N74-21190

Unclas
G3/19 16695

PHASE-LOCK LOOP CHARACTERISTICS IN THE PRESENCE OF NON-WHITE NOISE FOR BAND-PASS TYPES OF MODULATING SPECTRA

BY

ROBERT RICHARD HENRY, B.S., M.S.

A Dissertation submitted to the Graduate School

in partial fulfillment of the requirements

for the Degree

Doctor of Science

Major Subject: Electrical Engineering

Related Area: Mathematics

New Mexico State University

Las Cruces, New Mexico

December 1973

"Phase-Lock Loop Characteristics in the Presence of Non-White Noise for Band-Pass Types of Modulating Spectra," a dissertation prepared by Robert Richard Henry in partial fulfillment of the requirements for the degree, Doctor of Science, has been approved and accepted by the following:

Dean of the Graduate School

Frank F. Carden

Chairman of the Examining Committee

Date

Committee in Charge:

Dr. Frank F. Carden, Chairman

Dr. Lonnie C. Ludeman

Dr. Don D. Merrill

Dr. Keith R. Carver

Dr. William H. Julian

Dr. David W. Martin

ACKNOWLEDGEMENTS

The author would like to take this opportunity to express his gratitude to Dr. Frank Carden for his valuable counsel as graduate committee chairman and for his assistance in determining the course of action to be taken in solving problems associated with this Dissertation. The sponsorship of the majority of this research by the Telecommunications Systems Division of NASA's Manned Spacecraft Center along with the technical assistance of Dr. George D. Arndt is greatly appreciated. The author would also like to express his appreciation to his wife, Carolyn, for her understanding and patience; and to Dr. Lonnie Ludeman for his dedicated efforts to instill in the student the fundamentals of his profession.

VITA

April 22, 1945 - Born at Crowley, Louisiana

1967 - B.S.E.E., University of Southwestern Louisiana, Lafayette, Louisiana

1967 (Summer) - Service Technician, General Electric Company, New Orleans, Louisiana

1967-1969 - Graduate Assistant, University of Southwestern Louisiana, Lafayette, Louisiana

1968 (Summer) - Aerospace Summer Intern, NASA/Manned Spacecraft Center, Houston, Texas

1969 - M.S.E.E., University of Southwestern Louisiana, Lafayette, Louisiana

1969-1971 - Senior Engineer, Philco-Ford Corporation, Houston, Texas

1971-1973 - Communication Research Group, New Mexico State University, Las Cruces, New Mexico

PROFESSIONAL AND HONORARY SOCIETIES

Eta Kappa Nu Tau Beta Pi Gamma Beta Phi

Institute of Electrical and Electronic Engineers

PUBLICATIONS

"Multifilter Phase-Lock Nonlinear Analysis and Design Criterion," IEEE Transactions on Communications, Volume COM-21, February, 1973, pp. 135-142, co-author.

VITA (Continued)

PUBLICATIONS (Continued)

"The Nonlinear Analysis and Design Constraints of a Multi-Filter Phase-Lock Loop," National Telecommunications Conference Record, December 1972, Houston, Texas, co-author.

"Design and Development of a Variable Slope Delta Modulation System Encoder and Decoder," Technical Memorandum No. 7702-8, Philco-Ford Corporation, Houston, Texas, 26 June 1970.

"Optimum Transmission of a Single Voice Signal and 50 KBPS Telemetry Data," Technical Memorandum, Philco-Ford Corporation, Houston, Texas, 7 November 1969.

FIELDS OF STUDY

Major Field: Electrical Engineering (Communication Theory, System Theory)

Related Area: Mathematics (Algebra, Numerical Methods)

ABSTRACT

PHASE-LOCK LOOP CHARACTERISTICS IN THE PRESENCE OF NON-WHITE NOISE FOR BAND-PASS TYPES OF MODULATING SPECTRA

by

ROBERT R. HENRY, B.S., M.S.

Doctor of Science in Electrical Engineering

New Mexico State University

Las Cruces, New Mexico, 1973

Professor Frank F. Carden, Chairman

Conventional analytical techniques used to determine and optimize phase-lock loop (PLL) characteristics are most often based on a model which is valid only if the intermediate frequency (IF) filter bandwidth is large compared to the PLL bandwidth and the phase error is small. In this paper an improved model (called the Quasi-Linear Model) is developed which takes into account small IF Filter bandwidths and the non-linear effects associated with large phase errors. Results predicted by the Quasi-Linear Model for a second-order PLL are compared to experimental results to determine the accuracy of the model.

Due to its simplicity sinusoidal modulation is frequently used to make measurements on an experimental system. In the Experimental System used in this paper a more realistic modulating signal is used. The spectrum of the signal has a band-pass shape with

variable upper and lower break frequencies, with the rolloff rate determined by a fourth-order Chebyshev Polynominal. A rather complex measurement system utilizing cross-correlation techniques was required to determine the output signal-to-noise ratio, due to considerable overlap in the signal and noise spectra.

By comparison of theoretical and experimental results it is demonstrated that the Quasi-Linear Model accurately predicts PLL characteristics. This is true even for small IF Filter Bandwidths and large phase errors where the conventional model is invalid. The theoretical and experimental results are used to draw conclusions concerning threshold, multiplier output variance, phase error variance, output signal-to-noise ratio, and signal distortion. The relationship between these characteristics and IF Filter Bandwidth, modulating signal spectrum, and rms deviation is also determined.

TABLE OF CONTENTS

	Page
LIST OF TABLES	xi
LIST OF FIGURES	xii
Chapter	
1. PHASE-LOCK LOOP THEORETICAL ANAYLSIS	1
1.1 Introduction	1
1.2 The Phase-Lock Loop Model	3
1.3 Steady State Analysis	9
1.4 Relationship between σ_ϕ^2 and σ_x^2	12
2. THE EXPERIMENTAL SYSTEM	13
2.1 System Overview	13
2.2 The Band-pass Filter	13
2.3 The FM Transmitter	17
2.4 The IF Filter	19
2.5 The Post-Detection Filter	21
2.6 The Multiplier	21
2.7 The Loop Filter and PLL Transfer Function	22
2.8 CNR, SNR, and Voltage Measurements on the System	25
2.9 Experimental System Measurement Errors	29
3. THEORY APPLIED TO THE EXPERIMENTAL SYSTEM	31
3.1 RMS Deviation and Noise Power	31
3.2 Polynominal Form of the Spectra	32
3.3 Simplification of Results	35

TABLE OF CONTENTS (Continued)

Chapter Page

3.4 Computer Implementation of Equations 37

4. PLL CHARACTERISTICS IN THE ABSENCE OF NOISE . . . 40

4.1 Signal Distortion Due to the IF Filter and PLL Nonlinearity 40

4.2 Comparison of Theoretical and Experimental Results. 48

5. PLL CHARACTERISTICS IN THE ABSENCE OF MODULATION. 51

5.1 Introduction 51

5.2 Comparison of Theoretical and Experimental Results. 51

5.3 Comparison of the Quasi-Linear Model and Viterbi's Model. 56

6. PLL CHARACTERISTICS IN THE PRESENCE OF MODULATION AND NOISE 61

6.1 Comparison of Theoretical and Experimental Results. 61

6.2 PLL Characteristics as a Function of RMS Deviation. 75

6.3 PLL Characteristics as a Function of IF Filter Bandwidth 76

6.4 PLL Characteristics as a Function of the Signal Spectrum. 76

6.5 PLL Threshold Characteristics. 77

7. CONCLUSIONS AND RECOMMENDATIONS FOR FUTURE WORK . 79

7.1 Conclusions. 79

7.2 Recommendations for Future Work. 80

TABLE OF CONTENTS (Continued)

Chapter Page

BIBLIOGRAPHY. 81

APPENDICES

I. Spectral Densities of the PLL. 82

II. Band-pass Filter Transfer Function 84

LIST OF TABLES

Table Page

1. Output Signal Distortion Due to PLL Stress and Finite IF Filter Bandwidth for No Noise 46

2. Comparison of Theoretical (Quasi-Linear Model) and Experimental Results. 74

LIST OF FIGURES

Figure		Page
1.	Communication System Overview	2
2.	Receiver/Demodulator and Channel Block Diagram	4
3.	PLL Phase Model	7
4.	PLL Phase Model for Small Modulation Indices and/or Wide IF Bandwidths	8
5.	Quasi-Linear PLL Phase Model	10
6.	Experimental System Overview	14
7.	Multiplier and Summer Schematics	15
8.	Loop Filter, VCO, and Amplifier Schematics	16
9.	Band-pass Filter Frequency Response	18
10.	IF Filter Frequency Response	20
11.	PLL - Post-Detection Filter Frequency Response	24
12.	Measurement System Block Diagram	27
13.	Measurement System Computer Program Flow Chart	28
14.	Flow Chart of Computer Program Used to Calculate Theoretical Values Based on the Quasi-Linear Model	38
15.	SNR as a Function of Deviation for No Noise with f_1 = 56 Hz, f_2 = 440 Hz	41
16.	SNR as a Function of Deviation for No Noise with f_1 = 56 Hz, f_2 = 900 Hz	42
17.	SNR as a Function of Deviation for No Noise with f_1 = 56 Hz, f_2 = 1250 Hz	43
18.	SNR as a Function of Deviation for No Noise with f_1 = 560 Hz, f_2 = 900 Hz	44
19.	PLL Unlock Boundary as Function of f_2 for f_1 = 56 Hz	47

LIST OF FIGURES (Continued)

Figure Page

20. Multiplier Output Variance as a Function of RMS Deviation for No Noise and β = 5600 Hz. 49

21. Multiplier Output and Phase Variance as a Function of IF Filter Bandwidth for No Modulation and SNR_{loop} = 14.2 dB 52

22. Multiplier Output and Phase Variance as a Function of IF Filter Bandwidth for No Modulation and SNR_{loop} = 4.68 dB 53

23. Multiplier Output and Phase Variance as a Function of IF Filter Bandwidth for No Modulation and SNR_{loop} = 0.2 dB. 54

24. Multiplier Output Variance as a Function of CNR for No Modulation 57

25. Phase Error Variance Due to Additive Noise of Uniform Spectral Density (NSD). 59

26. Parameter Space Region for the Validity of the Quasi-Linear Model and Viterbi's Model. 60

27. SNR and σ_x^2 as a Function of CNR for β = 5600 Hz, f_1 = 56 Hz, f_2 = 440 Hz 62

28. SNR and σ_x^2 as a Function of CNR for β = 3300 Hz, f_1 = 56 Hz, f_2 = 440 Hz 63

29. SNR and σ_x^2 as a Function of CNR for β = 900 Hz, f_1 = 56 Hz, f_2 = 440 Hz 64

30. SNR and σ_x^2 as a Function of CNR for β = 5600 Hz, f_1 = 56 Hz, f_2 = 900 Hz 65

31. SNR and σ_x^2 as a Function of CNR for β = 3300 Hz, f_1 = 56 Hz, f_2 = 900 Hz 66

32. SNR and σ_x^2 as a Function of CNR for β = 900 Hz, f_1 = 56 Hz, f_2 = 900 Hz 67

LIST OF FIGURES (Continued)

Figure | Page

33. SNR and σ_x^2 as a Function of CNR for β = 5600 Hz, f_1 = 56 Hz, f_2 = 1250 Hz. 68

34. SNR and σ_x^2 as a Function of CNR for β = 3300 Hz, f_1 = 56 Hz, f_2 = 1250 Hz. 69

35. SNR and σ_x^2 as a Function of CNR for β = 900 Hz, f_1 = 56 Hz, f_2 = 1250 Hz. 70

36. SNR and σ_x^2 as a Function of CNR for β = 5600 Hz, f_1 = 560 Hz, f_2 = 900 Hz. 71

37. SNR and σ_x^2 as a Function of CNR for β = 3300 Hz, f_1 = 560 Hz, f_2 = 900 Hz. 72

38. SNR and σ_x^2 as a Function of CNR for β = 900 Hz, f_1 = 560 Hz, f_2 = 900 Hz. 73

Chapter 1

PHASE-LOCK LOOP THEORETICAL ANALYSIS

1.1 Introduction

The overview of a typical Communication System is shown in Figure 1. The source signal is transformed by the Modulator/Transmitter into a form suitable for transmission over the communication channel. By the time this transformed signal has reached the Receiver/Demodulator it has been corrupted by additive channel noise. The function of the Receiver/Demodulator is to perform an inverse transformation on the noise corrupted transformed signal and obtain a signal closely resembling the original signal.

This paper is concerned with a system such as in Figure 1, in which Frequency Modulation (FM) is used to perform the transformation. The Receiver/Demodulator function is performed by a Phase-lock loop (PLL). The PLL has become more widely used as an FM demodulator in the past several years. This is primarily due to the superior noise-rejection properties and threshold extension exhibited by the PLL. These characteristics are particularly useful in aerospace FM communication systems where receivers must operate in low carrier-to-noise ratio (CNR) environments.

In the development of the traditional PLL model, the additive channel noise is assumed to be "white". This implies that the intermediate frequency (IF) Filter bandwidth must be large compared

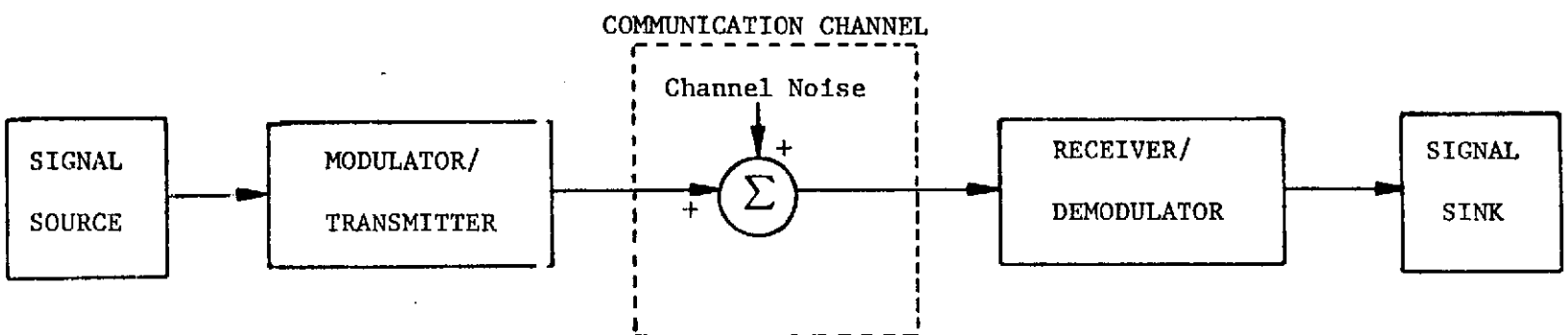

Figure 1. Communication System Overview.

to the PLL bandwidth. It is also usually assumed that the phase error is small so that the PLL is operating in the linear region. In this paper an improved model which takes into account small IF Filter bandwidths and the non-linear effect is developed.

1.2 The Phase-Lock Loop Model

Figure 2 is a more detailed block diagram of the Receiver/Demodulator and Communication Channel of Figure 1. The noise process $\bar{n}(t)$ is considered to have a spectral density which is "flat" over the passband of the IF Filter. It is assumed that the noise process has a Gaussian amplitude distribution with zero mean. This allows $\bar{n}(t)$ to be expressed as given in [1] by

$$\bar{n}(t) = \sqrt{2}\ [n_1(t) \sin(\omega_0 t) + n_2(t) \cos(\omega_0 t)]. \qquad (1\text{-}1)$$

$n_1(t)$ and $n_2(t)$ are independent Gaussian processes of zero mean and identical spectral densities which are the same as the spectral density of $n(t)$ but translated downward in frequency so that they are centered about zero frequency. Thus the spectrum of $n_1(t)$ and of $n_2(t)$ are low-pass extending to β rad./sec.

The signal input to the multiplier is given by

$$\sqrt{2}\ A \sin \theta(t) + \bar{n}(t) = \sqrt{2}\ \{A \sin [\omega_0 t + \theta_1(t)] + n_1(t) \sin \omega_0 t + n_2(t) \cos \omega_0 t\} \qquad (1\text{-}2)$$

where A is the rms voltage of the carrier, ω_0 the unmodulated carrier frequency in rad./sec., and $\theta_1(t)$ the carrier phase due to the modulating signal. The Voltage Controlled Oscillator (VCO) output

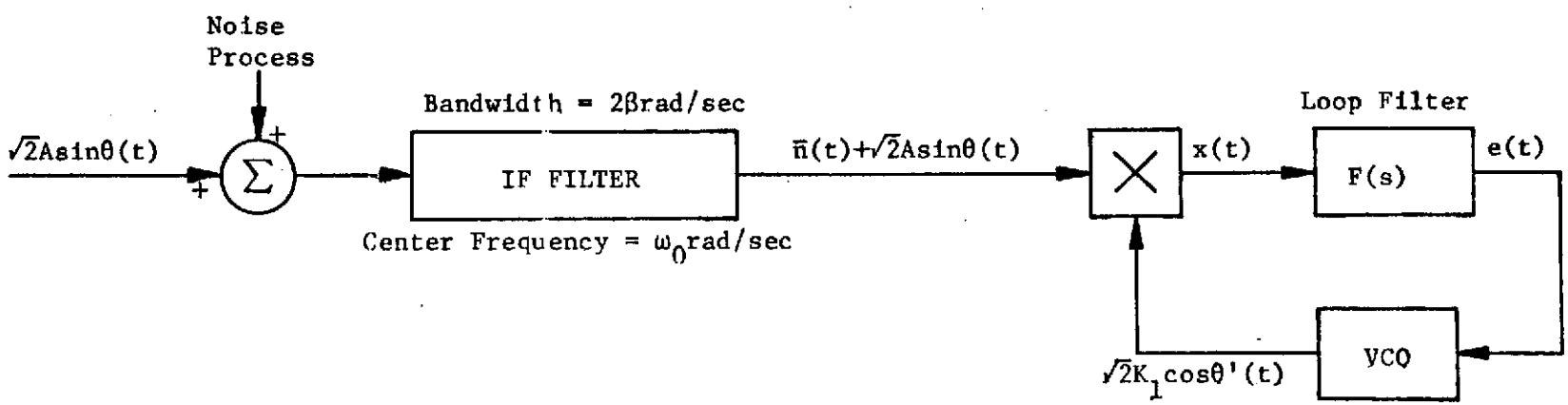

Figure 2. Receiver/Demodulator and Channel Block Diagram.

signal is

$$\sqrt{2}\ K_1 \cos \theta'(t) = \sqrt{2}\ K_1 \cos\ [\omega_0 t + \theta_2(t)] \tag{1-3}$$

where K_1 is the rms voltage of the VCO output, and $\theta_2(t)$ the phase of the VCO output.

From Equations (1-2) and (1-3) it is straightforward to verify that the multiplier output is

$$\begin{aligned} x(t) &= AK_1 \sin[\theta_1(t) - \theta_2(t)] - K_1 n_1(t) \sin \theta_2(t) \\ &+ K_1 n_2(t) \cos \theta_2(t) + AK_1 \sin[2\omega_0 t + \theta_1(t) + \theta_2(t)] \\ &+ K_1 n_1(t) \sin[2\omega_0 t + \theta_2(t)] + K_1 n_2(t) \cos[2\omega_0 t + \theta_2(t)]. \end{aligned} \tag{1-4}$$

By neglecting the double frequency terms in x(t), Equation (1-4) and Figure 2 yield the following for the VCO input

$$e(t) = K_1 \int_0^t [A \sin \phi(u) - n_1(u) \sin \theta_2(u) + n_2(u) \cos \theta_2(u)]\ f(t-u)du \tag{1-5}$$

where f(t) is the impulse response of the linear filter F(s), and

$$\phi(t) = \theta_1(t) - \theta_2(t). \tag{1-6}$$

Here the PLL is assumed to be locked at t=0 so that e(0) = 0. Let K_2 be the VCO constant (rad./sec./volt), then

$$\frac{d\theta_2(t)}{dt} = K_2 e(t) + \omega_0. \tag{1-7}$$

Also define a new constant

$$K \triangleq K_1\ K_2. \tag{1-8}$$

Now Equations (1-5) through (1-8) yield the phase model of the PLL shown in Figure 3.

Now consider the case in which $\theta_2(t)$ is small (less than 30°). This would be true for a small modulation index and high CNR. Since

$$n_2(t) \cos \theta_2(t) - n_1(t) \sin \theta_2(t) \longrightarrow n_2(t) \triangleq n(t) \qquad (1\text{-}9)$$

as $\theta_2(t) \longrightarrow 0$, the phase model of Figure 3 becomes that of Figure 4. The spectrum of $n(t)$ is low-pass with cutoff frequency β and spectral density the same as the noise process as discussed in the noise representation given by Equation (1-1). Viterbi [1] shows that the model of Figure 4 is valid for the case in which the IF filter bandwidth is wide compared to the PLL bandwidth. Thus the model given by Figure 4 is valid for small phase errors and/or wide IF Filter bandwidth compared to PLL bandwidth.

Since the multiplier output (neglecting double frequency terms) is

$$x(t) = K_{-}[A \sin \phi(t) + n(t)]. \qquad (1\text{-}10)$$

one finds that

$$x(t) = K_1 \, y(t). \qquad (1\text{-}11)$$

One of the difficulties in analyzing the PLL represented in Figure 4 is that a linear analysis is invalid [illegible] for small $\phi(t)$ since $\sin \phi(t) = \phi(t)$ only for $\phi(t) < 30°$. One [illegible] difficulty is to replace the non-linearity by an [illegible]valent linear gain which depends on $\phi(t)$. This quasi-linear a[illegible] [illegible]h was first applied to the PLL by Develet [2]. Replace the non-linearity by a

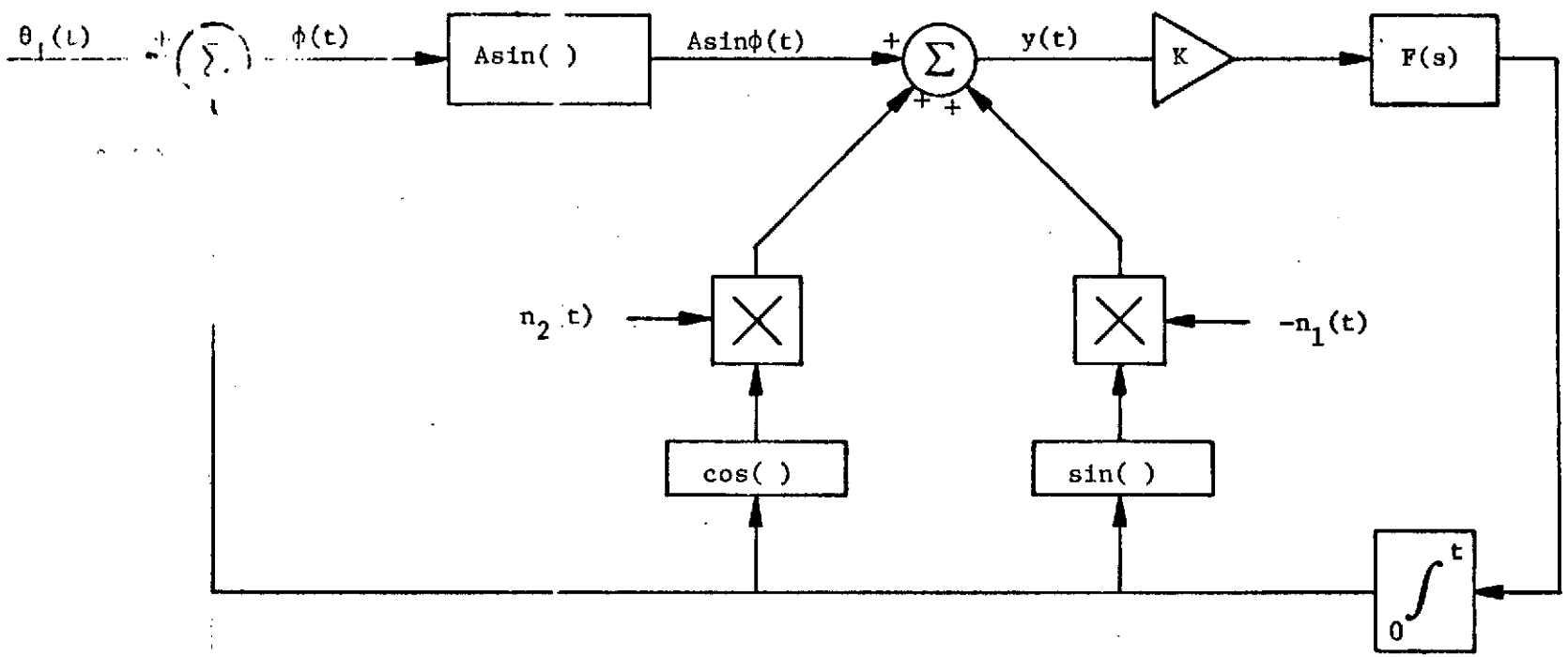

Figure 3. PLL Phase Model.

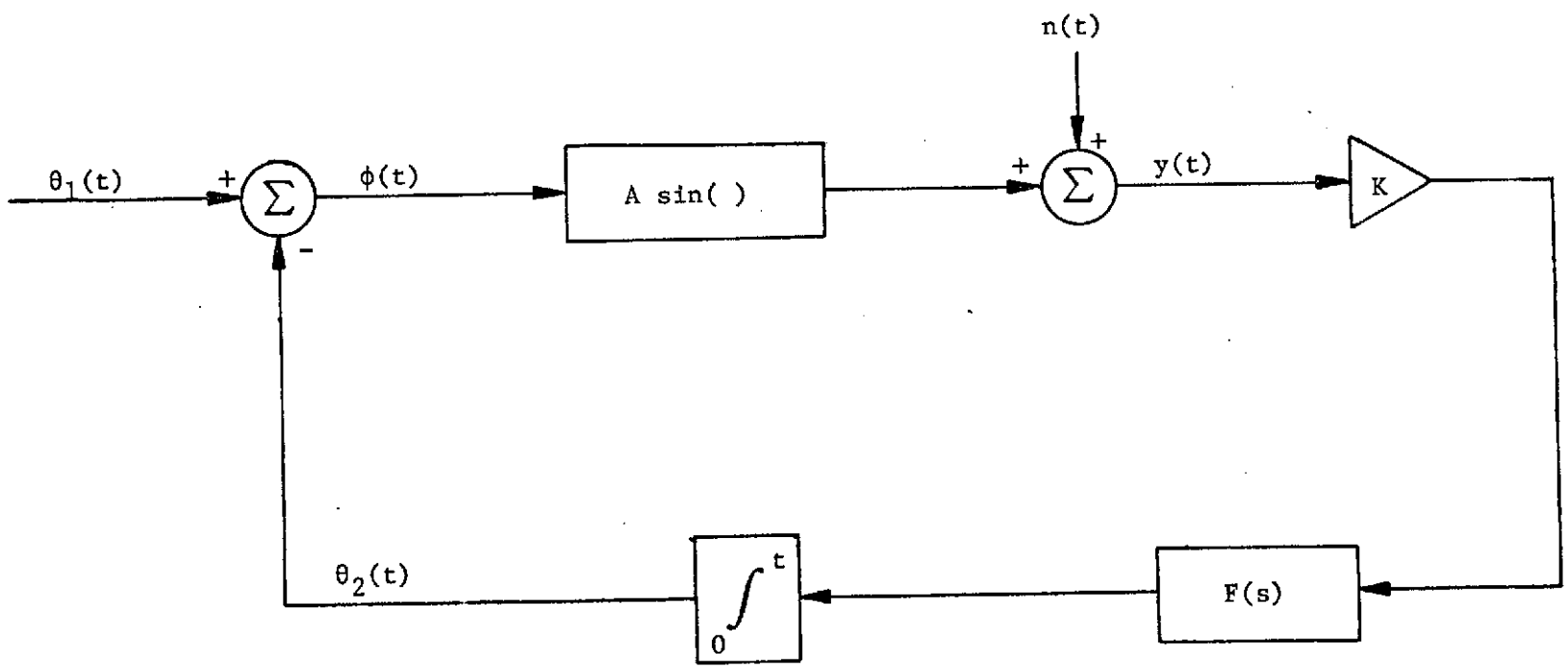

Figure 4. PLL Phase Model for Small Modulation Indices and/or Wide IF Bandwidths.

linear gain G so that the expected value of the square of the difference $E\{[A \sin \phi(t) - G\,\phi(t)]^2\}$ is minimized. Assuming that $\phi(t)$ is a zero-mean Gaussian process with $\sigma^2 = E[\phi^2(t)]$ it can be shown [3] that

$$G = A\, e^{-\sigma^2/2} \quad . \tag{1-12}$$

The assumption that $\phi(t)$ is Gaussian is justifiable only when the PLL is operating in the linear region. For large (>30°) ϕ the Gaussian assumption may no longer be valid, but the above procedure should be more accurate than replacing $A \sin \phi(t)$ with $A\,\phi(t)$. The phase model now becomes that illustrated in Figure 5. The transfer function D(s) represents a post-detection filter.

1.3 Steady State Analysis

Assuming that the modulation and additive noise processes are zero mean and wide sense stationary, it is straightforward to show [1] that $\phi(t)$, $y(t)$, $o(t)$, $\theta_1(t)$, and $\theta_2(t)$ are zero mean and that as $t \to \infty$ (steady state) the covariances are independent of t. Thus the corresponding spectral densities are well defined. Since the non-linearity is replaced by an equivalent linear gain G, the system in Figure 5 is linear and the superposition principle holds. This coupled with the hypothesis that the modulation process and the additive noise process are independent allows one to compute the effect of the modulation and of the noise independently and then combine the two.

Let $\overline{\Theta}_1(\omega)$, $\overline{\Theta}_2(\omega)$, $\overline{\Phi}(\omega)$, $\overline{N}(\omega)$, $\overline{Y}(\omega)$, and $\overline{O}(\omega)$ represent the spectral densities of $\theta_1(t)$, $\theta_2(t)$, $\phi(t)$, $n(t)$, $y(t)$, and $o(t)$

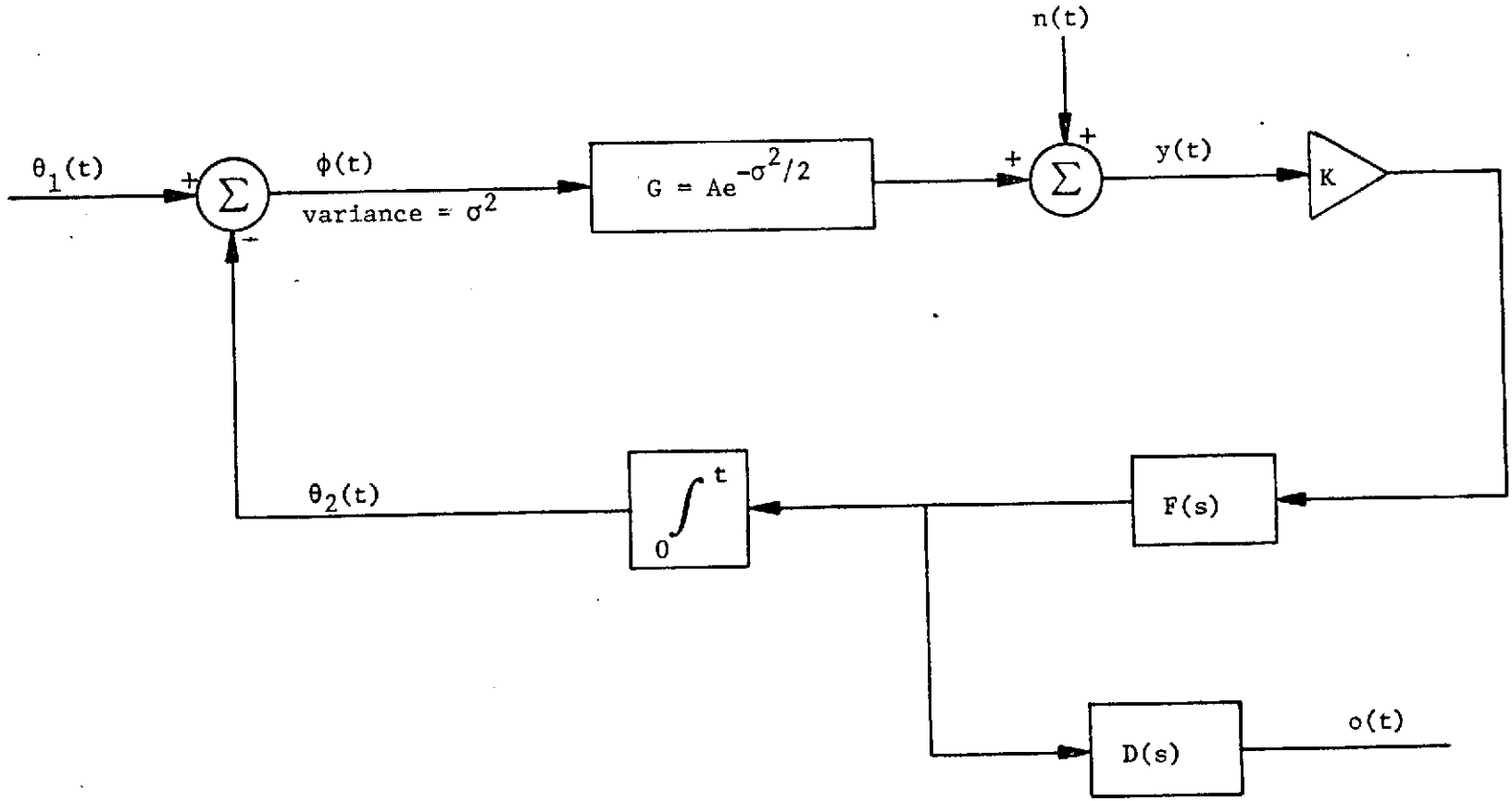

Figure 5. Quasi-Linear PLL Phase Model.

respectively. Throughout this paper it is understood that s is written in place of $j\omega$. It can be shown [4] that the frequency response of the PLL is given by

$$H(s) \triangleq \frac{\Theta_2(s)}{\Theta_1(s)} = \frac{GK\ F(s)}{s + GK\ F(s)} \tag{1-13}$$

where $\Theta_2(s)$ and $\Theta_1(s)$ are the Fourier Transforms of $\theta_2(t)$ and $\theta_1(t)$ respectively.

Equation (1-13) and Figure 5 give (see Appendix I)

$$\overline{\Phi}(\omega) = |1 - H(s)|^2 \overline{\Theta}_1(\omega) + \frac{1}{G^2}|H(s)|^2\ \overline{N}(\omega), \tag{1-14}$$

$$\overline{Y}(\omega) = G^2|1 - H(s)|^2 \overline{\Theta}_1(\omega) + |1 - H(s)|^2\ \overline{N}(\omega), \tag{1-15}$$

and

$$\overline{O}(\omega) = \omega^2|H(s)|^2 \overline{D}(\omega)\overline{\Theta}_1(\omega) + \frac{\omega^2}{G^2}|H(s)|^2 \overline{D}(\omega)\overline{N}(\omega). \tag{1-16}$$

From Equation (1-14) the variance of the phase error is

$$\sigma_\phi^2 = \int_{-\infty}^{\infty} \overline{\Phi}(\omega)\ \frac{d\omega}{2\pi}$$

$$= \int_{-\infty}^{\infty} |1 - H(s)|^2 \overline{\Theta}_1(\omega)\ \frac{d\omega}{2\pi} + \frac{1}{G^2} \int_{-\infty}^{\infty} |H(s)|^2 \overline{N}(\omega)\ \frac{d\omega}{2\pi}. \tag{1-17}$$

From Equation (1-11) and (1-15) the phase variance of the multiplier output is

$$\sigma_x^2 = \int_{-\infty}^{\infty} K_1^2\ \overline{Y}(\omega)\ \frac{d\omega}{2\pi}$$

$$= (GK_1)^2 \int_{-\infty}^{\infty} |1 - H(s)|^2 \overline{\Theta}_1(\omega)\ \frac{d\omega}{2\pi} + K_1^2 \int_{-\infty}^{\infty} |1 - H(s)|^2 \overline{N}(\omega)\ \frac{d\omega}{2\pi}. \tag{1-18}$$

Likewise Equation (1-16) gives the output variance as

$$\sigma_o^2 = \int_{-\infty}^{\infty} \overline{O}(\omega) \frac{d\omega}{2\pi}$$

$$= \int_{-\infty}^{\infty} \omega^2 |H(s)|^2 \overline{D}(\omega) \overline{\Theta}_1(\omega) \frac{d\omega}{2\pi} + \frac{1}{G^2} \int_{-\infty}^{\infty} \omega^2 |H(s)|^2 \overline{D}(\omega) \overline{N}(\omega) \frac{d\omega}{2\pi} . \tag{1-19}$$

1.4 Relationship Between σ_ϕ^2 and σ_x^2

In much of the literature the phase variance is often determined by measuring σ_x^2 and multiplying by the appropriate phase detector constant. From Equations (1-17, 1-18) it can be seen that this is true only for the no noise case (here $\sigma_\phi^2 = (GK_1)^2 \sigma_x^2$). For the general case with noise

$$\sigma_x^2 - \sigma_\phi^2 = [(GK_1)^2 - 1] \int_{-\infty}^{\infty} |1 - H(s)|^2 \overline{\Theta}_1(\omega) \frac{d\omega}{2\pi}$$
$$+ \int_{-\infty}^{\infty} \left[K_1^2 |1 - H(s)|^2 - \frac{1}{G^2} |H(s)|^2\right] \overline{N}(\omega) \frac{d\omega}{2\pi} . \tag{1-20}$$

Using the fact that

$$|1 - H(s)|^2 = |H(s)|^2 \frac{\omega^2}{(GK)^2 |F(s)|^2} \tag{1-21}$$

Equation (1-20) becomes

$$\sigma_x^2 - \sigma_y^2 = [(GK_1)^2 - 1] \int_{-\infty}^{\infty} |1 - H(s)|^2 \overline{\Theta}_1(\omega) \frac{d\omega}{2\pi}$$
$$+ \frac{1}{G^2} \int_{-\infty}^{\infty} \left[\frac{\omega^2}{K_2^2 |F(s)|^2} - 1\right] |H(s)|^2 \overline{N}(\omega) \frac{d\omega}{2\pi} . \tag{1-22}$$

Notice that the relationship involves the PLL parameters as well as the noise spectral density.

Chapter 2

THE EXPERIMENTAL SYSTEM

2.1 System Overview

An overview of the Experimental System is shown in Figure 6. Both the noise generator used to produce the signal and the one used to produce the additive channel noise have an essentially "flat" spectral density over the bandwidth of the corresponding filters which follow them (B(s) and I(s) respectively). The center frequency of the FM transmitter was chosen to be 455 kHz, so that the IF Filter is centered at 455 kHz. The noncommercial equipment schematics are shown in Figures 7 and 8.

2.2 The Band-pass Filter

The Band-pass Filter used to shape the "white" noise is the General Radio Type 1952 Universal Filter. The cutoff frequencies are selectable with the response being that of a 4-pole Chebyshev filter. Such a response for the low-pass section is given by

$$|G(s)|^2 = \frac{1}{1 + \varepsilon^2 \, T_4^2\left(\frac{\omega}{\omega_c}\right)} \tag{2-1}$$

where T_4 is a 4th order Chebyshev Polynominal and the peak-to-peak ripple is given by

$$1 - \frac{1}{\sqrt{1 + \varepsilon^2}} \tag{2-2}$$

The parameters as determined from comparison of the measured

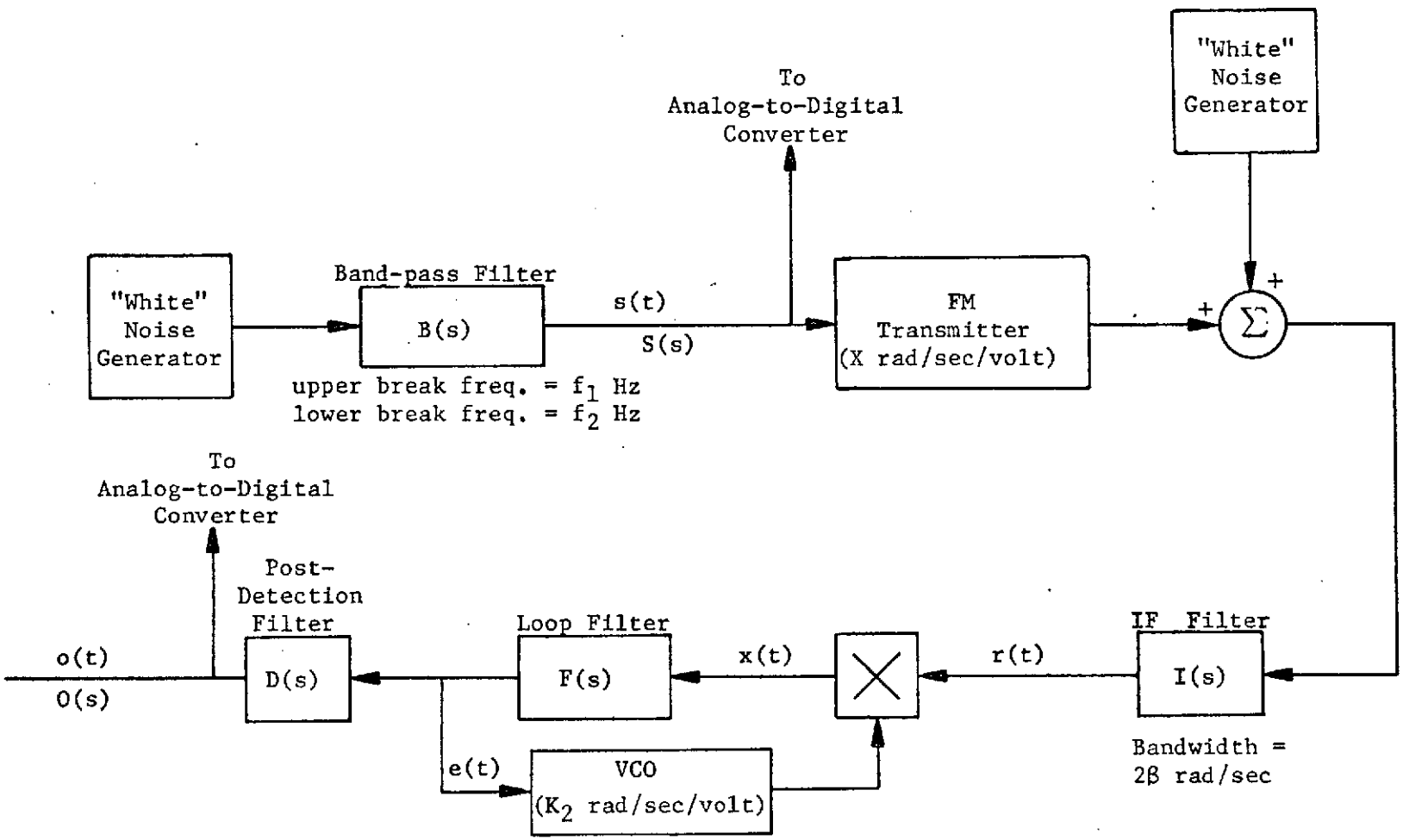

Figure 6. Experimental System Overview.

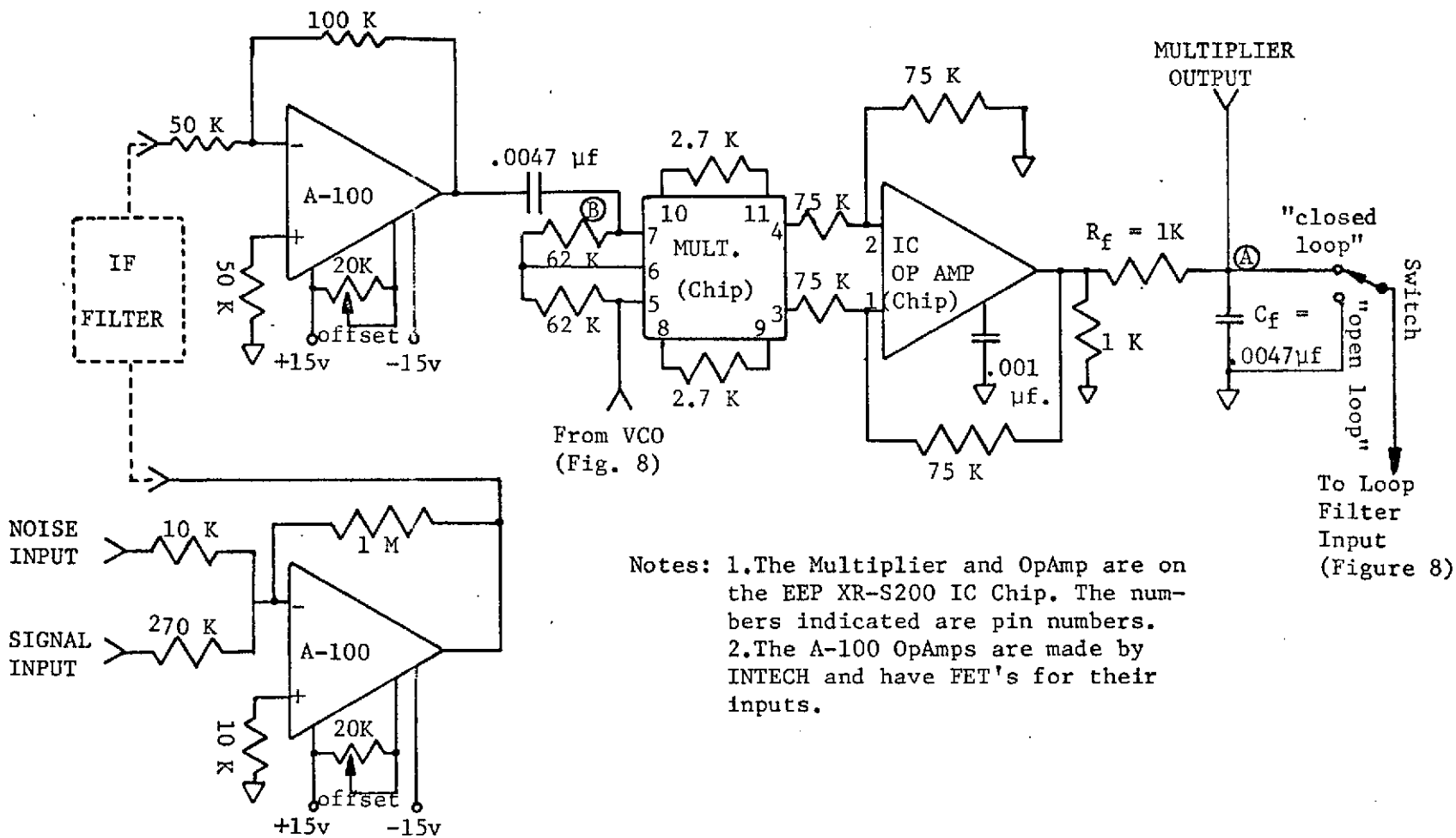

Notes: 1.The Multiplier and OpAmp are on the EEP XR-S200 IC Chip. The numbers indicated are pin numbers.
2.The A-100 OpAmps are made by INTECH and have FET's for their inputs.

Figure 7. Multiplier and Summer Schematics.

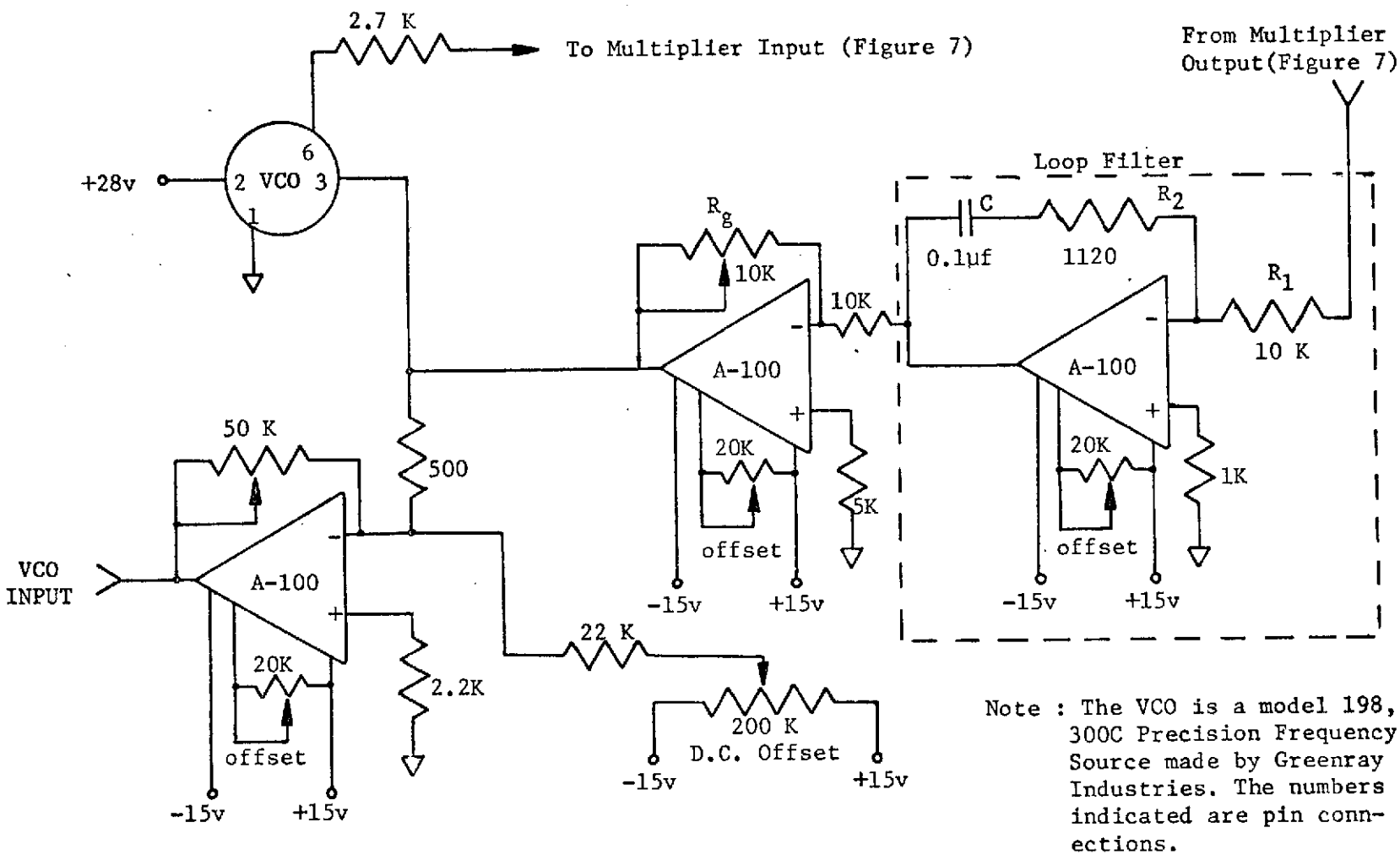

Note : The VCO is a model 198, 300C Precision Frequency Source made by Greenray Industries. The numbers indicated are pin connections.

Figure 8. Loop Filter, VCO, and Amplifier Schematics.

frequency response and theoretical response (see Figure 9) are:

$$\varepsilon^2 = 0.07,\ f_1 = 1.2\ f_{1,3dB},\ f_2 = 0.895\ f_{2,3dB} \qquad (2\text{-}3)$$

where $f_{1,3dB}$ is the selected cutoff frequency for the high-pass filter section, and f_1 the corresponding theoretical break frequency. A similar statement applies to $f_{2,3dB}$, f_2 for the low-pass section. By cascading the low-pass and high-pass sections the desired transfer function for the band-pass filter is obtained. The result is (see Appendix II)

$$B(s) = \frac{s^4}{g_8 s^8 + g_7 s^7 + \ldots\ldots\ldots + g_1 s + g_0} \quad . \qquad (2\text{-}4)$$

The constants g_0 through g_8 are functions of the upper and lower break frequencies and are given by Equations (II-5) and II-9).

2.3 The FM Transmitter

Consider the effect of applying a sinusoidal signal of frequency f_m Hz and zero-to-peak voltage of V to the input of the FM transmitter. Then the zero-to-peak deviation (Hz) Δf of the carrier is

$$2\pi\Delta f = XV. \qquad (2\text{-}5)$$

It is straightforward to verify that the zero-to-peak phase deviation is

$$\beta = \Delta f / f_m = \Delta\omega/\omega_m \qquad (2\text{-}6)$$

From Equation (2-5) and (2-6)

$$X = \frac{2\pi\beta\ f_m}{V} \qquad \frac{\text{rad/sec}}{\text{volt}} \quad . \qquad (2\text{-}7)$$

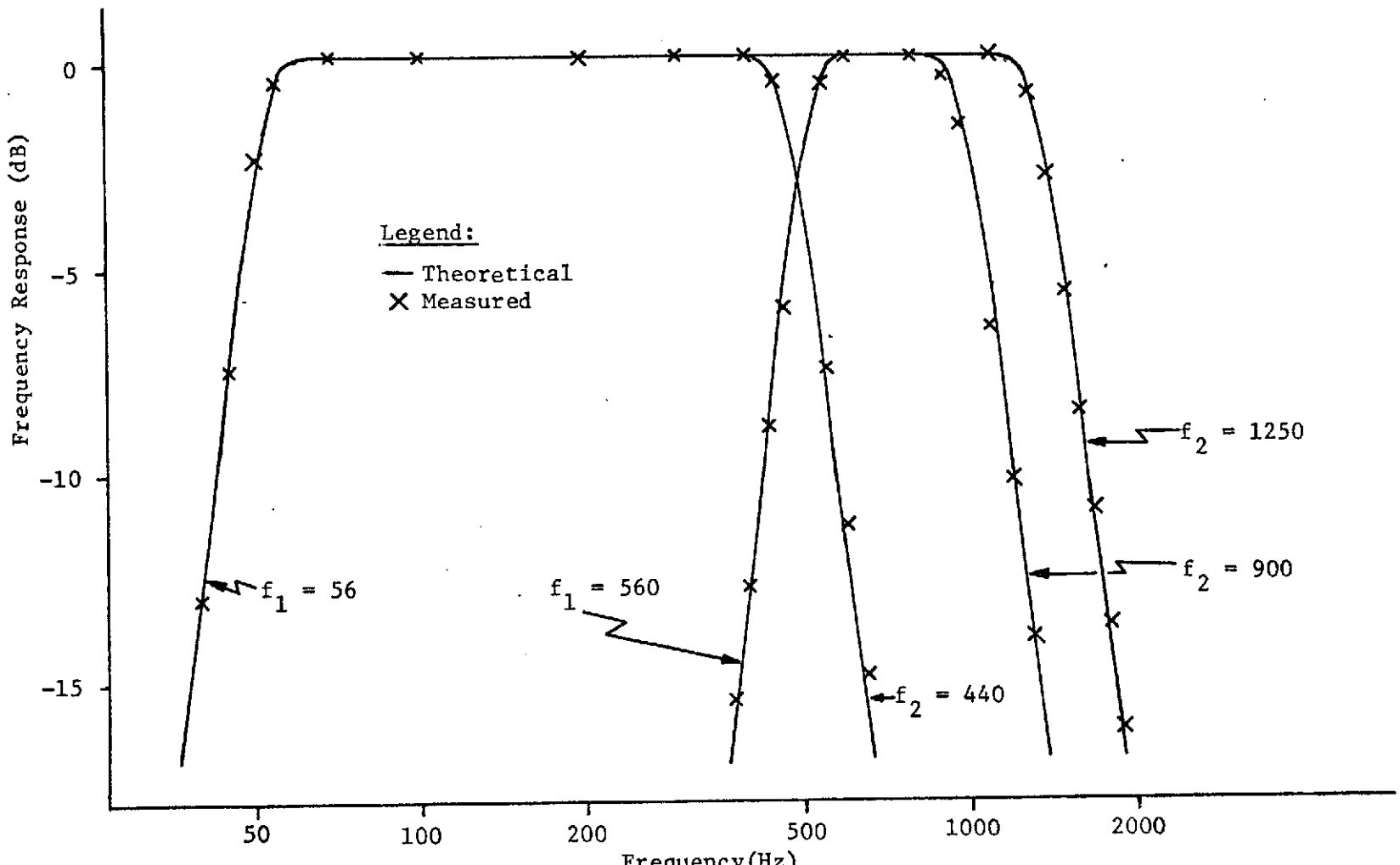

Figure 9. Band-pass Filter Frequency Response.

It is well known [5] that for sinusoidal modulation the amplitude of the carrier is proportional to $J_o(\beta)$ where $J_o(\ )$ is the Bessel function of the first kind of order zero. Thus for $\beta = 2.41$ the carrier component vanishes.

The above mentioned modulation was applied to the FM Transmitter and V increased until the carrier component of the Transmitter vanished as observed on a Spectrum Analyzer. The value of V and f_m were then recorded. Then Equation (2-7) with $\beta = 2.41$ was used to determine X. Values of f_m from 400 Hz to 2000 Hz were used with less than 0.1% difference in the corresponding values of X. X was determined to be

$$X = 2\pi(201000) \qquad \frac{\text{rad/sec}}{\text{volt}} \quad . \qquad (2\text{-}8)$$

2.4 The IF Filter

The measured frequency response of the four IF Filters used in the Experimental System is shown in Figure 10. The Figure is actually a plot of I(s) translated down in frequency so that the center frequency becomes zero. It is convenient for future calculations to define

$$C(s) \triangleq I\{j\ 2\pi(f - 455000)\} \qquad (2\text{-}9)$$

since it is the translated version of I(s) that is needed.

The frequency response of $B(s)_{LP}$ determined in Appendix II with the appropriate break frequency fits the frequency response of C(s) reasonably well as illustrated in Figure 10. Therefore from Equation (II-6)

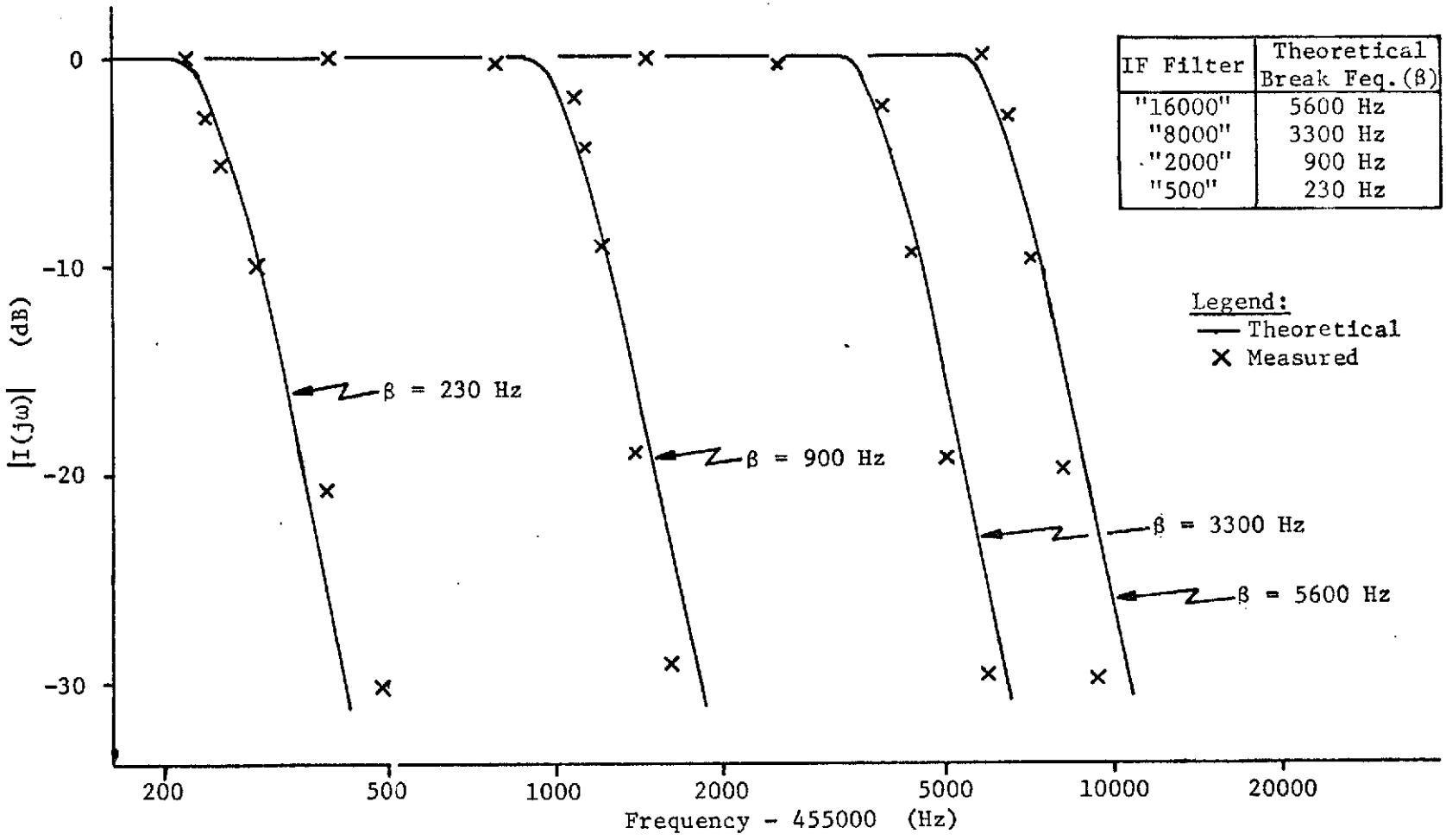

IF Filter	Theoretical Break Feq. (β)
"16000"	5600 Hz
"8000"	3300 Hz
"2000"	900 Hz
"500"	230 Hz

Figure 10. IF Filter Frequency Response.

$$C(s) = \frac{1}{p_4 s^4 + p_3 s^3 + p_2 s^2 + p_1 s + f_o} \tag{2-10}$$

where $p_1 = f_1/\beta$ $\qquad p_3 = f_3/\beta^3$

$$p_2 = f_2/\beta^2 \qquad p_4 = 1/\beta^4 \tag{2-11}$$

and β is the break frequency in rad/sec. The values of β for the four mechanical filters that could be used as the IF filter are given in Figure 10 along with the theoretical and measured frequency responses.

2.5 The Post-Detection Filter

The Post-Detection Filter used has a first order low-pass response given by

$$D(s) = \frac{b}{b + s} \tag{2-12}$$

where b is the break frequency in rad/sec. The filter is used to eliminate output noise outside of the signal spectral characteristic and thus enhance the output signal-to-noise-ratio.

2.6 The Multiplier

The Multiplier is shown in Figure 7 and is part of the EEP XR-S200 Multifunction Integrated Circuit. The resistor-capacitor combination R_f-C_f filters out the double frequency terms of the multiplier output. The multiplier output measurements were made at point Ⓐ of Figure 7. With the loop switch set to the "open loop" position and with no noise, the multiplier output was observed on an oscilloscope for various offsets in frequency between the VCO and FM

transmitter. The observed waveform was sinusoidal with constant amplitude for offset frequency differences up to 5 kHz. Since the highest modulating frequency used in the system was about 1.5 kHz, the multiplier response is essentially flat over the frequencies of interest. The zero-to-peak voltage output of the multiplier output was measured to be 1.4 volts. Thus from Equation (1-10) with n(t) = 0

$$K_1 A = 1.4(\text{volts})^2 \tag{2-13}$$

The voltage of A measured at (B) in Figure 7 was found to be 0.776 volts rms. Thus from Equation (2-13)

$$K_1 = \frac{1.4}{0.776} = 1.8 \text{ volts} \tag{2-14}$$

2.7 The Loop Filter and PLL Transfer Function

A very common loop filter used in PLL's is one with an "integral plus proportional" transfer characteristic. This type filter is used in the Experimental System and has a transfer function given by

$$F(s) = 1 + \frac{a}{s} . \tag{2-15}$$

It follows from Equation (1-13) that

$$H(s) = \frac{GK(s + a)}{s^2 + GKs + aGK} = \frac{x_1 s + x_0}{s^2 + x_1 s + x_0} \tag{2-16}$$

where

$$x_0 = GKa, \; x_1 = GK. \tag{2-17}$$

Since the largest exponent of s in the denominator of Equation (2-16) is 2 the PLL is classified as second order. The actual loop

filter is shown in Figure 8. It can be shown [4] that for a large operational amplifier gain this active filter has a transfer function given by

$$\frac{\tau_2}{\tau_1} + \frac{\tau_1}{\tau_1 s} = \frac{s\tau_2 + 1}{s\tau_1} = \frac{\tau_2}{\tau_1}\left[1 + \frac{1}{\tau_2 s}\right] \tag{2-18}$$

where $\tau_1 = R_1 C, \qquad \tau_2 = R_2 C$. (2-19)

Comparing Equations (2-15) and (2-18) one finds that

$$a = 1/\tau_2 \tag{2-20}$$

From Equations (1-13), (2-15) and (2-18) it can be seen that the loop gain K is modified by the factor τ_2/τ_1. Gardner [4] shows that

$$\omega_n^2 = \frac{GK}{\tau_1} \quad \text{and} \quad \zeta = \frac{\tau_2}{2}\,\omega_n, \tag{2-21}$$

where ω_n is the natural frequency and ζ the damping factor for the second order system. In this system the following values for ω_n and ζ were chosen

$$\omega_n = 2\pi(860), \quad \zeta = 0.707 \tag{2-22}$$

The values of R_1, R_2, and C were chosen to give the approximate values for ω_n and ζ. Then the loop gain was changed (by varying R_g) until the measured frequency response agreed closely with the theoretical response [4].

The Post-Detection filter was chosen so that

$$b = 2\pi(1300) \ . \tag{2-23}$$

The overall measured frequency response of the PLL is shown in Figure 11. Also included for comparison is the theoretical response for

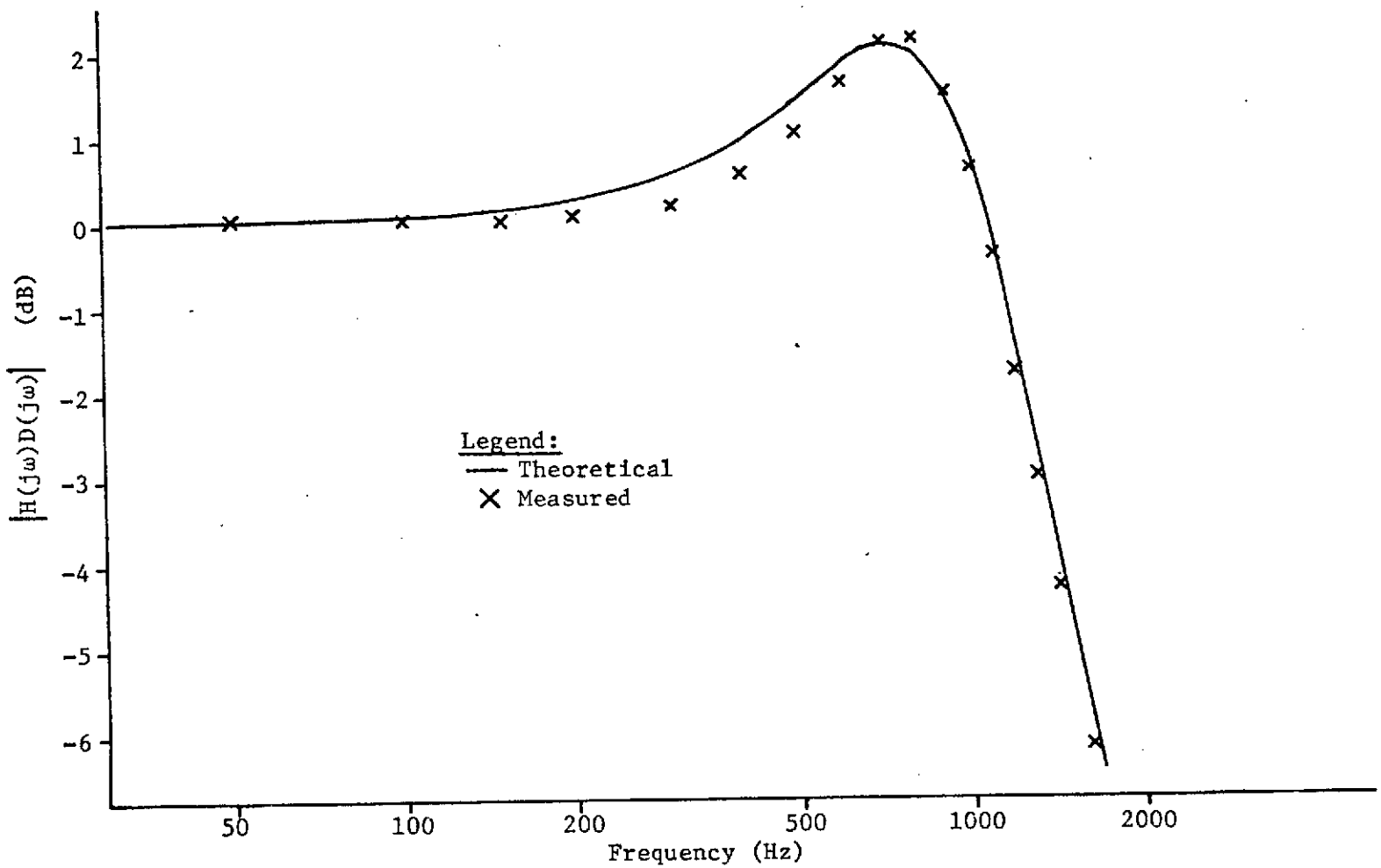

Figure 11. PLL - Post-Detection Filter Frequency Response.

the parameters given in Equations (2-22) and (2-23).

2.8 CNR, SNR, and Voltage Measurements on the System

CNR measurements were made with a rms voltmeter at point Ⓑ in Figure 7. This is equivalent to measuring r(t) in Figure 6. The carrier rms voltage (V_c) was measured with no modulation applied to the FM transmitter and no channel noise added. A calibration chart was then made for each IF Filter which gives the voltage at point Ⓑ (V_n) for a given voltage at the channel noise generator output with the carrier turned off. From this calibration chart the CNR was determined by reading the rms voltage at the channel noise generator output. That is

$$\text{CNR} = 20 \log_{10} (V_c/V_n) \tag{2-24}$$

where V_n was determined from the calibration chart and the noise generator output reading.

The multiplier output voltage was measured with a rms voltmeter at point Ⓐ of Figure 7. This point corresponds to the measurement of x(t) in Figure 6. Thus the rms voltage reading squared gives the multiplier output variance.

The measurement of the output SNR presented a problem that is not encountered when the modulating spectrum is narrow compared to the loop bandwidth. The solution required the use of a relatively complex and powerful measurement device, namely a HP 2116 computer connected to two analog-to-digital converters via a HP 2115 computer. Quite often SNR measurements are made by using filters to "filter out" most of the noise or the signal to determine the

signal-to-noise ratio. The fact that the signal and noise output spectrum overlap considerably precludes the use of such a technique in this system. The inherent non-linearity of FM and the PLL also preclude the use of superposition to measure each effect separately.

Since frequency-domain diversity characteristics could not be exploited, time-domain differences were utilized. The cross correlation ($R_{so}(\tau)$) between the input signal (s(t)) to the FM Transmitter and the output signal (o(t)) was the fundamental characteristic used to determine the SNR. Figure 12 is a block diagram of the measurement system. The pulse generator was adjusted so that both s(t) and o(t) were sampled at a 25 kHz rate. Since the highest frequency content of the signal was about 1400 kHz, the sampling rate was approximately 18 times the highest frequency. The analog-to-digital converters (ADC) were adjusted to quantize the signals into a 10 bit word (1024 levels). Since the ADC's required a 0-10 volt input, the signals were offset by approximately 5 volts and amplified to cover a dynamic range from about 2 to 8 volts. One thousand samples were transferred to the 2116 computer by first setting parameters on the experimental system and then running the computer program.

A block diagram of the computer program used to calculate the SNR is shown in Figure 13. Due to the IF Filter and PLL characteristics the output signal is delayed with respect to the input signal. The approximate delay was determined by observation of the signals on an oscilloscope. Then two numbers (ID1, and ID2) such that

$$ID1 < \# \text{ of samples of delay} < ID2$$

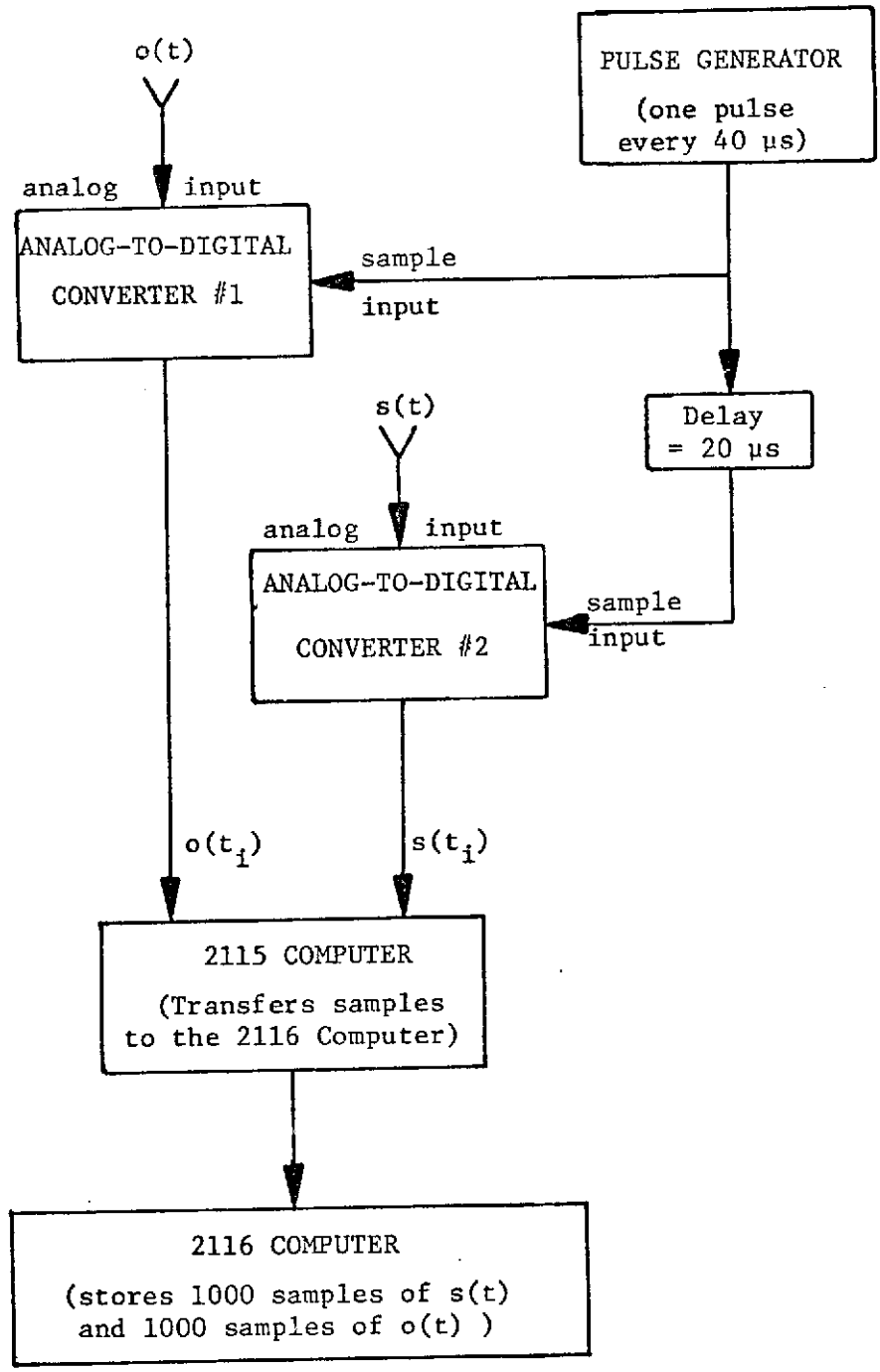

Figure 12. Measurement System Block Diagram.

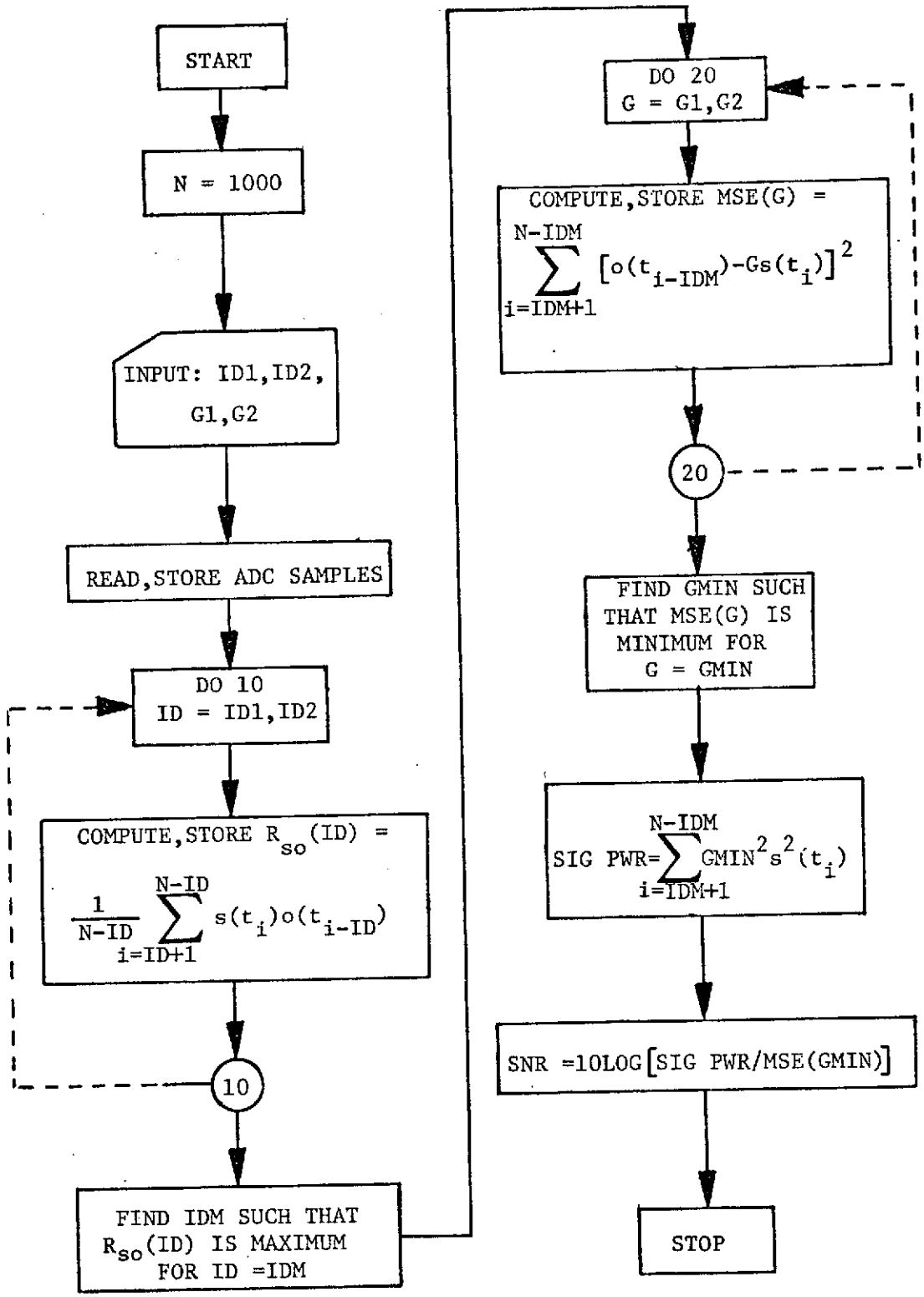

Figure 13. Measurement System Computer Program Flow Chart.

were read into the computer. The program then determined the delay (IDM) for which the cross correlation $R_{so}(\tau)$ was maximum, in the domain ID1 to ID2. Next the mean-square-error (MSE($\overline{G}$)) between s(t) and o(t) was determined for the input signal delayed by IDM samples and the output signal multiplied by a gain $\overline{G}$, for $G1 \leq \overline{G} \leq G2$. The values G1 and G2 were previously input into the computer such that a plot of MSE($\overline{G}$) showed a distinct minimum. The output SNR was then calculated as shown in Figure 13. In summary then, the SNR was calculated by delaying the input signal s(t) by IDM samples such that the cross correlation $R_{so}(\tau)$ was maximum, and multiplying the input signal by a constant G such that the mean-square-error MSE($\overline{G}$) was minimum.

2.9 Experimental System Measurement Errors

The ideal Experimental System would have components which are described exactly by their mathematical representation. However, this is not usually the case. For example, a resistor may not exhibit a linear relationship between voltage and current although it is modeled this way. Thus, there are errors introduced by the Experimental System which are not accounted for by the mathematical model. In well designed systems these errors are kept small so that they will not interfere with the primary purpose of the system.

The Measurement System illustrated in Figure 12 introduces some error in the SNR measurement. This is due to the slight differences between and the quantization errors of the two Analog-to-digital Converters, as well as the finite sampling rate. To determine the

magnitude of these errors, the same analog signal was applied to the inputs of both ADC's and the output SNR calculation observed. For signals in the frequency and amplitude range of those used in this paper the SNR reading was greater than 30dB. Ideally the reading would be infinite since the two signals are identical and the mean-square-error is zero. Thus the "noise" introduced by the measurement system is at least 30dB below the signal being measured.

The main source of error in the Experimental System is the "phase jitter" introduced by the VCO. With no modulation applied to the system the phase error should be zero for the ideal system. However, oscillator instability in the VCO and Transmitter cause "noise" at the output of the multiplier. The magnitude of these and other errors were determined as follows. The Transmitter was modulated by the signals with spectra as illustrated in Figure 9 using a small modulation index so that the PLL was operating in the "linear" region. The Measurement System was then used to calculate the output SNR. This value ranged between 18 and 20dB for the various signals.

The combined "noise" of the Measurement and Experimental Systems is approximately 20dB below the signal being measured. The majority of this noise is caused by "phase jitter" of the VCO and Transmitter. Thus SNR measurements below 20dB should be accurate in the sense that it is the Experimental System characteristics and not system design errors which are dominant in causing the reading.

Chapter 3

THEORY APPLIED TO THE EXPERIMENTAL SYSTEM

3.1 RMS Deviation and Noise Power

Since the input signal to the FM transmitter is essentially a white noise process shaped by a band-pass filter, the spectrum of s(t) assumes the filter spectral shape and is given by (see Equation (2-4))

$$S(s) = R\,B(s) = \frac{Rs^4}{g_8 s^8 + g_7 s^7 + \ldots + g_1 s + g_0} \tag{3-1}$$

where R is a constant which is related to the rms voltage of s(t) via

$$v_{rms}^2 = R^2 \int_{-\infty}^{\infty} \overline{B}(\omega)\,\frac{d\omega}{2\pi} \qquad \text{where } \overline{B}(\omega) = |B(s)|^2 \tag{3-2}$$

Let X be the FM transmitter constant in rad/sec./volt, then

$$(\text{RMS Deviation})^2 = (XR)^2 \int_{-\infty}^{\infty} \overline{B}(\omega)\,\frac{d\omega}{2\pi} \cdot (\text{rad/sec})^2 \quad . \tag{3-3}$$

The phase of the carrier is given by the integral of the frequency of the carrier with the appropriate initial conditions. Assuming zero initial conditions, Equation (3-1) gives

$$\Theta_1(s) = \frac{X}{s} S(s) = RX\,\frac{B(s)}{x} \quad . \tag{3-4}$$

Thus the spectral density of the carrier phase due to the signal s(t) is

$$\overline{\Theta}_1(\omega) = \frac{(RX)^2\,\overline{B}(\omega)}{\omega^2} \quad . \tag{3-5}$$

The noise process n(t) has a low-pass spectrum with cutoff frequency β rad/sec. (see Section 1.2) Since the shape is determined by the IF Filter one finds from Equation (2-10) that

$$N(s) = TC(s) = \frac{T}{p_4 s^4 + p_3 s^3 + p_2 s^2 + p_1 s + f_0} . \tag{3-6}$$

T is a constant which is related to the rms noise voltage into the multiplier via

$$\text{noise power} = v_{rms}^2 = 2 \int_{-\infty}^{\infty} \overline{N}(\omega) \frac{d\omega}{2\pi} \tag{3-7}$$

where

$$\overline{N}(\omega) = |N(s)|^2 . \tag{3-8}$$

3.2 Polynominal Form of the Spectra

The general equations developed in Chapter 1 for the PLL spectral densities are now specialized for the Experimental System of Chapter 2. From Equations (2-16), (2-4), and (3-4)

$$[1 - H(s)][\Theta_1(s)] = \left[\frac{s^2}{s^2 + x_1 s + x_0}\right]\left[\frac{RXs^3}{g_8 s^8 + \ldots + g_1 s + g_0}\right]$$

$$= \frac{RXs^5}{h_{10} s^{10} + h_9 s^9 + \ldots + h_1 s + h_0} , \tag{3-9}$$

where

$$\begin{aligned} h_0 &= x_0 g_0 \\ h_1 &= x_1 g_0 + x_0 g_1 \\ h_i &= g_{i-2} + x_1 g_{i-1} + x_0 g_i \qquad \text{for } 2 \le i \le 8 \\ h_9 &= g_7 + x_1 g_8 \\ h_{10} &= g_8 . \end{aligned} \tag{3-10}$$

Equations (2-16) and (3-6) yield

$$[1 - H(s)][N(s)] = \left[\frac{s^2}{s^2 + x_1 s + x_0}\right]\left[\frac{T}{p_4 s^4 + \ldots + p_1 s + f_0}\right]$$

$$= \frac{Ts^2}{e_6 s^6 + \ldots + e_1 s + e_0} \qquad (3\text{-}11)$$

where

$$e_0 = x_0 f_0 \qquad e_4 = p_2 + x_1 p_3 + x_0 p_4$$

$$e_1 = x_1 f_0 + x_0 p_1 \qquad e_5 = p_3 + x_1 p_4$$

$$e_2 + f_0 + x_1 p_1 + x_0 p_2 \qquad e_6 = p_4 \quad .$$

$$e_3 = p_1 + x_1 p_2 + x_0 p_3 \qquad (3\text{-}12)$$

From Equations (2-16) and (3-6)

$$H(s)\ N(s) = \left[\frac{x_1 s + x_0}{s^2 + x_1 s + x_0}\right]\left[\frac{T}{p_4 s^4 + \ldots + p_1 s + f_0}\right]$$

$$= \frac{Tx_1 s + Tx_0}{e_6 s^6 + \ldots + e_1 s + e_0} \qquad (3\text{-}13)$$

Using Equations (2-16), (2-12), and (3-4)

$$sH(s)\ D(s)\ \Theta_1(s) = \left[\frac{x_1 s^2 + x_0 s}{s^2 + x_1 s + x_0}\right]\left[\frac{b}{b + s}\right]\left[\frac{RXs^3}{g_8 s^8 + \ldots + g_1 s + g_0}\right]$$

$$= \left[\frac{d_3 s^2 + d_0 s}{s^3 + d_2 s^2 + d_1 s + d_0}\right]\left[\frac{RXs^3}{g_8 s^8 + \ldots + g_1 s + g_0}\right] \qquad (3\text{-}14)$$

where

$$d_0 = x_0 b \qquad d_2 = b + x_1$$

$$d_1 = x_1 b + x_0 \qquad d_3 = bx_1 \ . \qquad (3\text{-}15)$$

Further algebraic manipulation of Equation (3-14) gives

$$s\ H(s)\ D(s)\ \Theta_1(s) = \frac{RX\left[d_3 s^5 + d_0 s^4\right]}{\bar{h}_{11} s^{11} + \bar{h}_{10} s^{10} + \ldots + \bar{h}_1 s + \bar{h}_0} \tag{3-16}$$

where

$$\begin{aligned}
\bar{h}_0 &= g_0 d_0 \\
\bar{h}_1 &= g_0 d_1 + g_1 d_0 \\
\bar{h}_2 &= g_0 d_2 + g_1 d_1 + g_2 d_0 \\
\bar{h}_i &= g_{i-3} + g_{i-2} d_2 + g_{i-1} d_1 + g_i d_0 \qquad 3 \leq i \leq 8 \\
\bar{h}_9 &= g_6 + g_7 d_2 + g_8 d_1 \\
\bar{h}_{10} &= g_7 + g_8 d_2 \\
\bar{h}_{11} &= g_8 \ .
\end{aligned} \tag{3-17}$$

Equations (3-6), and (3-14) give

$$s\ H(s)\ D(s)\ N(s) = \left[\frac{d_3 s^2 + d_0 s}{s^3 + d_2 s^2 + d_1 s + d_0}\right]\left[\frac{T}{p_4 s^4 + \ldots + p_1 s + f_0}\right]$$

$$= \frac{T\ (d_3 s^2 + d_0 s)}{\bar{e}_7 s^7 + \ldots + \bar{e}_1 s + \bar{e}_0} \tag{3-18}$$

where

$$\begin{aligned}
\bar{e}_0 &= f_0 d_0 & \bar{e}_5 &= p_2 + p_3 d_2 + p_4 d_1 \\
\bar{e}_1 &= f_0 d_1 + p_1 d_0 & \bar{e}_6 &= p_3 + p_4 d_2 \\
\bar{e}_2 &= f_0 d_2 + p_1 d_1 + p_2 d_0 & \bar{e}_7 &= p_4 \ . \\
\bar{e}_3 &= f_0 + p_1 d_2 + p_2 d_1 + p_3 d_0 \\
\bar{e}_4 &= p_1 + p_2 d_2 + p_3 d_1 + p_4 d_0
\end{aligned} \tag{3-19}$$

3.3 Simplification of Results

The following definitions are now made to simplify notation. Recalling that $s = j\omega$,

$$\text{INT1} \triangleq \int_{-\infty}^{\infty} \left| \frac{s^5}{h_{10}s^{10} + \ldots + h_1 s + h_0} \right|^2 \frac{d\omega}{2\pi}$$

$$\text{INT2} \triangleq \int_{-\infty}^{\infty} \left| \frac{d_3 s^5 + d_0 s^4}{\bar{h}_{11}s^{11} + \ldots + \bar{h}_1 s + \bar{h}_0} \right|^2 \frac{d\omega}{2\pi}$$

$$\text{INT3} \triangleq \int_{-\infty}^{\infty} \left| \frac{s^2}{e_6 s^6 + \ldots + e_1 s + e_0} \right|^2 \frac{d\omega}{2\pi}$$

$$\text{INT4} \triangleq \int_{-\infty}^{\infty} \left| \frac{x_1 s + x_0}{e_6 s^6 + \ldots + e_1 s + e_0} \right|^2 \frac{d\omega}{2\pi}$$

$$\text{INT5} \triangleq \int_{-\infty}^{\infty} \left| \frac{d_3 s^2 + d_0 s}{\bar{e}_7 s^7 + \ldots + \bar{e}_1 s + \bar{e}_0} \right|^2 \frac{d\omega}{2\pi}$$

$$\text{INT6} \triangleq \int_{-\infty}^{\infty} \left| \frac{s^4}{g_8 s^8 + \ldots + g_1 s + g_0} \right|^2 \frac{d\omega}{2\pi}$$

$$\text{INT7} \triangleq \int_{-\infty}^{\infty} \left| \frac{1}{p_4 s^4 + \ldots + p_1 s + f_0} \right|^2 \frac{d\omega}{2\pi} \quad . \qquad (3\text{-}20)$$

By combining Equations (1-17), (3-9), (3-13) and (3-20) one

obtains

$$\sigma_\phi^2 = \underbrace{(RX)^2(INT1)}_{\sigma_{\phi,s}^2} + \underbrace{\frac{T^2}{G^2}(INT4)}_{\sigma_{\phi,n}^2} \tag{3-21}$$

In the above $\sigma_{\phi,s}^2$ is the phase error variance due to the signal while $\sigma_{\phi,n}^2$ is the variance due to the noise.

In a similar manner Equations (1-18), (3-9), (3-11) and (3-20) give

$$\sigma_x^2 = \underbrace{(GK_1)^2\ (RX)^2\ (INT1)}_{\sigma_{x,s}^2} + \underbrace{(K_1T)^2\ (INT3)}_{\sigma_{x,n}^2} \tag{3-22}$$

while Equations (1-19), (3-14), (3-16), and (3-20) give

$$\sigma_o^2 = \underbrace{(RX)^2\ (INT2)}_{\sigma_{o,s}^2} + \underbrace{\frac{T^2}{G^2}(INT5)}_{\sigma_{o,n}^2} \tag{3-23}$$

where $\sigma_{x,s}^2$, $\sigma_{x,n}^2$, $\sigma_{o,s}^2$, and $\sigma_{o,n}^2$ are defined in a manner similar to $\sigma_{\phi,s}^2$ and $\sigma_{\phi,n}^2$.

From Equations (3-20) and (3-1), Equation (3-3) becomes

$$(\text{RMS Deviation})^2 = X^2\ R^2\ (INT6), \tag{3-24}$$

while the from Equations (3-7), (3-6), and (3-20) the noise power at the input to the multiplier is given by

$$\text{noise power} = 2T^2\ (INT7). \tag{3-25}$$

3.4 Computer Implementation of Equations

A Computer Program was written to evaluate the quantities in Equations (3-22) through (3-25). The block diagram of the Program is shown in Figure 14. For the input parameters ω_1, ω_2 (signal break frequencies), β(half the IF bandwidth), and DEV (rms voltage into FM Transmitter), the program calculates the indicated values for CNR's from 0 to 27dB in 3dB steps. The output values for each CNR is punched on paper tape for later use.

The value for G was determined by first setting G = A, calculating σ_ϕ^2, then setting $G = A \exp(-\sigma_\phi^2/2)$ as indicated by Equation (1-12). Then σ_ϕ^2 was re-calculated using the new value of G. This process was iterated three times to obtain a third-order estimate of G.

The integrals were evaluated by numerical integration (Simpson's Rule) after much difficulty was encountered with analytical techniques. The equations for the analytical method were quite complex and often caused overflow and underflow during computer calculations. The integration increment used for the numerical integration was 60 rad/sec (about 10 Hz). This value was decided on since reducing the increment 100 times changed the integrals by less than 0.001%. The lower limit of the integration was zero while the upper limit a frequency which corresponds to the response being 30dB smaller than the maximum. The 30dB figure was chosen since setting the value to 90dB caused less than 0.01% change in the value.

The computer used was a HP 2116 programmed using the Fortran IV language. Typically about 15 minutes was required to obtain a complete

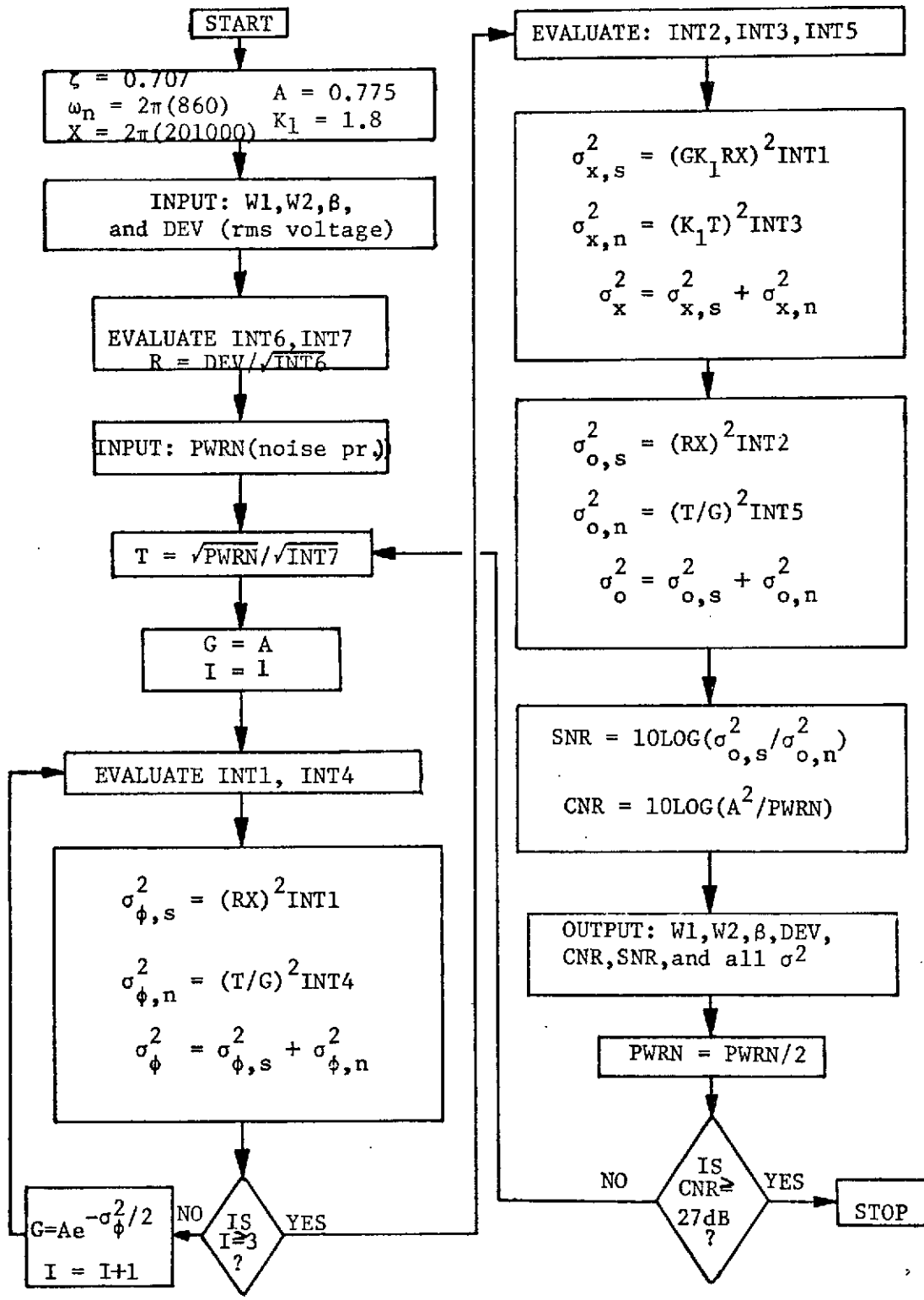

Figure 14. Flow Chart of Computer Program Used to Calculate Theoretical Values Based on the Quasi-Linear Model.

set of output data for a given set of input parameters. Over 95% of this time was used to evaluate the integrals by the numerical technique.

Chapter 4

PLL CHARACTERISTICS IN THE ABSENCE OF NOISE

4.1 Signal Distortion Due to the IF Filter and PLL Nonlinearity.

The spectrum of the transmitter output is a function of the signal and deviation of the carrier. For sinusoidal modulation, 98% of the total power in the FM signal is contained in a bandwidth (B) given by Carson's rule [5]:

$$B = 2(\Delta f + f_m) \tag{4-1}$$

where Δf is the zero-to-peak frequency deviation and f_m is the modulating frequency. For a modulating signal with a bandpass spectrum the corresponding FM signal bandwidth is difficult to determine. Van Trees (pp. 100-104 of [7]) indicates that a measure of the bandwidth for a modulating signal with a low-pass Gaussian spectrum is $2\sigma_a d_f$, where σ_a is the signal rms voltage and d_f the Transmitter constant.

From the above it is reasonable to assume that the larger the rms deviation the larger the bandwidth occupied by the FM signal. Thus increasing the rms deviation and/or decreasing the IF Filter Bandwidth causes more of the FM signal to be filtered out and results in more distortion in the demodulated output. This effect is illustrated in Figures 15 through 18. Note that a decrease in IF Bandwidth and/or an increase rms deviation results in a lower SNR (larger signal distortion).

In addition to the signal distortion caused by the IF Filter, distortion is also caused by the fact that the PLL is non-linear.

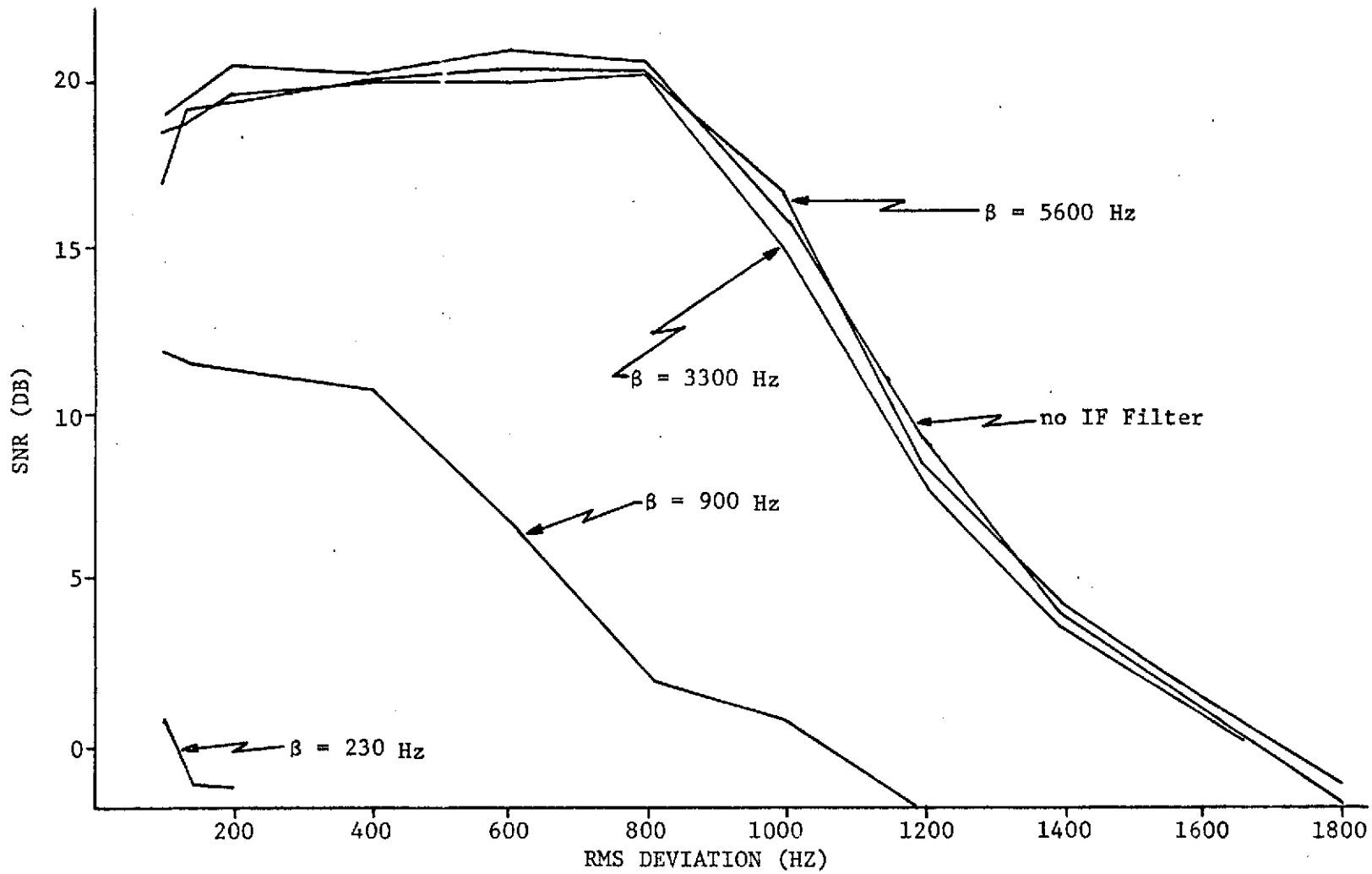

Figure 15. SNR as a Function of Deviation for No Noise with f_1=56Hz,f_2=440Hz.

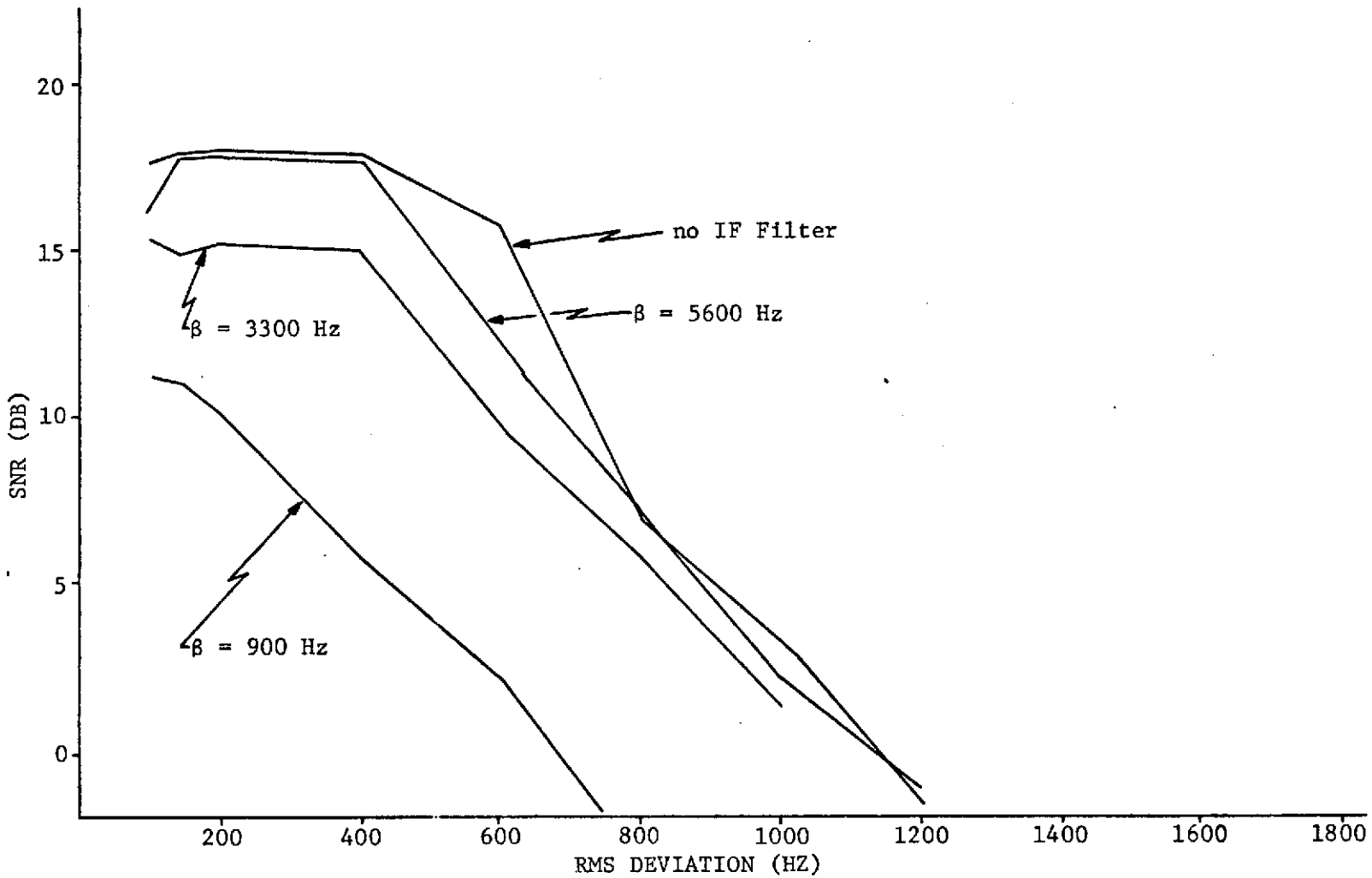

Figure 16. SNR as a Function of Deviation for No Noise with f_1 = 56 Hz, f_2 = 900 Hz.

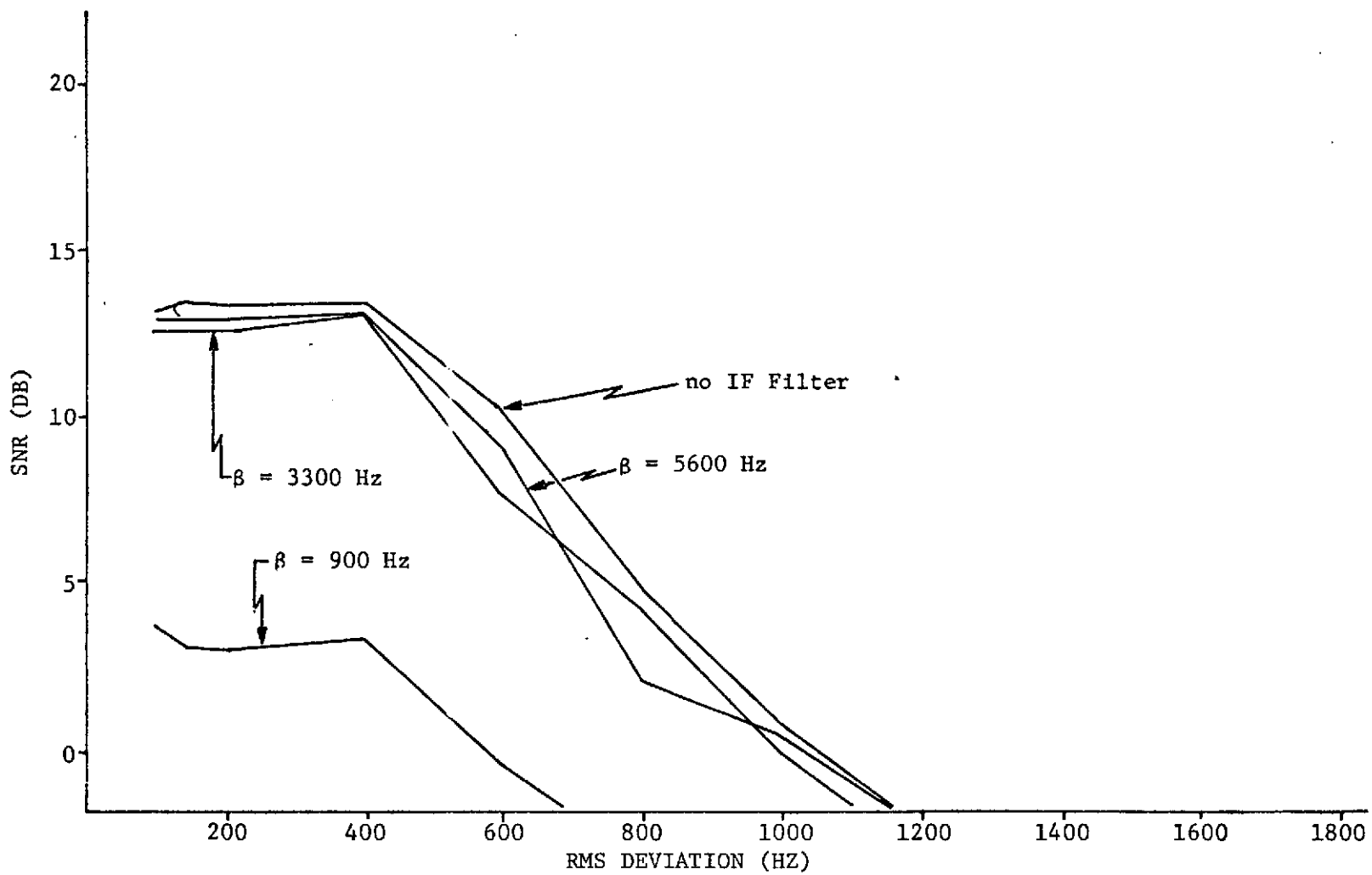

Figure 17. SNR as a Function of Deviation for No Noise with f_1 = 56 Hz, f_2 = 1250 Hz.

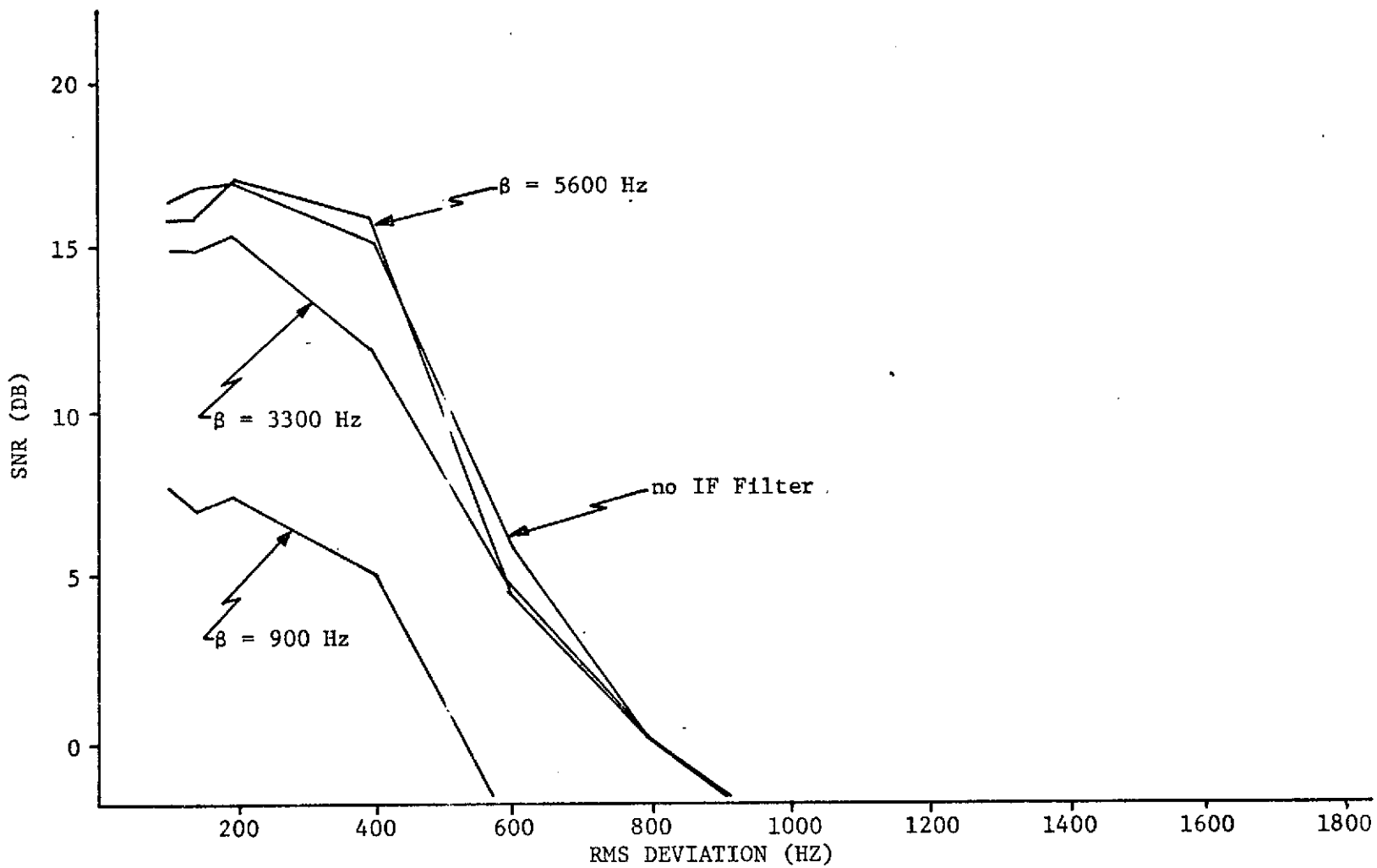

Figure 18. SNR as a Function of Deviation for No Noise with f_1 = 560 Hz, f_2 = 900 Hz.

This distortion is more pronounced for larger σ_ϕ^2 since the non-linearity sin σ_ϕ is nearly linear for small σ_ϕ but non-linear for large (>30°) σ_ϕ. Now an increase in the rms deviation "stresses" the PLL more and results in an increase in σ_ϕ. Thus as the rms deviation is increased the PLL output SNR decreases (distortion increases). If the loop "stress" is sufficient a phenomenon known as "cycle-slipping" will occur [8,12] resulting in impulse noise at the PLL output. A further increase in the rms deviation will normally result in a complete loss of phase lock [9]. The "cycle-slipping" and "loss of lock" phenomenon was observed as the rms deviation was increased for all four signals and four IF Filters used in the Experimental System. A summary of distortion due to PLL Stress and Finite IF Filter bandwidth is presented in Table 1. Data for this Table was obtained from Figures 15 through 18.

Figures 15 through 18 illustrate that for no IF Filter (infinitely wide IF bandwidth) an increase in the signal upper cut-off frequency results in a lower output SNR. In obtaining the data the deviation was increased until the loop would not maintain lock. The rms deviation at which loss of lock occurs (obtained from Figures 15-18) as a function of f_2 for f_1 = 56 Hz is plotted in Figure 19. A non-linear analysis of the second-order PLL for sinusoidal modulation [10,11] has shown that the PLL unlock boundary for $f_m < 0.85 f_n$ is given by:

$$\Delta f\ (f_m) = 1.15\ f_n^{\ 2} \qquad (4\text{-}2)$$

where Δf is the zero-to-peak deviation, f_m the modulating frequency, and f_n the PLL natural frequency. Since it is the highest modulating

Table 1

Output Signal Distortion Due to PLL Stress
and Finite IF Filter Bandwidth for No Noise

SIGNAL ($f_1 - f_2$) \ IF FILTER BANDWIDTH (β)	5600 HZ	3300 HZ	900 HZ
56 HZ - 440 HZ	1. 0dB 2. 0dB 3. 0dB	1. 0dB 2. 0dB 3. 0dB	1. -8dB,IF 2. -10dB,IF 3. -15dB,IF
56 HZ - 900 HZ	1. -3dB,PLL 2. -3dB,PLL 3. -6dB,IF	1. -5dB,PLL 2. -5dB,PLL 3. -10dB,IF	1. -10dB,IF 2. -15dB,IF 3. -18dB,IF
56 HZ - 1250 HZ	1. -6dB,PLL 2. -6dB,PLL 3. -10dB,IF	1. -6dB,PLL 2. -6dB,PLL 3. -11dB,IF	1. -16dB,IF 2. -18dB,IF 3. -20dB,IF
560 HZ - 900 HZ	1. -4dB,PLL 2. -4dB,PLL 3. -12dB,IF	1. -5dB,PLL 2. -7dB,IF 3. -16dB,IF	1. -14dB,IF 2. -16dB,IF 3. -22dB,IF

Legend:
1. rms deviation equal to 201 Hz
2. rms deviation equal to 402 Hz
3. rms deviation equal to 603 Hz

IF IF Filter dominant cause of distortion
PLL PLL stress dominant cause of distortion

Note: the number indicated is the output SNR in dB relative to the SNR for the case in which there is no distortion.

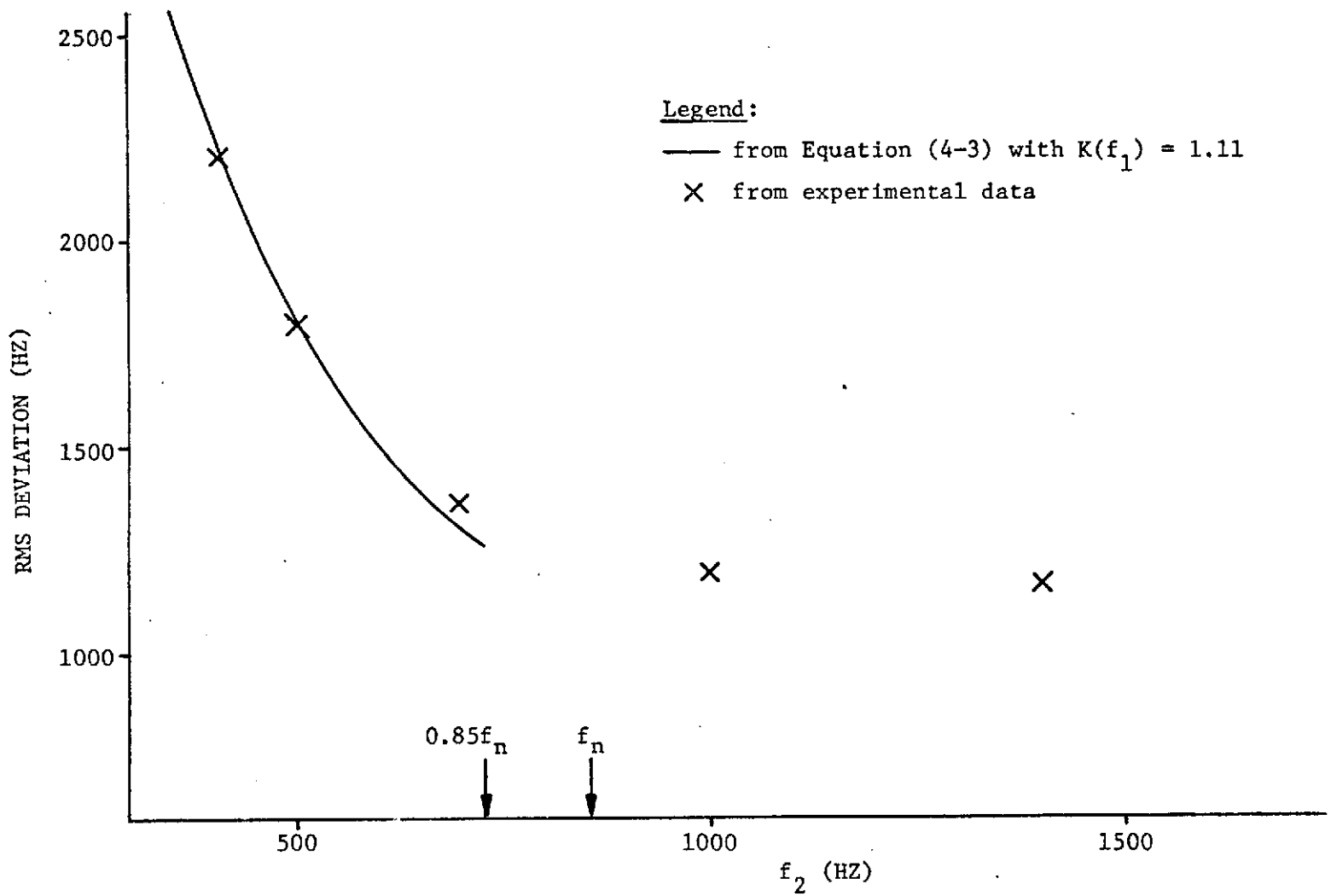

Figure 19. PLL Unlock Boundary as a Function of f_2 for f_1 = 56 Hz.

frequency (f_m) which determines the boundary it is conjectured that an approximation to the PLL unlock boundary for the Experimental System is given by:

$$(\Delta f_{rms})(f_2) = K(f_1)\ f_n^{\ 2} \qquad (4\text{-}3)$$

where Δf_{rms} is the rms deviation, $f_n^{\ 2}$ the PLL natural frequency (860 Hz), and $K(f_1)$ a function of f_1. Equation (4-3) is valid only for $f_2 \leq .85\ f_n$, and is plotted with $K(f_1) = 1.11$ in Figure 19. As can be seen there is good agreement between the measured values and those given by Equation (4-3). It is beyond the scope of this paper to attempt to derive an analytical expression for the unlock boundary valid for $f_2 > 0.85\ f_n$. However, as can be seen in Figure 19, the unlock boundary seems to approach a constant value of $f_2 \to \infty$.

In summary then, it is desirable to choose an IF Filter bandwidth and rms deviation so that the output signal undergoes negligible distortion. The deviation should be small enough so that the PLL is not "stressed" excessively. The IF Filter bandwidth should be wide enough to attenuate only a negligible percentage of the FM spectrum.

4.2 Comparison of Theoretical and Experimental Results

Figure 20 is a plot of σ_x^2 as a function of the rms deviation. S3 and S4 have essentially the same bandwidth, yet S4 which is centered around a higher frequency causes a larger multiplier output variance. Thus higher frequency components of the signal cause larger σ_x^2 and are consequently distorted more than are lower frequency components. There is excellent agreement between the Experimental

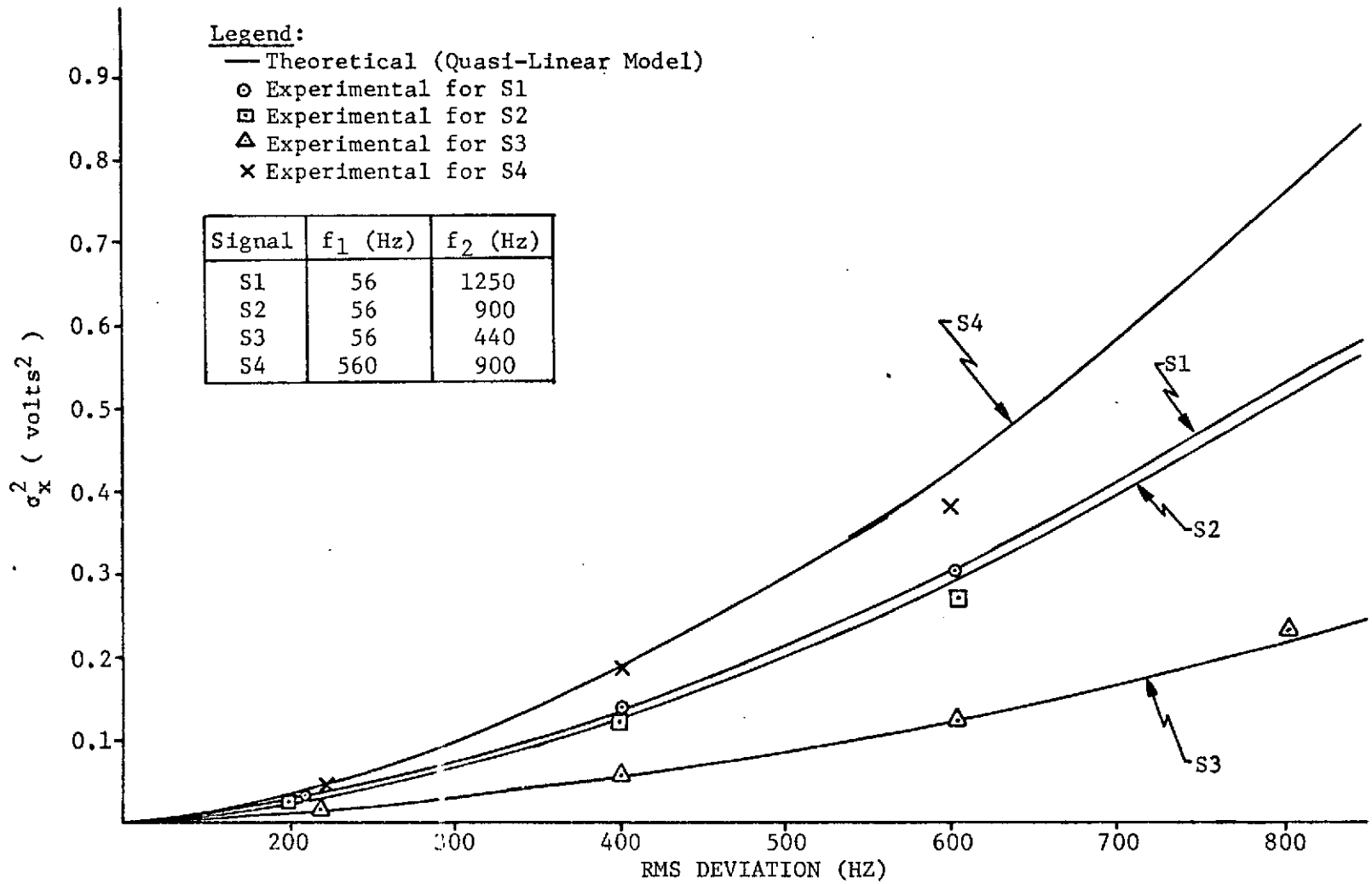

Figure 20. Multiplier Output Variance as a Function of RMS Deviation for No Noise and β= 5600 Hz.

and Theoretical values (less than 2% error) for $\sigma_x^2 < .25$. For $\sigma_x^2 > .25$ the agreement is not as good, probably due to the fact that the PLL becomes non-linear for larger σ_x^2.

Chapter 5

PLL CHARACTERISTICS IN THE ABSENCE OF MODULATION

5.1 Introduction

The purpose of this section is to show that the PLL characteristics predicted by the Quasi-Linear Model agree well (within 10%) with actual characteristics measured from the Experimental System. Since Viterbi's model is often used (and misused) in determining PLL characteristics a comparison is then made between the Quasi-Linear Model and Viterbi's Model. It is shown that Viterbi's Model is a special case of the Quasi-Linear Model and the regions in the PLL parameter space in which each is valid is discussed.

5.2 Comparison of Theoretical and Experimental Results

Since there was no junction in the Experimental System from which to measure $\phi(t)$, the multiplier output variance (ϕ_x^2) was measured and used to compare to the results predicted by the Quasi-Linear Model. Both the theoretical and experimental results are plotted in Figures 21 through 23. In each Figure the noise-spectral-density (NSD) is held constant while the IF Filter Bandwidth is varied. The corresponding PLL signal-to-noise ratio (SNR_{loop}) for a wide IF Bandwidth is also indicated as determined from the definition [3,4]

$$SNR_{loop} = 10 \log_{10} [A^2/NSD \int_{-\infty}^{\infty} |H(s)|^2 \frac{d\omega}{2\pi}]. \qquad (5\text{-}1)$$

This quantity is commonly used as a measure of the noise in the

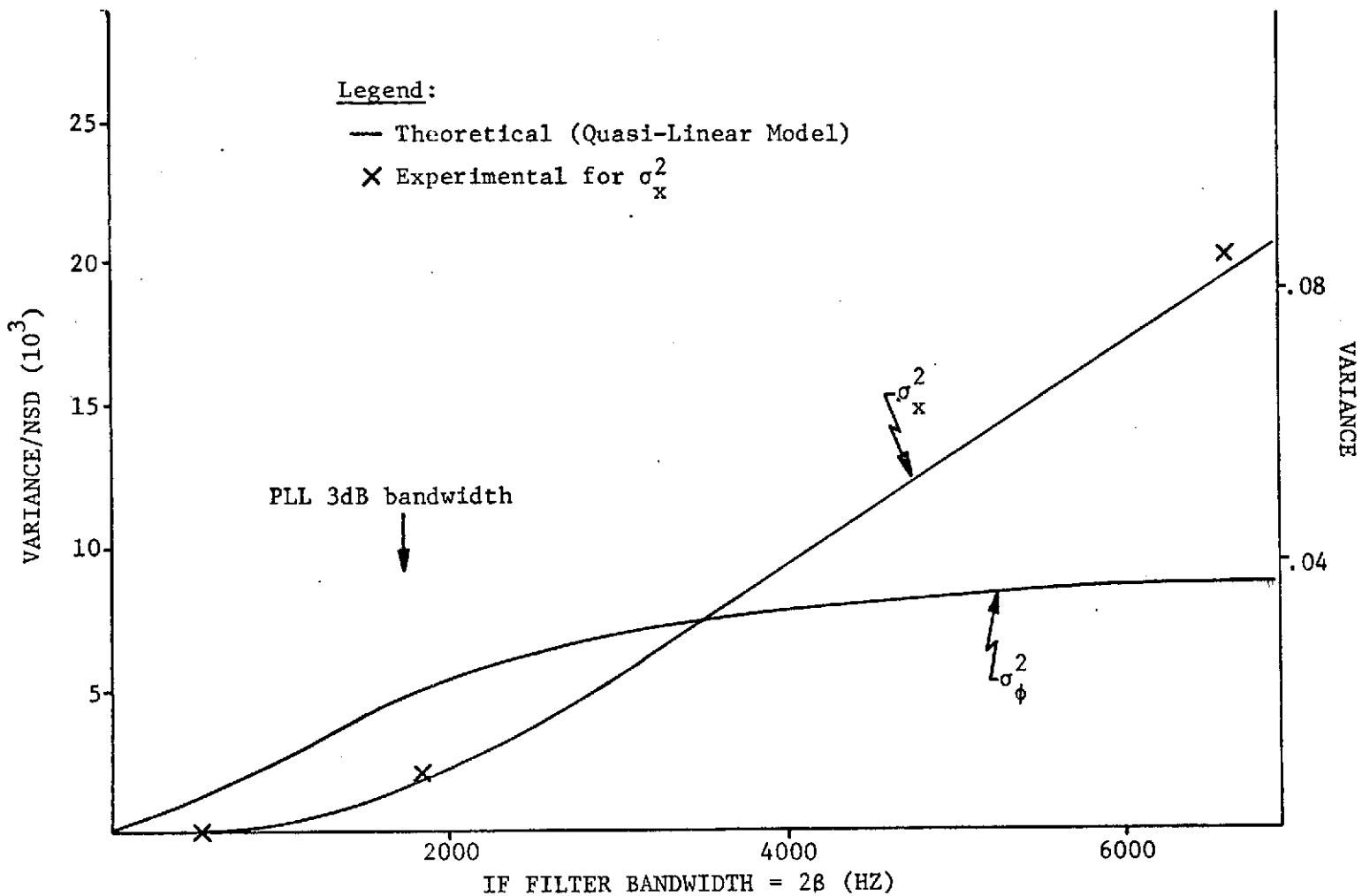

Figure 21. Multiplier Output and Phase Variance as a Function of IF Filter Bandwidth for No Modulation and SNR_{loop} = 14.2 dB.

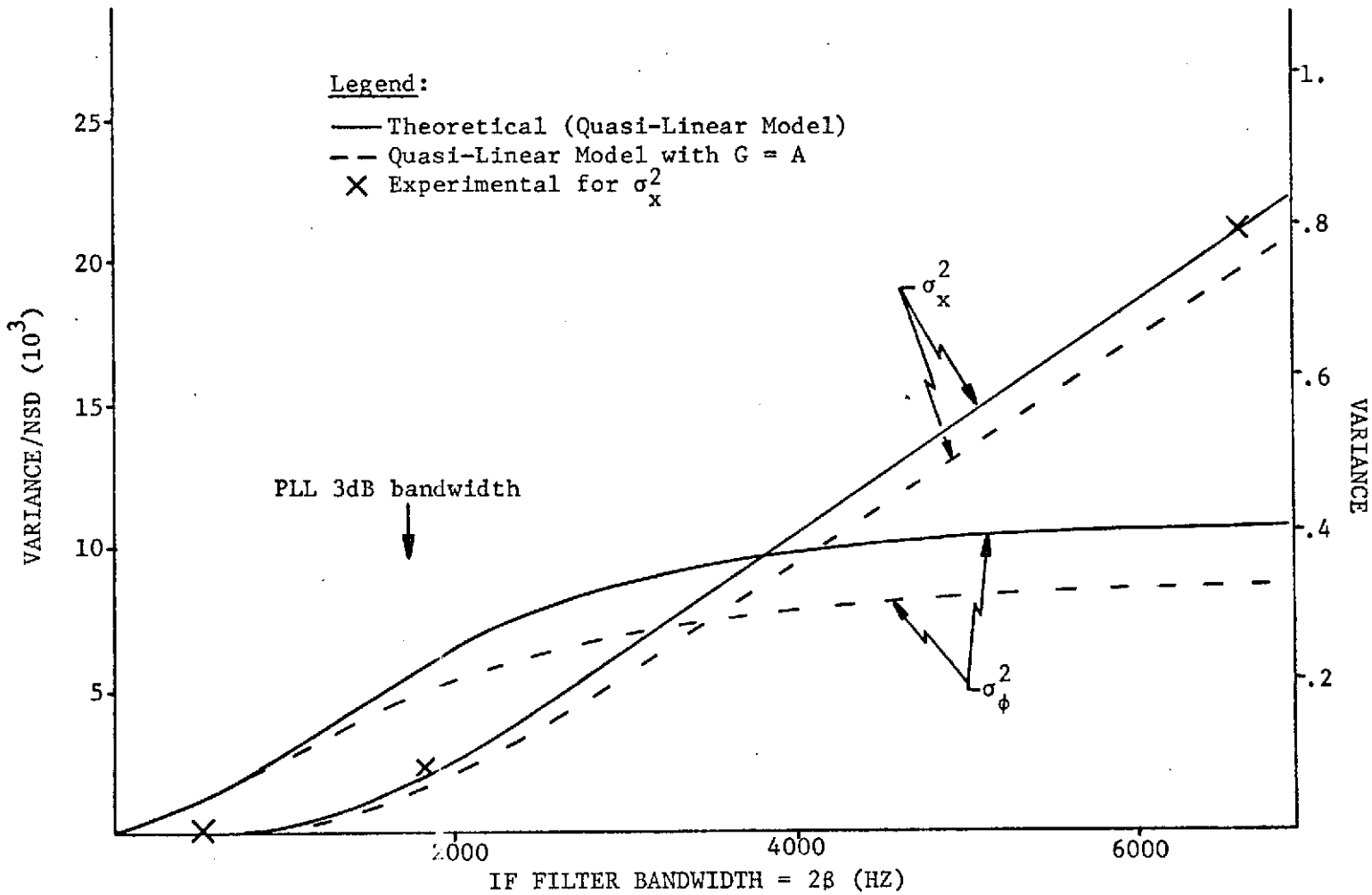

Figure 22. Multiplier Output and Phase Variance as a Function of IF Filter Bandwidth for No Modulation and SNR_{loop} = 4.68 dB.

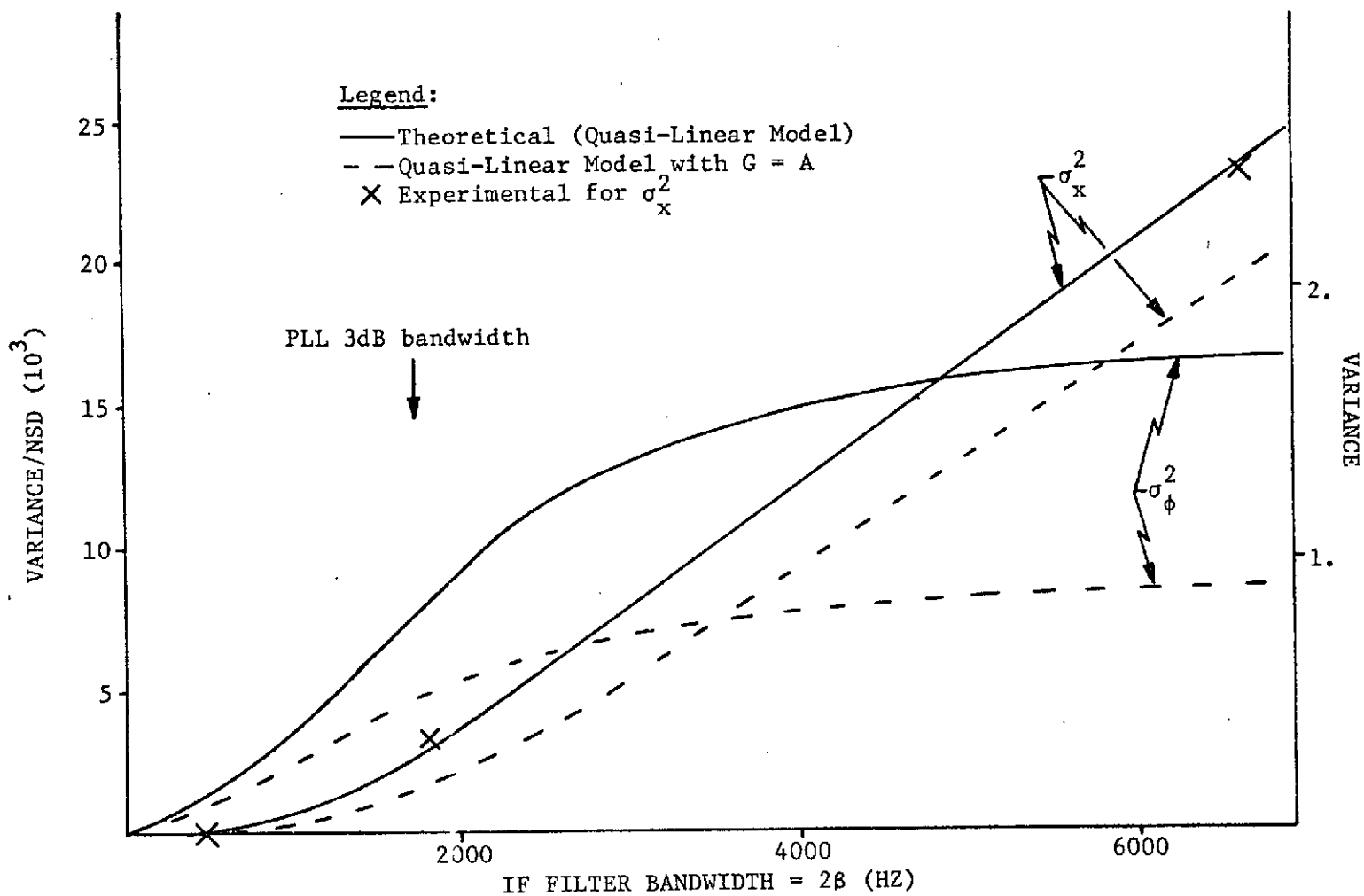

Figure 23. Multiplier Output and Phase Variance as a Function of IF Filter Bandwidth for No Modulation and SNR_{loop} = 0.2 dB.

loop for the case in which the IF Filter Bandwidth is large compared to the PLL Bandwidth. It is emphasized that this quantity is included just as a matter of convenience and has no meaning when the IF Bandwidth is of the same order of magnitude as the PLL Bandwidth. The important parameter is the NSD which is related to the SNR_{loop} by Equation (5-1).

In Figure 21 SNR_{loop} = 14.2dB and corresponds to small values for the NSD and σ_ϕ^2. Thus the PLL is operating in the linear region and replacing G with A in the Quasi-Linear Model gives almost identical results. Notice that the error between the experimental and theoretical data is less than about 5% even for small IF Bandwidth. For small IF Filter Bandwidth the phase variance (σ_ϕ^2) is larger than multiplier output variance (σ_x^2). As the IF Filter Bandwidth is increased, σ_ϕ^2 approaches a constant value while σ_x^2 increases without bound. The latter is true since the noise power (variance) increases without bound as the IF Filter Bandwidth is increased for a constant NSD. Since the PLL does not "track" noise outside of its bandwidth, an increase in IF Bandwidth beyond the PLL Bandwidth only adds frequency components outside this Bandwidth. Thus the former is true since phase error is caused only by frequencies that the PLL "tracks."

The result of increasing the NSD is shown in Figures 22 and 23. As the NSD is increased the values predicted by the Quasi-Linear Model and the Quasi-Linear Model with G = A differ considerably. This is due to the increase in σ_ϕ^2 causing the PLL to operate in a

non-linear manner. The Experimental results for σ_x^2 agree well with that predicted by the Quasi-Linear Model while differing considerably from that predicted by the linear model. This result supports the validity of replacing A by $Ae^{-\sigma_\phi^2/2}$ as developed in Chapter 1. Figures 21 through 23 illustrate the complex relationship between σ_x^2 and σ_ϕ^2. In general σ_x^2 is quite different from σ_ϕ^2 and in order to determine σ_ϕ^2 knowing σ_x^2, these plots (or the equations used for these plots) must be used.

Figure 24 is a plot of σ_x^2 as a function of CNR for three of the IF Filters used in the Experimental System. As can be seen, the error between Experimental data and data predicted by the Quasi-Linear Model is less than about 20% for all cases. In general, error is larger for larger σ_x^2 and/or smaller IF Filter Bandwidths. This is consistent with the assumptions made in developing the Quasi-Linear Model (Section 1).

5.3 Comparison of the Quasi-Linear Model and Viterbi's Model

By replacing the equivalent non-linear gain G in Figure 5 by A, and allowing the IF bandwidth to become large compared to the loop bandwidth, the Quasi-Linear PLL Phase Model becomes similar to the model developed by Viterbi [3]. The main difference is that the Quasi-Linear Model gives a finite variance for the multiplier output while Viterbi's model yields an infinite variance (which is of course a physical impossibility). The reason for this discrepancy is that Viterbi's model does not account for the fact that in an actual system the IF Filter causes the input noise spectrum to have a band-pass shape rather than a flat ("white") spectrum. However,

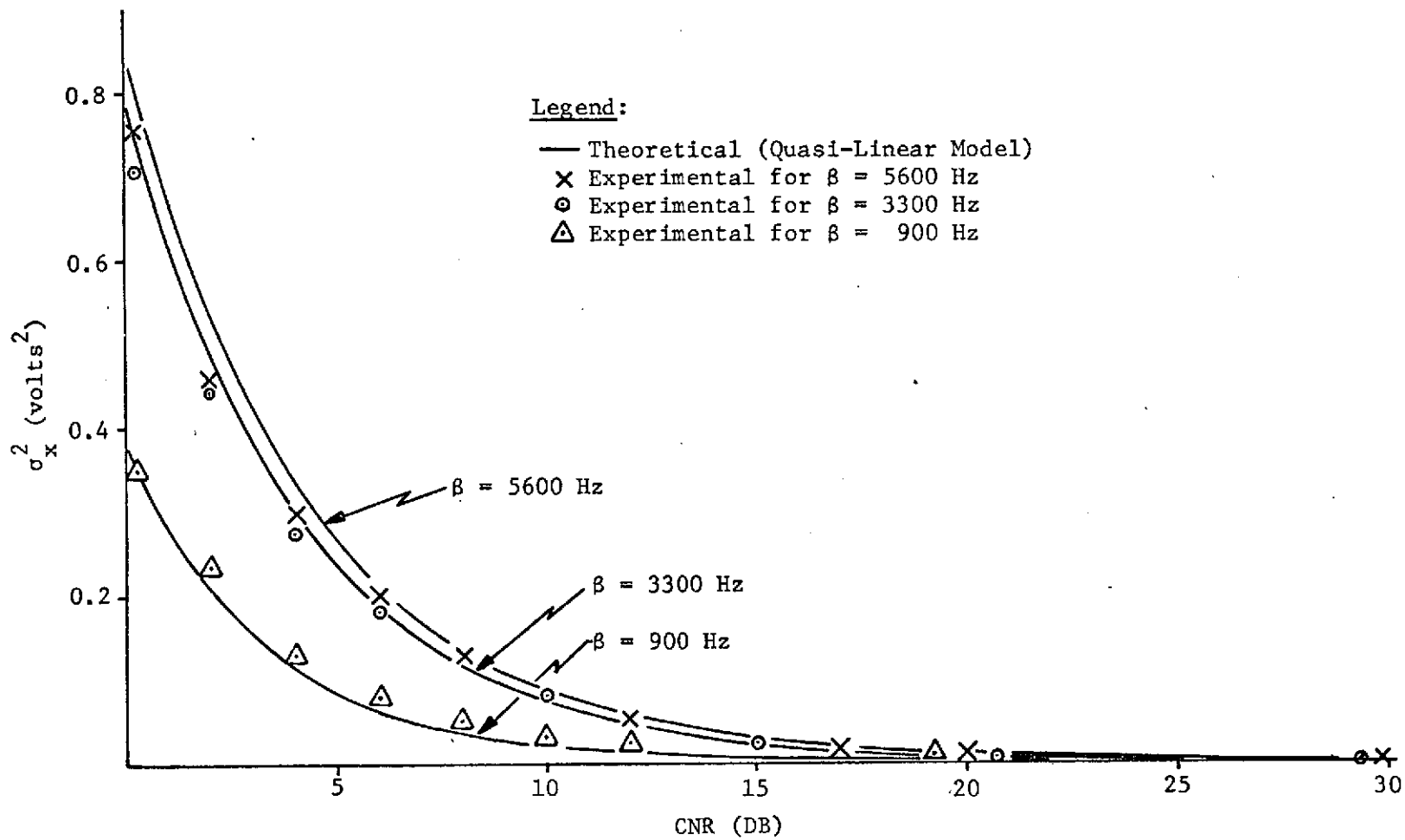

Figure 24. Multiplier Output Variance as a Function of CNR for No Modulation.

the two models do agree on the value for the phase error variance, subject to the above mentioned conditions being satisfied.

Figure 25 illustrates the phase error variance predicted by the two models as a function of IF Filter bandwidth for G = A in the Quasi-Linear Model. As can be seen, the two models agree to within about 2% for $BW_{IF} > 10\ B_{PLL}$. However, the difference becomes progressively worse as BW_{IF} approaches zero. For $B_{IF} = 0$ the phase error variance should be zero since all the noise is filter out by the IF Filter. The Quasi-Linear Model prediction coincides with this point while Viterbi's Model does not. As was shown in Section 2.2, the Quasi-Linear Model predictions agree well with actual experimental data. Thus for small σ_ϕ^2 (so that $G \simeq A$ in the Quasi-Linear Model) and $BW_{IF} > 10\ B_{PLL}$ Viterbi's model is essentially equivalent to the Quasi-Linear Model. The region in the PLL parameter space in which each model is valid is illustrated in Figure 26. The boundaries illustrated are approximately where the error between σ_x^2 predicted by the models and actual experimental data is 10%. As can be seen, Viterbi's Model is valid in a subspace of the space in which the Quasi-Linear Model is valid. Although Figure 26 was determined for no modulation, subsequent data indicates that it is valid whether σ_ϕ^2 is due to modulation or noise or a combination of the two.

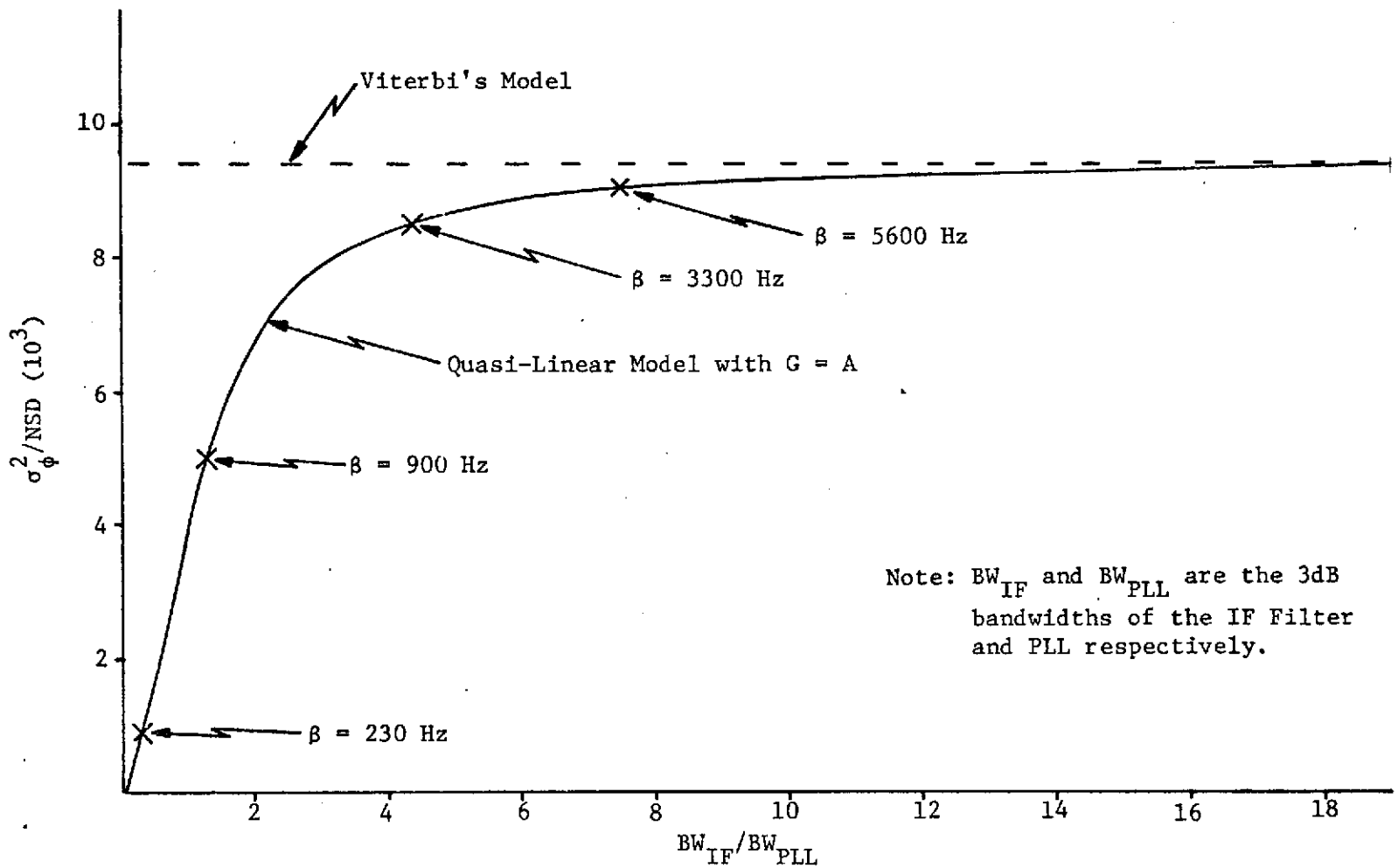

Figure 25. Phase Error Variance Due to Additive Noise of Uniform Spectral Density (NSD).

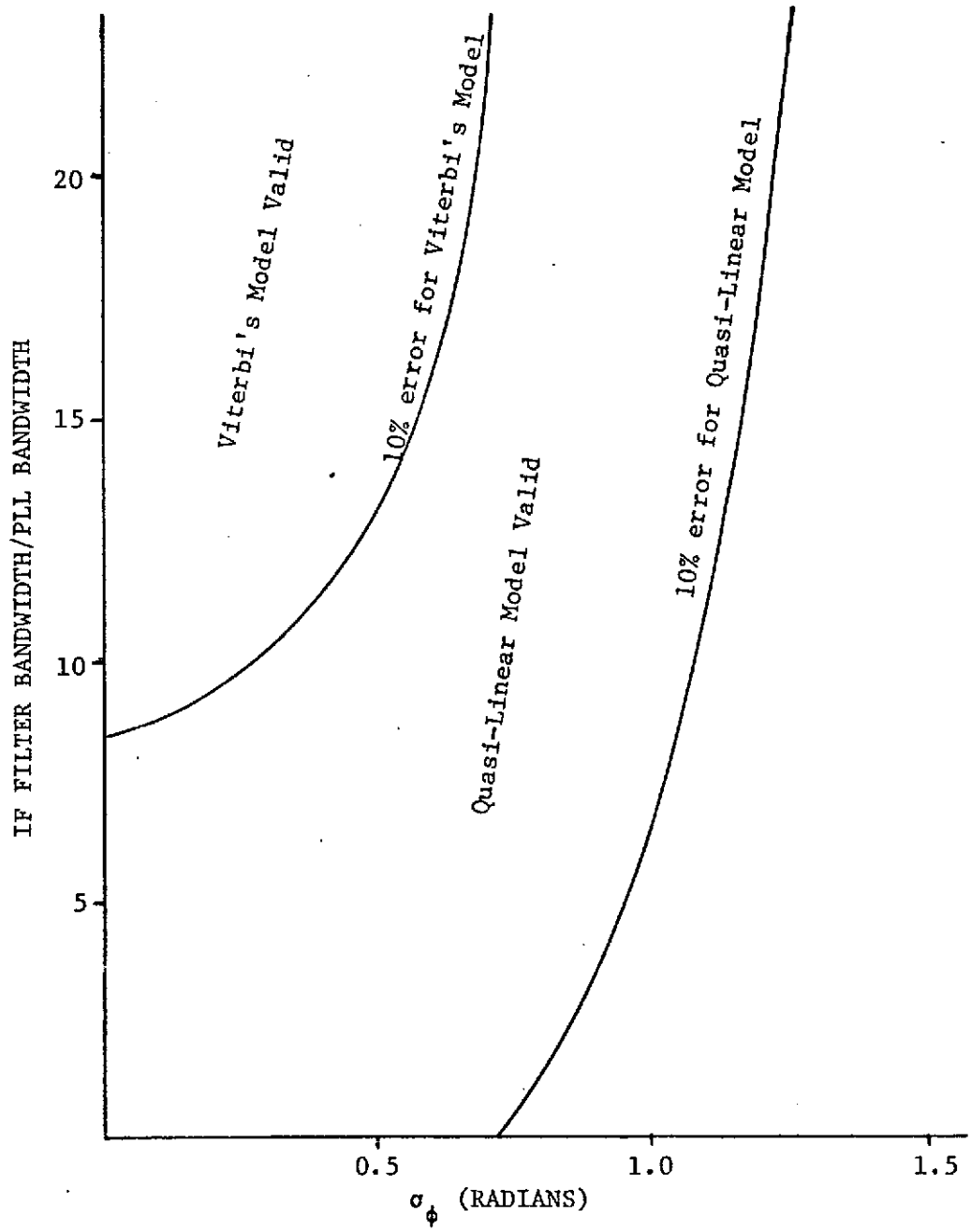

Figure 26. Parameter Space Region for the Validity of the Quasi-Linear Model and Viterbi's Model.

Chapter 6

PLL CHARACTERISTICS IN THE PRESENCE OF MODULATION AND NOISE

6.1 Comparison of Theoretical and Experimental Results

Both Experimental and Theoretical Data was obtained for combinations of three different IF Filter Bandwidths, four different signals, and three different deviations. The data obtained is plotted in Figures 27 through 38. In each Figure the IF Filter Bandwidth and Signal spectrum is held constant while the deviation is changed. The Figure numbers are listed in Table 2 which may be used as an index. A summary of the maximum errors is also presented in Table 2. The first number is the maximum error in dB between the Theoretical calculation of output SNR (as determined from the Quasi-Linear Model) and the output SNR measured from the Experimental System. The second number is the maximum % error between Theoretical and Experimental values for σ_x^2.

As indicated in Section 4.1 the finite IF Filter Bandwidth causes output signal distortion for certain combinations of system parameters. When such distortion exists it is indicated by an asterisk (*) in Table 2. Since the effect of IF distortion on the signal was not incorporated in the Quasi-Linear Model it is reasonable to compare the Model results to Experimental results when IF distortion does not exist. As can be seen from Table 2, the maximum error for all cases in which IF distortion does not exist is 4dB for the output

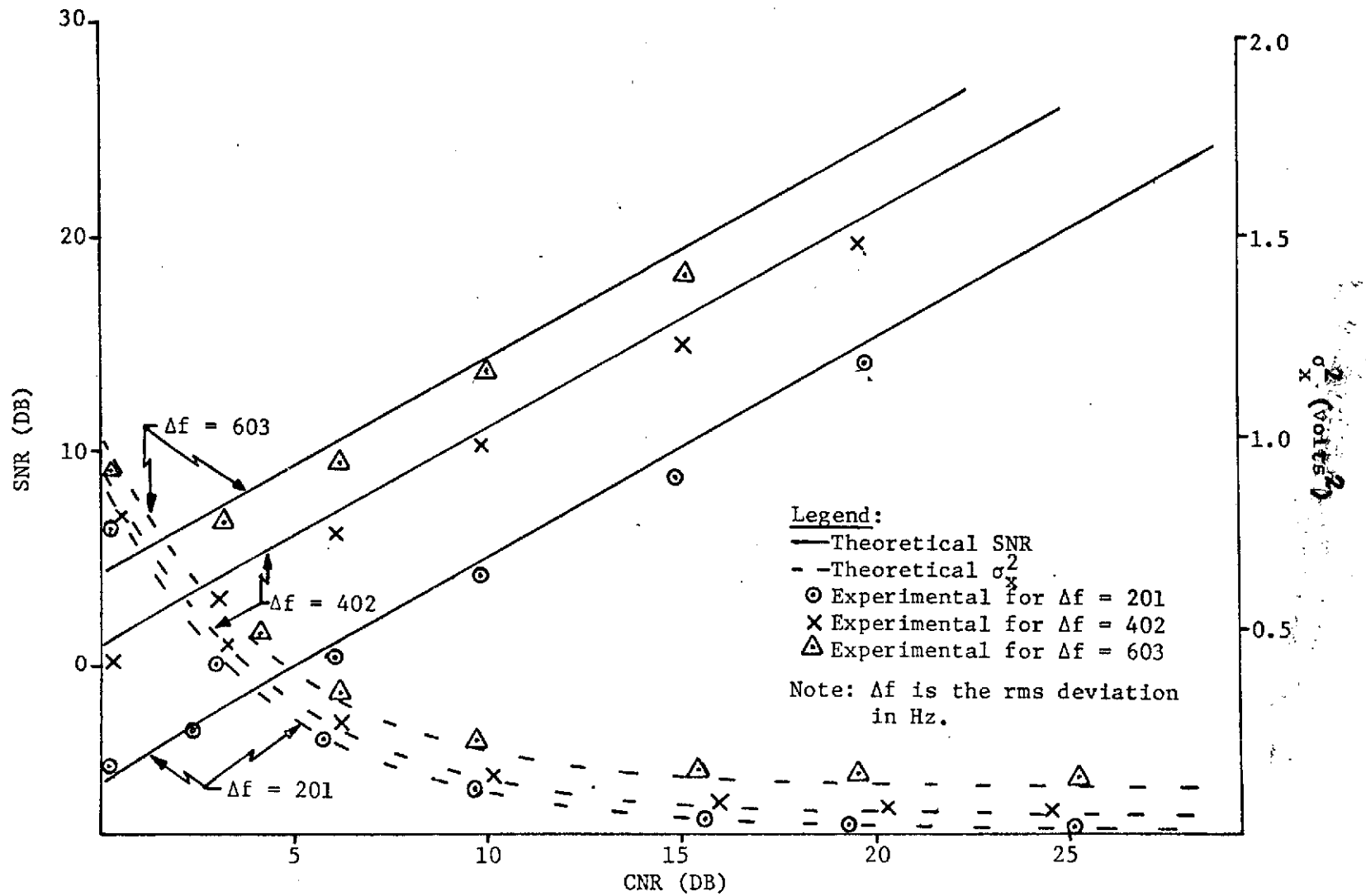

Figure 27. SNR and σ_x^2 as a Function of CNR for β = 5600 Hz, f_1 = 56 Hz, f_2 = 440 Hz.

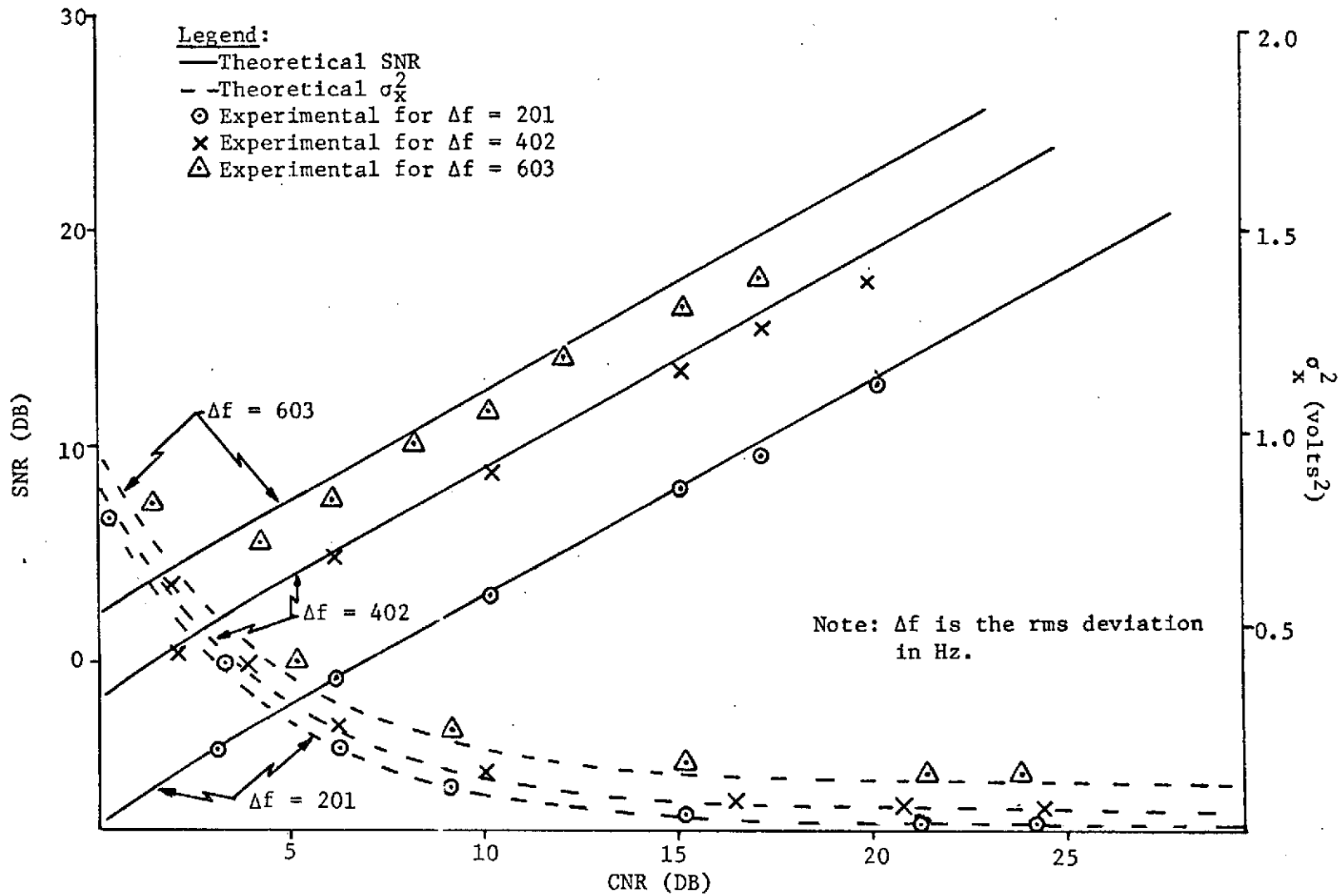

Figure 28. SNR and σ_x^2 as a Function of CNR for β= 3300 Hz, f_1 = 56 Hz, f_2 = 440 Hz.

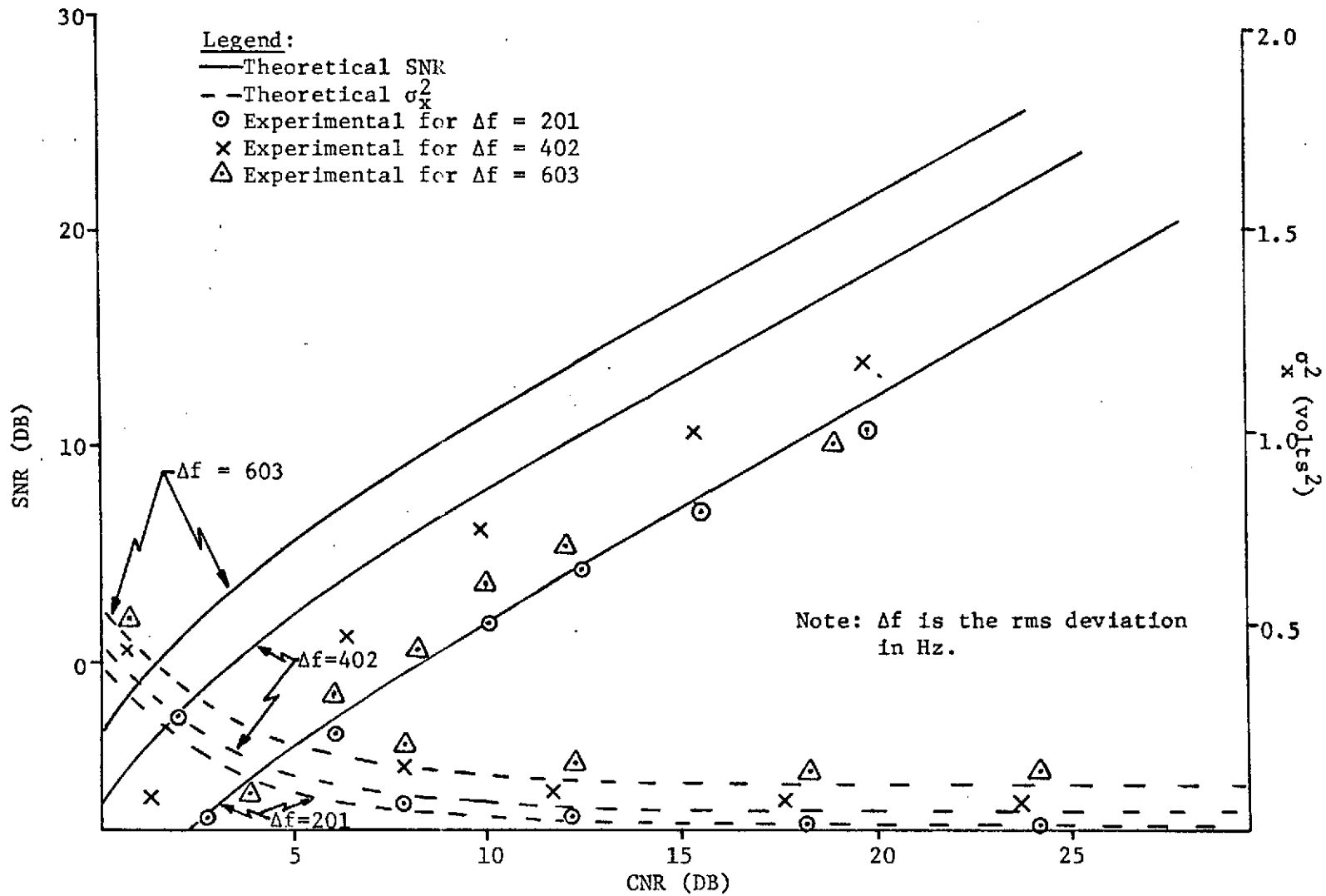

Figure 29. SNR and σ_x^2 as a Function of CNR for β = 900 Hz, f_1 = 56 Hz, f_2 = 440 Hz.

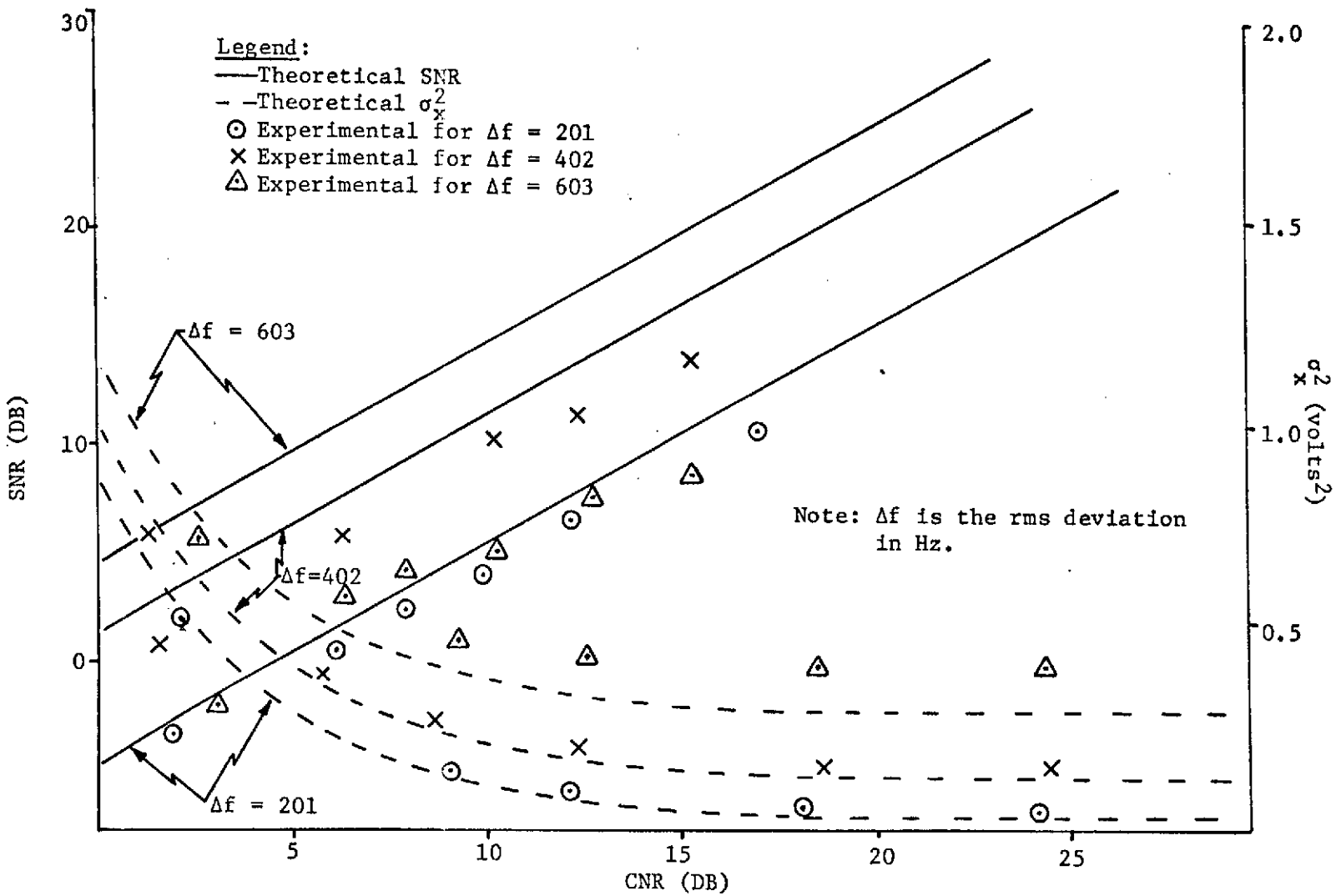

Figure 30. SNR and σ_x^2 as a Function of CNR for β = 5600 Hz, f_1 = 56 Hz, f_2 = 900 Hz.

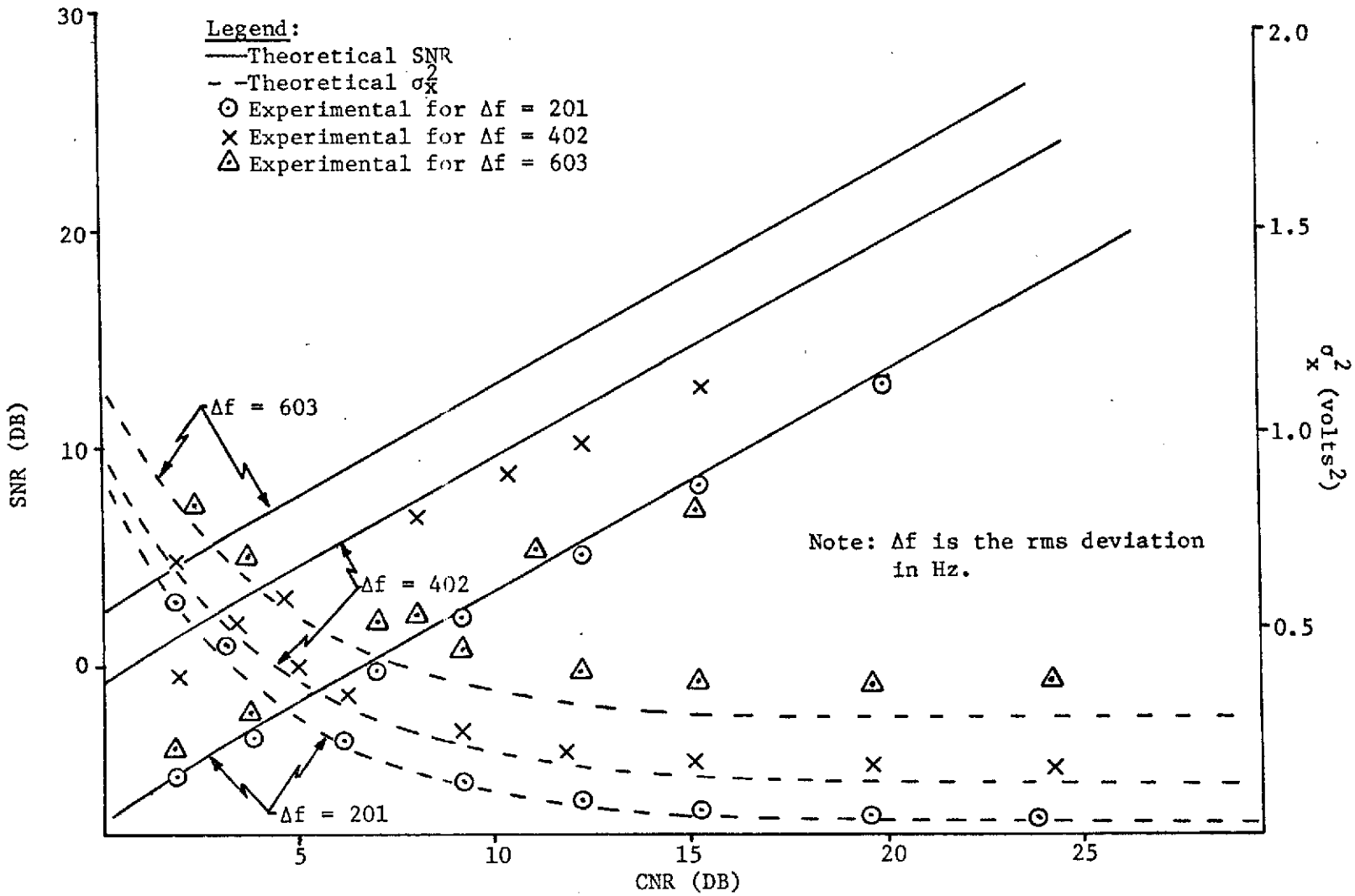

Figure 31. SNR and σ_x^2 as a Function of CNR for β = 3300 Hz, f_1 = 56 Hz, f_2 = 900 Hz.

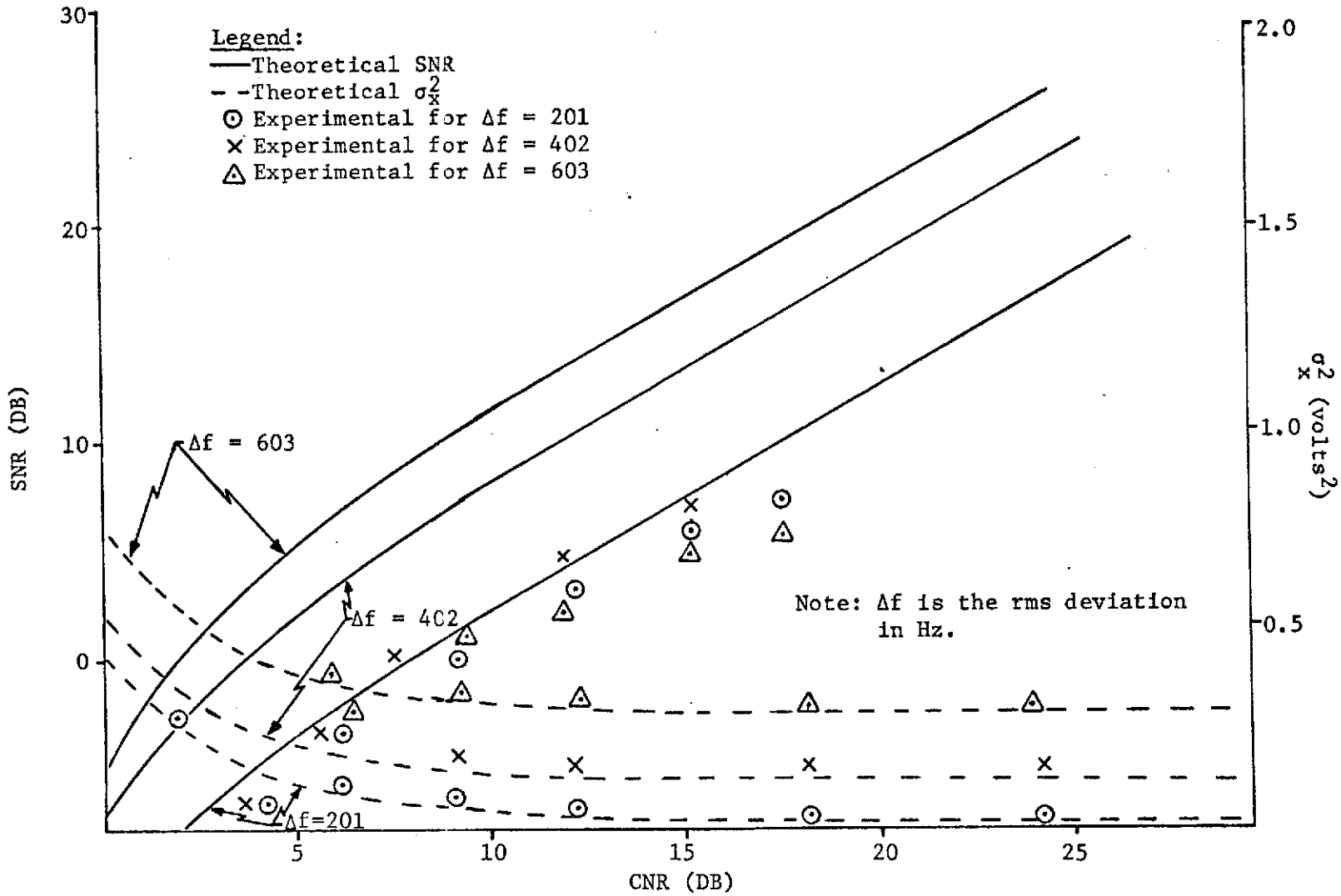

Figure 32. SNR and σ_x^2 as a Function of CNR for β = 900 Hz, f_1 = 56 Hz, f_2 = 900 Hz.

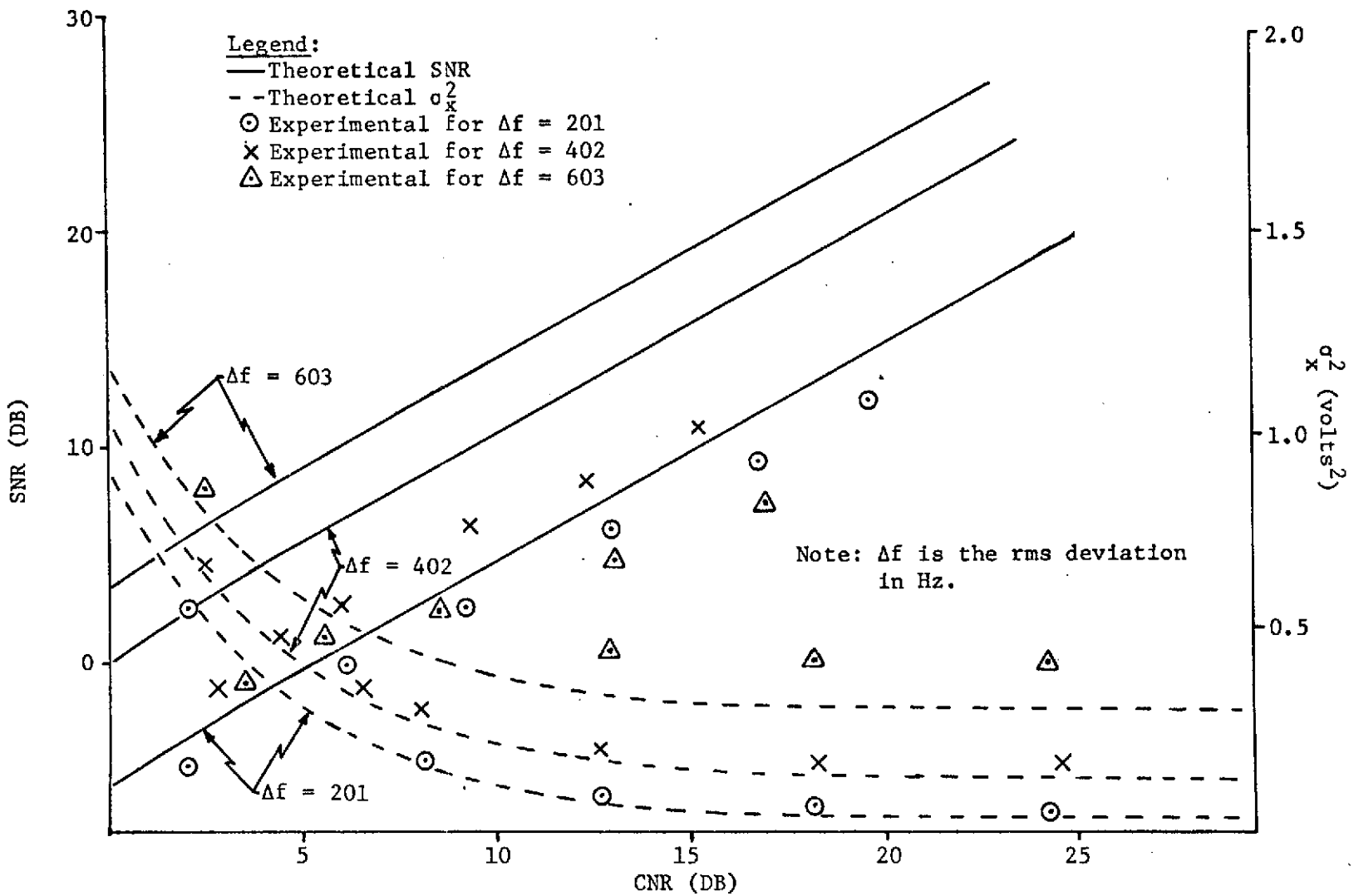

Figure 33. SNR and σ_x^2 as a Function of CNR for β = 5600 Hz, f_1 = 56 Hz, f_2 = 1250 Hz.

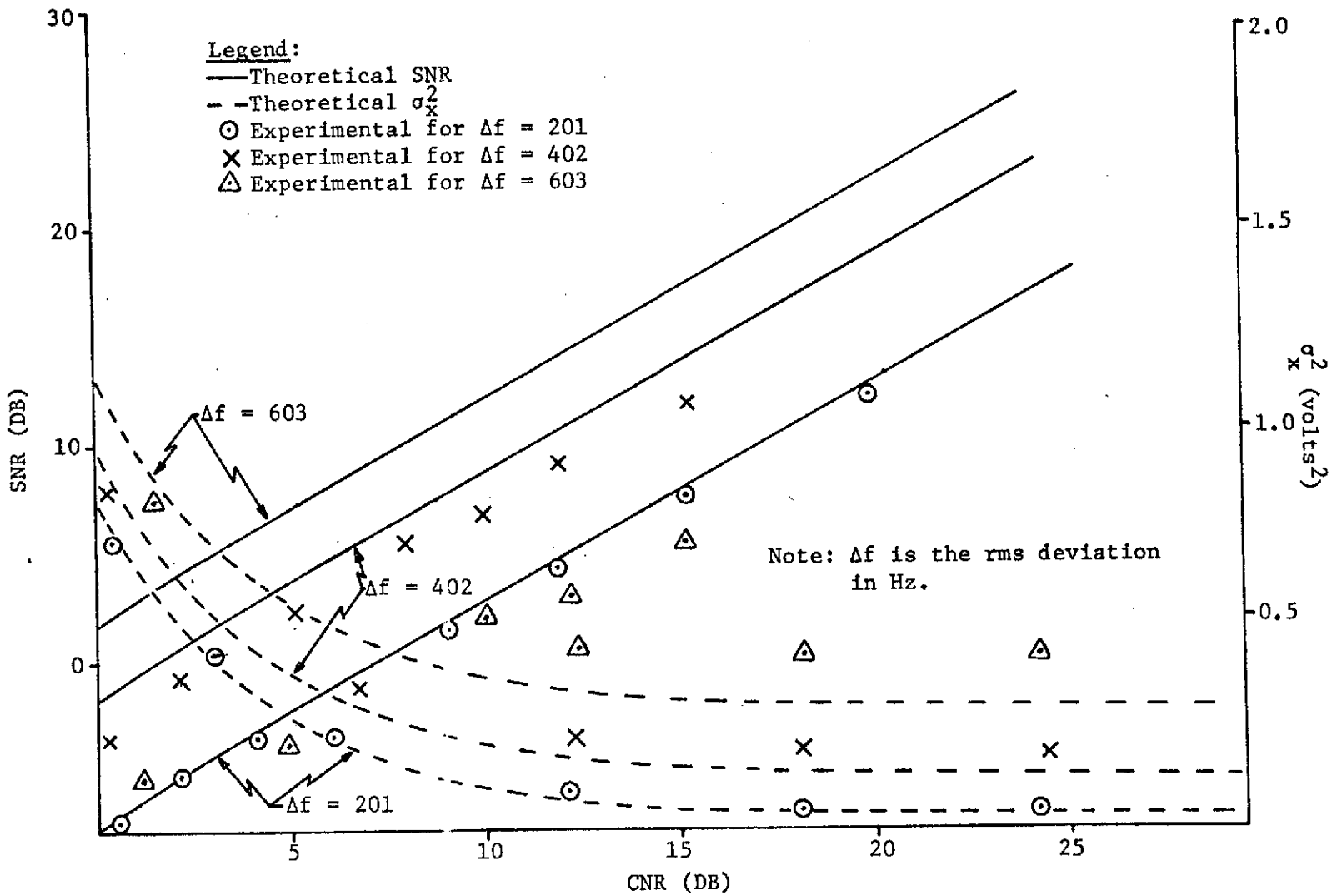

Figure 34. SNR and σ_x^2 as a Function of CNR for β = 3300 Hz, f_1 = 56 Hz, f_2 = 1250 Hz.

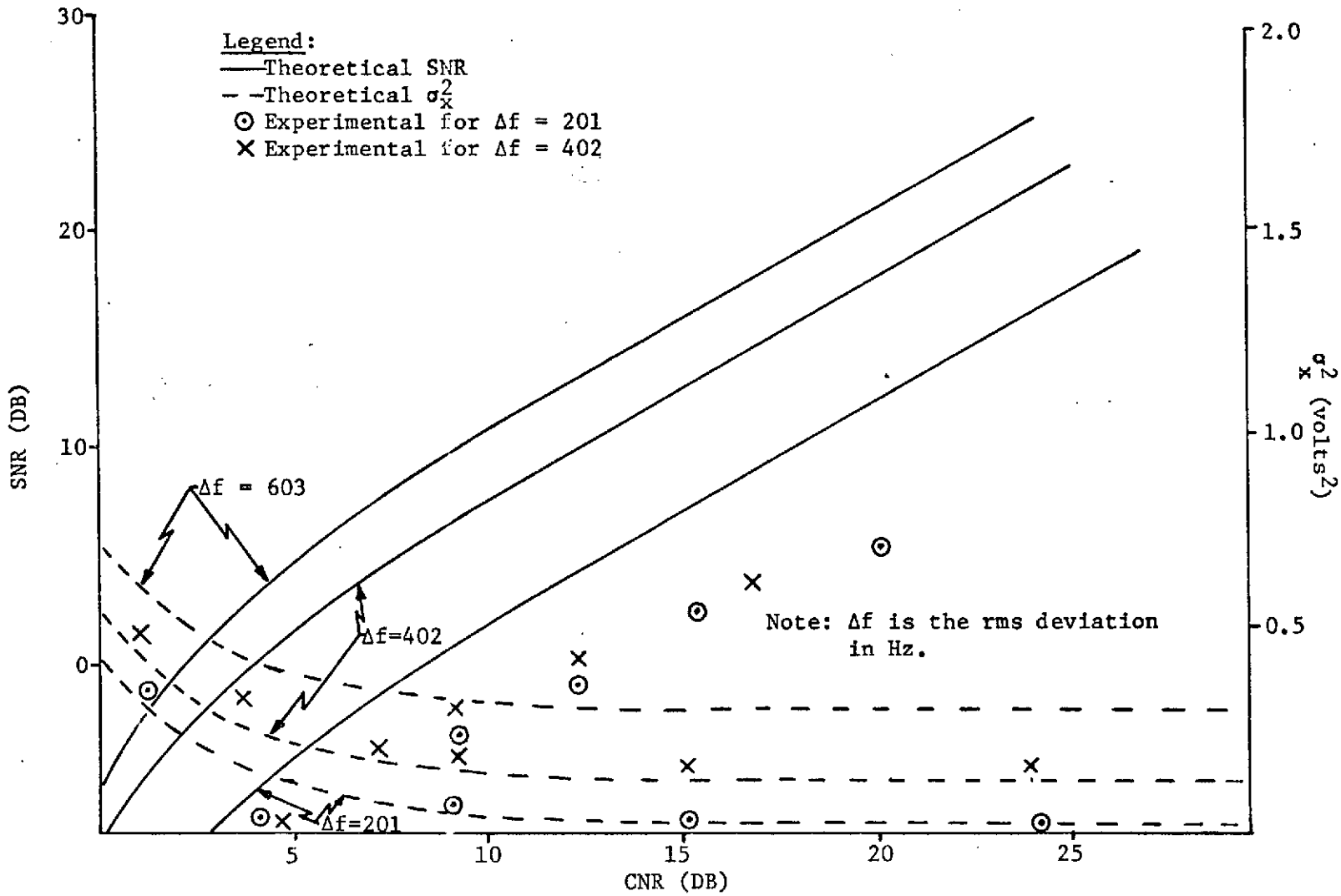

Figure 35. SNR and σ_x^2 as a Function of CNR for β = 900 Hz, f_1 = 56 Hz, f_2 = 1250 Hz.

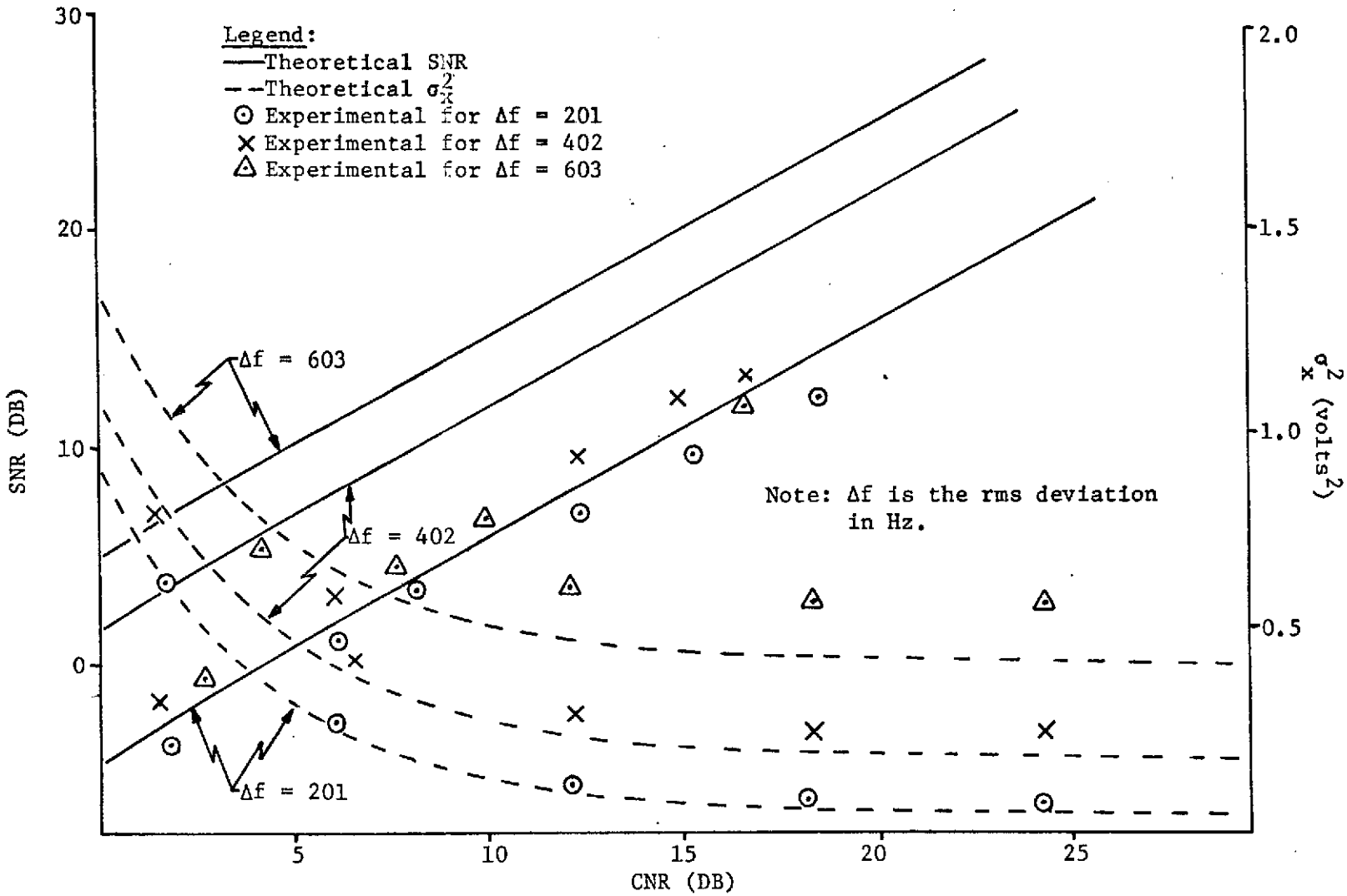

Figure 36. SNR and σ_x^2 as a Function of CNR for β = 5600 Hz, f_1 = 560 Hz, f_2 = 900 Hz.

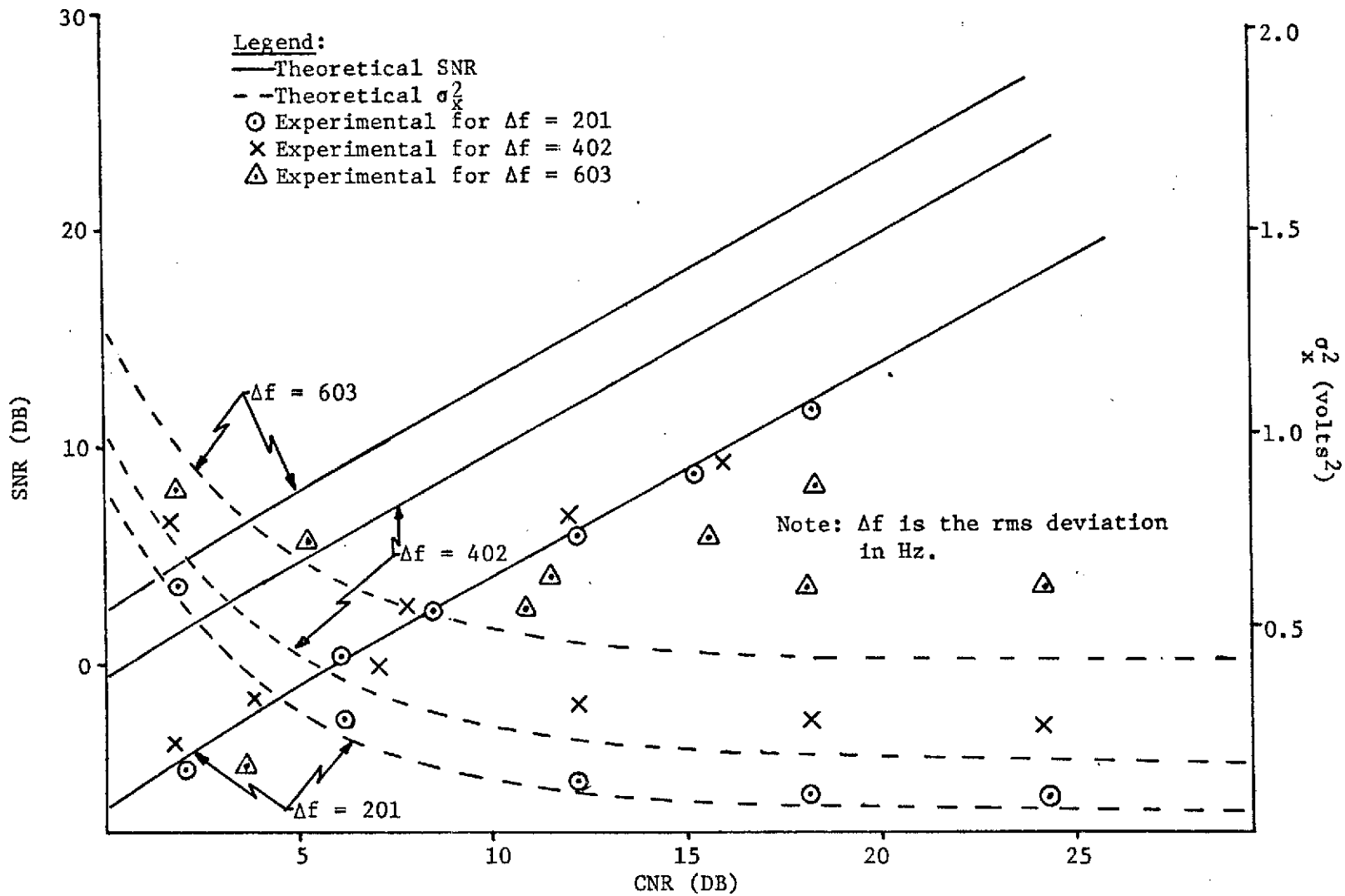

Figure 37. SNR and σ_x^2 as a Function of CNR for β = 3300 Hz, f_1 = 560 Hz, f_2 = 900 Hz.

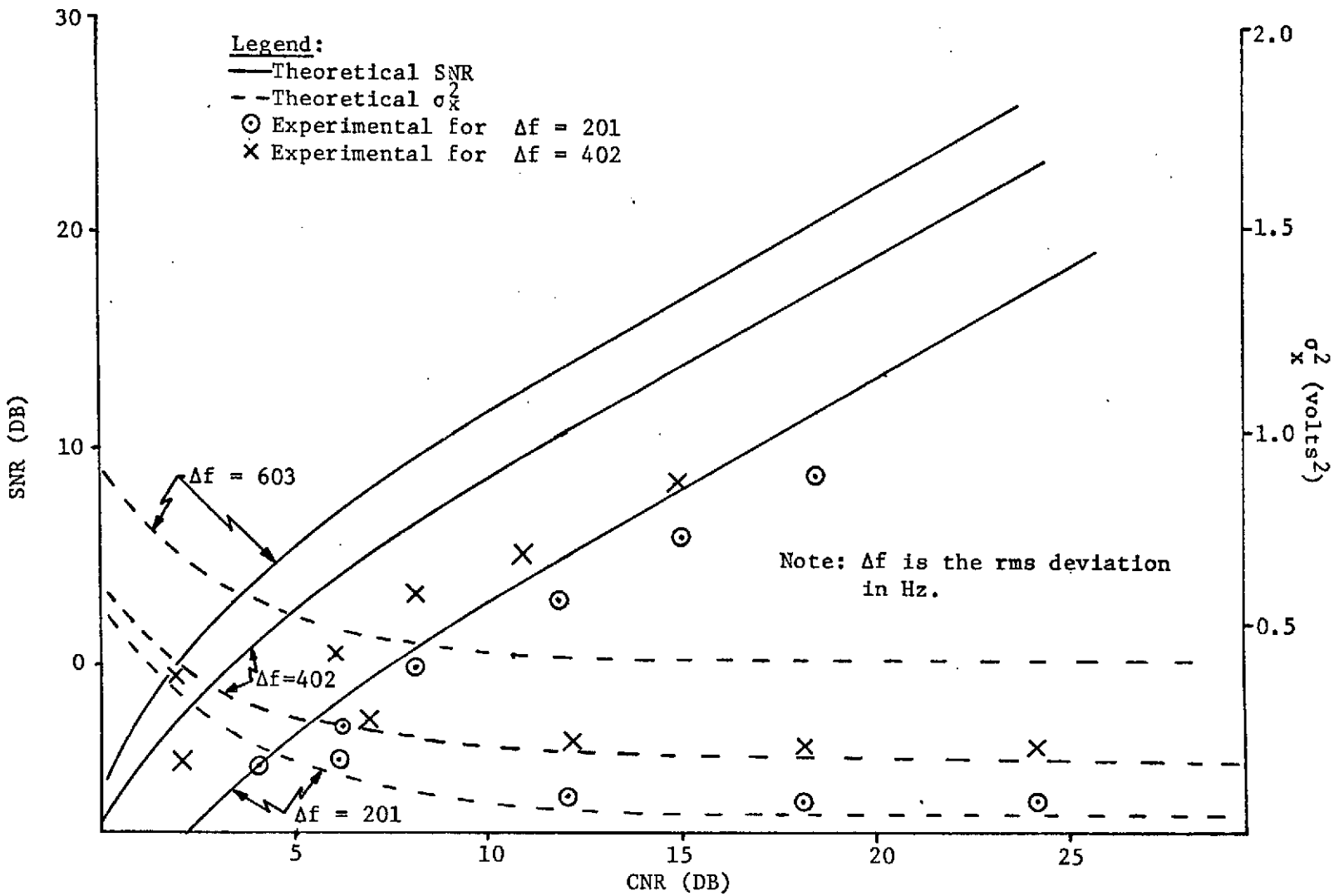

Figure 38. SNR and σ_x^2 as a Function of CNR for β = 900 Hz, f_1 = 560 Hz, f_2 = 900 Hz.

Table 2

Comparison of Theoretical (Quasi-Linear Model) and Experimental Results

SIGNAL ($f_1 - f_2$) \ IF FILTER BANDWIDTH (β)	5600 HZ	3300 HZ	900 HZ
	Figure 27	Figure 28	Figure 29
56 HZ - 440 HZ	1. 1dB,10%	1. 0.5dB,5%	1.*2dB,15%
	2. 1dB,10%	2. 0.5dB,10%	2.*5dB,30%
	3. 1dB,10%	3. 2dB,10%	3.*10dB,30%
	Figure 30	Figure 31	Figure 32
56 HZ - 900 HZ	1. 2dB,10%	1. 0.5dB,5%	1.*2dB,10%
	2. 3dB,10%	2. 2dB,15%	2.*5dB,15%
	3.*12dB,40%	3.*10dB,30%	3.*12dB,10%
	Figure 33	Figure 34	Figure 35
56 HZ - 1250 HZ	1. 2dB,5%	1. 0.5dB,5%	1.*5dB,20%
	2. 4dB,15%	2. 3dB,15%	2.*10dB,20%
	3.*13dB,30%	3.*12dB,40%	
	Figure 36	Figure 37	Figure 38
560 HZ - 900 HZ	1. 2dB,10%	1. 0.5dB,15%	1.*3dB,20%
	2. 4dB,15%	2.*5dB,40%	2.*5dB,20%
	3.*10dB,40%	3.*15dB,40%	

Legend:
1. rms deviation equal to 201 Hz
2. rms deviation equal to 402 Hz
3. rms deviation equal to 603 Hz

* indicates IF Filter distortion (see Table 2)

Note: the first number is the maximum difference between theoretical and experimental SNR in dB, while the second number is the maximum percent difference between theoretical and experimental values of σ_x^2.

SNR and 15% for σ_x^2. It is emphasized that this is the maximum error and that the error is usually much smaller than the above values as can be seen from Figures 27 through 38. Table 2 also indicates that the error increases as σ_x^2 increases and/or IF Filter Bandwidth increases. This is consistent with the assumptions used in developing the Quasi-Linear Model (Chapter 1).

6.2 PLL Characteristics as a Function of RMS Deviation

One of the advantages of using FM is that there is a so called "FM improvement" for large modulation indices. Essentially what this means is that the output SNR can be improved (increased) by using a larger modulation index. This of course assumes that the larger modulation index does not cause IF Filter distortion or PLL distortion due to loop "stress." Thus there is a "tradeoff" between "FM improvement" and distortion when the modulation index is increased.

Figure 27 illustrates the "FM improvement" effect. In this case there is no IF or PLL distortion, and an increase in the rms deviation (modulation index) causes an increase in output SNR. An increase in the deviation by a factor of 2 causes an increase in SNR by a factor of 4 (6dB). Figure 37 illustrates the effect of IF Filter Distortion. In this case an increase in rms deviation causes a decrease in the output SNR. This is true since IF Filter distortion increases with an increase in the rms deviation and for this case the IF distortion dominates over any "FM improvement" effect. It should be noted that the theoretical values do not conform to the IF Filter distortion since this effect was not incorporated into the Quasi-Linear Model.

From the above discussion it is clear that there is an optimum deviation for a given IF Filter and PLL in the sense that the output SNR is maximized.

6.3 PLL Characteristics as a Function of IF Filter Bandwidth

When the IF Filter Bandwidth is of the same order of magnitude as the PLL Bandwidth, the noise spectrum is within a frequency range that can be tracked by the PLL. Thus the PLL tracks the noise and results in a reduced output SNR. As the noise amplitude is increased, the probability that the carrier will undergo a 2π step in phase increases [13]. Since the PLL tracks the input noise when such an event occurs, there is an impulse noise event at the PLL output. This impulse noise event is referred to as a "Type I click" [12]. This phenomenon was observed during operation of the Experimental System when the IF Filter Bandwidth was narrow and the CNR was low. For wider IF bandwidths, the frequency of occurance of these "Type I clicks" decreases which agrees with previous work [12,13].

From Figures 27, 28, and 29 it can be seen that a decrease in IF Filter Bandwidth results in a larger value for σ_x^2 and a lower value for the SNR if the CNR is kept constant. This is consistent with the above mentioned fact that the PLL tracks the noise frequency components within the PLL Bandwidth.

6.4 PLL Characteristics as a Function of the Signal Spectrum

By comparing the results in Figure 27 with the results in Figure 36, it can be seen that higher frequency components of the signal

undergo more IF and PLL distortion than do lower frequency components. This can also be seen by comparing Figures 27, 31, and 33 in which the upper cutoff frequency (f_2) is increased. Equation (1-19) indicates that the output NSD is parabolic (i.e. increases in proportion to ω^2). Therefore, the higher frequency signal components are "imbedded" in more noise than are lower frequency components. Both the parabolic NSD and the IF Filter and PLL distortion effects mentioned above contribute to the characteristic that in general low frequency signal components are demodulated with greater fidelity than are high-frequency signal components.

6.5 PLL Threshold Characteristics

If the PLL were a linear device the plot of SNR as a function of CNR shown in Figures 27 through 38 would be linear. However, due to the non-linearity of the PLL the plot departs from that given by the linear model for sufficiently small CNR. The point at which the actual output SNR is 1dB less than the SNR predicted by the linear model is termed "threshold" [5]. As can be seen from Figures 27 through 38 the "threshold" effect is more pronounced for certain conditions. In general the "threshold" effect is more pronounced (has a sharper "bend" in the SNR/CNR plot) for larger deviations, smaller IF Filter Bandwidths, and smaller Signal Bandwidths.

Quite often an attempt to predict threshold is made by setting σ_ϕ^2 equal to some value [1,4,7] and determining the corresponding CNR for the linear model. To check on the validity of this approach, the

threshold point was determined for Figures 27 through 38 when the "bend" in the SNR/CNR plot was pronounced enough to give an accurate reading. The corresponding values for σ_ϕ^2 were then determined from the print out generated during runs of the computer program which calculated theoretical values. The following observations were made. For wide signal bandwidths, threshold occurs at higher values for σ_x^2 and σ_ϕ^2. The phase variance (σ_ϕ^2) at threshold depends mainly on the signal spectrum and is fairly insensitive to changes in IF Filter Bandwidth and deviation. In particular, for f_1 = 56Hz, and f_2 = 900Hz at threshold $\sigma_\phi^2 \simeq 0.12$; while for f_1 = 560Hz and f_2 = 900H_z at threshold $\sigma_\phi^2 \simeq 0.13$.

Chapter 7

CONCLUSIONS AND RECOMMENDATIONS FOR FUTURE WORK

7.1 Conclusions

The Quasi-Linear PLL Phase Model developed in Chapter 1 is realistic and useful in the sense that it accurately predicts phase error and multiplier output variances as well as output SNR of an actual PLL. It is an improvement over previous models in that it accounts for (in a statistical sense) the fact that the IF Filter Bandwidth may be narrow compared to the PLL Bandwidth and that the phase error may be large enough to cause operation in a non-linear region. The use of a realistic modulating signal contributes to the usefulness of the results of this paper. For the second-order PLL and band-pass type modulating signals used in the Experimental System the error between actual and predicted data was less than 15%. However, there is no reason to believe that a similar bound on errors would not be found for different order PLL's and modulating signals.

The following observations were made concerning the occurence of threshold. The threshold effect is more pronounced (has a sharper "bend" in the SNR/CNR plot) for narrow IF Filter bandwidths, for larger modulation indices, and for narrow signal bandwidths. The phase error variance at threshold depends mainly on the modulating signal spectrum, and varies considerably as the signal bandwidth or

center frequency of the signal spectrum is changed. The above threshold information is important since it is desirable to operate the PLL above threshold.

7.2 Recommendations for Future Work

One of the difficulties encountered in using the Experimental System was that the VCO "phase jitter" made measurements of the output SNR above approximately 18dB inaccurate. The use of a voltage-controlled crystal oscillator might reduce this inaccuracy and allow measurements at larger SNR's, and variances. Then threshold characteristics for large modulation indices could be investigated.

An important effect encountered when making measurements on the Experimental System was output signal distortion caused by the finite IF Filter Bandwidth. It would be very helpful if an analytical expression could be developed which gives the relationship between IF Filter distortion as a function of the IF Filter Bandwidth, modulation index, and signal spectrum.

The theoretical and experimental techniques developed in this paper were applied to a second-order PLL. These same techniques could be applied to PLL's that are other than second-order. One particular PLL which has received attention [10] to which these techniques may be applied is the Multifilter PLL.

BIBLIOGRAPHY

[1] Viterbi, A. J., Principles of Coherent Communication, pp. 7-36, McGraw-Hill, 1966.

[2] Develet, J. A., Jr., "A Threshold Criterion for Phase-Lock Demodulation," Proceedings of the IEEE, Vol. 51, February 1963, pp. 349-356.

[3] Viterbi, A. J. and C. R. Cahn, "Optimum Coherent Phase and Frequency Demodulation of a Class of Modulating Spectra," IEEE Transactions on Space Electronics and Telemetry, Vol. SET-10, No. 3, September 1964, pp. 95-102.

[4] Gardner, F. M., Phaselock Techniques, pp. 7-27, John Wiley and Sons, 1966.

[5] Taub, H. and D. L. Schilling, Principles of Communication Systems, pp. 118-125, McGraw-Hill, 1971.

[6] Weinberg, L., Network Analysis and Synthesis, pp. 507-518, McGraw-Hill, 1962.

[7] Van Trees, H. L., Detection, Estimation, and Modulation Theory, Part II Nonlinear Modulation Theory, Wiley and Sons, 1971.

[8] Uhran, J. J., Jr., "Cycle-Slipping Effects on the Output Signal of a Phase-Locked Demodulator," Proceedings of the IEEE, Vol. 56, No. 1, January 1968, pp. 80-81.

[9] Carden, F. F., L. R. Kelly and T. B. Hintz, "The FDM Demodulating Characteristics of Non-linear Phase-Locked Loops," IEEE National Telemetering Conference, Houston, Texas, 1968, pp. 30-35.

[10] Henry, R. R. and F. F. Carden, "Multifilter Phase-Lock Loop Nonlinear Analysis and Design Criterion," IEEE Transactions on Communications, Vol. COM-21, February 1973, pp. 135-142.

[11] Henry, R. R. and F. F. Carden, "Phase Error Characteristics of a Second-Order Phase-Lock Loop," to be published.

[12] Hess, D. T., "Cycle-Slipping in a First-Order Phase-Locked Loop," IEEE Transactions on Communications, Vol. COM-16, No. 2, April 1968, pp. 255-260.

[13] Rice, S. O., "Noise in FM Receivers," in Time Series Analysis, M. Rosenblatt, Ed., Chapter 25, John Wiley and Sons, 1963.

Appendix I

SPECTRAL DENSITIES OF THE PLL

Let $\Theta_1(s)$, $\Theta_2(s)$, $\Phi(s)$, $N(s)$, $Y(s)$, and $O(s)$ represent the Fourier Transforms of $\Theta_1(t)$, $\Theta_2(t)$, $\phi(t)$, $n(t)$, $y(t)$, and $o(t)$ respectively. Then, from Figure 5,

$$\Phi(s) = \Theta_1(s) - \Theta_2(s)$$

$$= \Theta_1(s) - \left[\frac{K' F(s)}{s}\right] [N(s) + G\,\Phi(s)],$$

or $$\Phi(s)\left[\frac{GK\,F(s)}{s} + 1\right] = \Theta_1(s) - \frac{K\,F(s)}{s} N(s).$$

Thus $$\Phi(s) = \frac{s\Theta_1(s)}{s + GK\,F(s)} - \frac{K\,F(s)\,N(s)}{s + GK\,F(s)}. \qquad \text{(I-1)}$$

Since $$H(s) = \frac{GK\,F(s)}{s + GK\,F(s)} \text{ and } 1 - H(s) = \frac{s}{s + GKF(s)} \qquad \text{(I-2)}$$

Equation I-1 becomes

$$\Phi(s) = [1 - H(s)]\,\Theta_1(s) - \frac{1}{G} H(s)\,N(s). \qquad \text{(I-3)}$$

Since $_1(t)$ and $n(t)$ are independent

$$\overline{\Phi}(\omega) = |1 - H(s)|^2\,\overline{\Theta}_1(\omega) + \frac{1}{G^2}\,|H(s)|^2\,\overline{N}(\omega). \qquad \text{(I-4)}$$

Again from Figure 5

$$Y(s) = N(s) + G\,\Phi(s). \qquad \text{(I-5)}$$

substituting for $\Phi(s)$ as given by Equation (I-3)

$$Y(s) = N(s) + G[\{1 - H(s)\}\Theta_1(s) - \frac{1}{G} H(s)\,N(s)]$$

$$= G[1 - H(s)]\Theta_1(s) + [1 - H(s)]\,N(s) \quad . \qquad \text{(I-6)}$$

Thus the spectral density is

$$\overline{Y}(\omega) = G^2 \, |1 - H(s)|^2 \, \overline{\Theta}_1(\omega) + |1 - H(s)|^2 \, \overline{N}(\omega) \; . \qquad \text{(I-7)}$$

From Figure 5 and Equation (I-6)

$$\begin{aligned} O(s) &= K \, D(s) \, F(s) \, Y(s) = GK[1 - H(s)] \, D(s) \, F(s) \, \Theta_1(s) \\ &\qquad + K[1 - H(s)] \, F(s) \, N(s) \\ &= s \, D(s) \, H(s) \, \Theta_1(s) + \frac{1}{G} \, s \, D(s) \, H(s) \, N(s). \end{aligned} \qquad \text{(I-8)}$$

Therefore

$$\overline{O}(\omega) = \omega^2 |H(s)|^2 \, \overline{D}(\omega) \, \overline{\Theta}_1(\omega) + \frac{\omega^2}{G^2} |H(s)|^2 \, \overline{D}(\omega) \, \overline{N}(\omega) \qquad \text{(I-9)}$$

where $\overline{D}(\omega) = |D(s)|^2$.

Appendix II

BAND-PASS FILTER TRANSFER FUNCTION

Consider first the low-pass section of the Filter. Since Equation (2-1) is the transfer function squared it is necessary to find the polynominal $V_4(s)$ such that

$$\frac{1}{V_4(s)\ V_4(-s)} = \frac{64\varepsilon^2}{1 + \varepsilon^2\ T_4^2(s)} \tag{II-1}$$

$$= \frac{64\varepsilon^2}{1 + \varepsilon^2[64s^8 - 128s^6 + 80s^4 - 16s^2 + 1]} \quad .$$

Thus one must find the roots of

$$1 + \varepsilon^2\ T_4^2(s) = 0. \tag{II-2}$$

The procedure to do so is given by [6] and yields the following 4 roots in the left-hand complex plane

$$\begin{aligned} r_1 &= -a_1 + jb_1 \qquad \text{where} \qquad a_1 = 0.203721927 \\ r_2 &= -a_1 - jb_1 \qquad\qquad\quad\ \ b_1 = 1.046636712 \\ r_3 &= -a_2 + jb_2 \qquad\qquad\quad\ \ a_2 = 0.491828394 \\ r_4 &= -a_2 - jb_2 \qquad\qquad\quad\ \ b_2 = 0.433531121 \end{aligned} \tag{II-3}$$

Therefore

$$\begin{aligned} V_4(s) &= (s + a_1 - jb_1)(s + a_1 + jb_1)(s + a_2 - jb_2)(s + a_2 + jb_2) \\ &= s^4 + 2(a_1 + a_2)s^3 + (A_1 + A_2 + 4a_1a_2)s^2 \\ &\quad + 2(a_1A_2 + a_2A_1)s + A_1A_2 \quad , \end{aligned} \tag{II-4}$$

where $\qquad A_1 = a_1^2 + b_1^2$, and $A_2 = a_2^2 + b_2^2$.

Substitution of Equation (II-3) into Equation (II-4) yields

$$V_4(s) = s^4 + f_3 s^3 + f_2 s^2 + f_1 s + f_0$$

where

$$f_0 = 0.4887118438 \qquad f_2 = 1.96758027$$
$$f_1 = 1.29350660 \qquad f_3 = 1.39100322 \quad . \tag{II-5}$$

Thus the transfer function for the low-pass section is

$$B(s)_{LP} = \frac{1}{\left(\frac{s}{\omega_2}\right)^4 + f_3\left(\frac{s}{\omega_2}\right)^3 + f_2\left(\frac{s}{\omega_2}\right)^2 + f_1\left(\frac{s}{\omega_2}\right) + f_0} \tag{II-6}$$

where ω_2 is the upper break frequency of B(s). Likewise the transfer function of the high-pass section is

$$B(s)_{HP} = \frac{1}{\left(\frac{\omega_1}{s}\right)^4 + f_3\left(\frac{\omega_1}{s}\right)^3 + f_2\left(\frac{\omega_1}{s}\right)^2 + f_1\left(\frac{\omega_1}{s}\right) + f_0} \tag{II-7}$$

where ω_1 is the lower break frequency of B(s).

The overall transfer function (B(s)) is

$$B(s) = B(s)_{LP}\, B(s)_{HP}$$
$$= \frac{s^4}{g_8 s^8 + g_7 s^7 + \ldots\ldots\ldots\ldots + g_2 s^2 + g_1 s + g_0} \tag{II-8}$$

where

$$g_0 = f_0 \omega_1^4$$

$$g_1 = \frac{f_1 \omega_1^4}{\omega_2} + f_0 f_3 \omega_1^3$$

$$g_2 = \frac{f_2\omega_1^4}{\omega_2^2} + \frac{f_1 f_3 \omega_1^3}{\omega_2} + f_0 f_2 \omega_1^2$$

$$g_3 = \frac{f_3\omega_1^4}{\omega_2} + \frac{f_2 f_3 \omega_1^3}{\omega_2^2} + \frac{f_1 f_2 \omega_1^2}{\omega_2} + f_0 f_1 \omega_1$$

$$g_4 = \frac{\omega_1^4}{\omega_2^4} + \frac{f_3^2\omega_1^3}{\omega_2^3} + \frac{f_2^2\omega_1^2}{\omega_2^2} + \frac{f_1^2\omega_1}{\omega_2} + f_0^2 \qquad \text{(II-9)}$$

$$g_5 = \frac{f_3\omega_1^3}{\omega_2^4} + \frac{f_2 f_3 \omega_1^2}{\omega_2^3} + \frac{f_2 f_1 \omega_1}{\omega_2^2} + \frac{f_1 f_0}{\omega_2}$$

$$g_6 = \frac{f_2\omega_1^2}{\omega_2^4} + \frac{f_3 f_1 \omega_1}{\omega_2^3} + \frac{f_2 f_0}{\omega_2^2}$$

$$g_7 = \frac{f_1\omega_1}{\omega_2^4} + \frac{f_3 f_0}{\omega_2^3}$$

$$g_8 = \frac{f_0}{\omega_2^4}$$